Functional Carbon Nanotubes for Photonic Applications

Raz N Arif

Doctor of Philosophy

Aston University
Birmingham

30th September, 2014

Declaration

The work in this thesis is the results of research carried out in Aston Institute of Technologies and Nanoscience Research Group at School of Engineering and Applied Physics, Aston University, Birmingham, United Kingdom. I declare it to be my own work unless referenced to the contrary in the text.

To

Kurdish peshmerga

Acknowledgement

I would like to express my sincere gratitude and appreciation to my Supervisor Dr Alex Rozhin who offered me the great opportunity to do research in this field and kindly guided me throughout my time at Aston University. With great patience and the utmost dedication he introduced me to the scientific community and always was keen on helping me succeed with the many challenges and opportunities that arose. I am truly thankful for your support, inspiration, and for expanding my horizon in a most profound way.

Professor Sergei K. Turitsyn did not hesitate in giving me a great opportunity in welcoming me into his group. Your stance, generosity and incredible support were paramount in the beginning and without your encouragement it would have been impossible for me to partake in this great experience.

I cannot express enough and emphasize my gratitude to my husband Mariwan for his immense understanding and sacrifice throughout these long years. You were and are as always my bedrock and my greatest support. I am so very glad to have you in my life.

I am most grateful to my father, Noori Arif who was always there for me. Thank you for all the time you have invested in me, and for your great patience. You have comforted and supported me in ways I cannot express. It is an honour to have followed in your footsteps and you have been such an inspiration and role model.

To my lovely brother Ahmad. Thank you for everything you have done for me. I know you are under great pressure but although you are busy with your difficult and demanding medical studies, you have always made time for me.

My deepest love and affection to my angels, my boys, Meer and Aland. I appreciate your understanding during these years, which meant great changes and challenges for you. Your well-being and success will always be my ultimate happiness.

It is a great pleasure to express my gratitude towards Dr. Govand Sherwani, to the Kurdistan Ministry of Higher Education and Scientific Research, and dear Dr. Mohammed Rasheed Mochtar, of Salahaddin University, Erbil. I am deeply grateful for your advice and guidance which has been essential. I will never forget your endorsement and encouragement.

My appreciation and thanks to dear Rozhen Kamal, a friend and part of my family. Thank you for your ever-so important assistance.

I would like to acknowledge the NATO Science for Peace and Security project “Novel Macromolecular Complexes for Rapid Detection of Hazardous Agents” (SFP 984 189), which supported a significant part of this thesis. Also I wish express my sincere gratitude to all NATO project team members in Institute of Physics and Institute of Organic Chemistry, National Academy of Sciences of Ukraine. Thank you very much honourable colleagues, especially Dr Petro Lutsyk, for developing great organic dye materials and for stimulating discussions.

Lastly, but in no way least, many thanks go to all of my beloved colleagues and friends at Aston University, especially Dr Chengbo Mou, and to all my colleagues at Sulaimani University.

Aston University
Birmingham

Abstract

Carbon nanomaterials are an active frontier of research in current nanotechnology. Single wall Carbon Nanotube (SWNT) is a unique material which has already found several applications in photonics, electronics, sensors and drug delivery. This thesis presents a summary of the author's research on functionalisation of SWNTs, a study of their optical properties, and potential for an application in laser physics.

The first significant result is a breakthrough in controlling the size of SWNT bundles by varying the salt concentrations in N-methyl 2-pyrrolidone (NMP) through a salting out effect. The addition of Sodium iodide leads to self-assembly of CNTs into recognizable bundles. Furthermore, a stable dispersion can be made via addition polyvinylpyrrolidone (PVP) polymer to SWNTs-NMP dispersion, which indicates a promising direction for SWNT bundle engineering in organic solvents.

The second set of experiments are concerned with enhancement of photoluminescence (PL), through the formation of novel macromolecular complexes of SWNTs with polymethine dyes with emission from enhanced nanotubes in the range of dye excitation. The effect appears to originate from exciton energy transfer within the solution.

Thirdly, SWNT base-saturable absorbers (SA) were developed and applied to mode locking of fibre lasers. SWNT-based SAs were applied in both composite and liquid dispersion forms and achieved stable ultrashort generation at 1000nm, 1550nm, and 1800 nm for Ytterbium, Erbium and Thulium-doped fibre laser respectively.

The work presented here demonstrates several innovative approaches for development of rapid functionalised SWNT-based dispersions and composites with potential for application in various photonic devices at low cost.

Key Words: carbon nanotubes, polymers, poltymethine dye, photoluminescence spectroscopy, saturable absorber, mode locked fibre laser.

Relevant Publications

Maxim V. Fedorov, **Raz N. Arif**, Andrey I. Frolov, Martin Kolar, Anastasia O. Romanovaa and Aleksey G. Rozhin, Salting out in organic solvents: a new route to carbon nanotube bundle engineerin, Phys. Chem. Chem. Phys., 13, 12399 (2011).

Andrey I. Frolov, **Raz N. Arif**, Martin Kolar, Anastasia O. Romanova, Maxim V. Fedorov and Aleksey G. Rozhin, Molecular mechanisms of salt effects on carbon nanotube dispersions in organic solvent (N-methyl-2-pyrrolidone), Chem. Sci., 3, 541 (2012).

C. Mou, A. G. Rozhin, **R. Arif**, K. Zhou, and S. Turitsyn, Polarization insensitive in-fiber mode-locker based on carbon nanotube with N-methyl-2-pryrrolidone solvent filled fiber microchamber, Appl. Phys. Lett. 100(10), 101110 (2012).

Chengbo Mou, **Raz Arif**, Aleksey Rozhin, and Sergei Turitsyn, Passively harmonic mode locked erbium doped fiber soliton laser with carbon nanotubes based saturable absorber, Optical Material Express, Vol. 2 Issue 6, pp 884-890 (2012)

Y. S. Fedotov, S. M. Kobtsev, **R. N. Arif**, A. G. Rozhin, C. Mou, and S. K. Turitsyn, Spectrum-, pulsewidth-, and wavelength-switchable all-fiber mode-locked Yb laser with fiber based birefringent filter, Optics Express, Vol. 20 Issue 16, pp.17797-17805 (2012)

M. Chernysheva, A. Krylov, C. Mou, **R. Arif**, A. Rozhin, M.H. Rmmeli, S. Turitsyn, E.M. Dianov 300-mW average output power hybrid modelocked thulium-doped fiber laser, in Proc. ECOC, 2013, paper P.1.9.

Maria A. Chernysheva, Alexander A. Krylov, Chengbo Mou, **Raz N. Arif**, Alex G. Rozhin, Mark H. Rmmeli, Sergey K. Turitsyn, and Evgeny M. Dianov, Higher-Order Soliton Generation in Hybrid Mode-Locked Thulium-doped Fiber Ring Laser, IEEE JOURNAL OF SELECTED TOPICS IN QUANTUM ELECTRONICS, VOL. 20, NO. 5, pp 1100908 (2014)

R.N. Arif, C. Mou, Yu.P. Piryatinski, A. Pud, K. Zhou, S.K. Turitsyn, A.G. Rozhin, Carbon Nanotubes Dispersion in N-methyl-2-Pyrrolidone: Optical Properties and Application as Micro-channel Mode-Locker Device in Fibre Laser, Journal of Experimental Nanoscience, accepted

M. P. Shandura, Yu. P. Kovtun, V. P. Yakubovskyi, Yu. P. Piryatinski, P. M. Lutsyk, R. J. Perminov, **R. N. Arif**, A. B. Verbitsky, and A. Rozhin, Dehydroacetic Acid based Dioxaborine

Styryl Dye: Effective Fluorescent Probe for Detection of Ammonia, Amine and Carbon Nanotubes. Sensor Letters, accepted.

Chengbo Mou, **Raz Arif**, Anatoly Lobach, Nataliya Spitsina, Valery Kazakov, Aleksey Rozhin, and Sergei K. Turitsyn, Erbium Doped Fiber Laser Mode Locked by Graphene in Carboxymethylcellulose Polymer Composite, Optical Fiber Communication Conference San Francisco, California United States, Optics InfoBase, March 9-13, 2014.

C. Mou, S. Sergeyev, **R. Arif**, A. Rozhin, S. Kolpakov, Z. Zhang, and S. K. Turitsyn, Polarization switching in stretched pulse fiber laser,CLEO: QELS_Fundamental Science San Jose, California United States, Optics InfoBase, June 8-13, 2014.

Maria Chernysheva, Alexander Krylov, Chengbo Mou, **Raz N. Arif**, Alex Rozhin, Mark Ruemmeli, Natalia Arutyunyan, Elena Obraztsova, Sergei K. Turitsyn, and Evgeny Dianov, Inversed-modified Soliton Generation in Mode-locked Fibre Laser at Normal Dispersion, Conference Paper, Optical Sensors, Barcelona Spain,July 27-31, 2014.

Maria Chernysheva, Alexander Krylov, Chengbo Mou, **Raz N. Arif**, Alex Rozhin, Mark Ruemmeli, Sergei K. Turitsyn, and Evgeny Dianov, Higher-order Femtosecond Solitons Generation in a Hybrid Mode-locked Tm-doped Fibre Laser, Conference Paper, Specialty Optical Fibers,Barcelona Spain,July 27-31, 2014.

Contents

Abbreviations

SWNT	Single walled carbon nanotube
NMP	N-Methyl-2-pyrrolidone
PVP	Polyvinylpyrrolidone
PL	Photoluminescence
SA	Saturable absorber
CNT	Carbon nanotube
MWNTs	Multi Walled Carbon Nanotubes
1D	One dimensional
DC	Direct current
CVD	Chemical vapor deposition
CoMoCAT	Synthesis of SWNT
HiPco	Synthesis of SWNT
LA	Laser ablation
SDS	Sodium dodecyl sulphate
SDBS	Sodium dodecylbenzenesulfonate
AFM	Atomic force microscopy
SC	Sodium cholate
DUG	Ultracentrifugation
DNA	Deoxyribonucleic acid
DOC	Deoxycholic acid
TDOC	Taurodeoxycholic acid
DMF	Dimethylformamide

RBM	Radial breathing mode
EET	Exciton energy transfer
SBM	polystyrene-block-polybutadiene-block-poly(methyl methacrylate)
SESAMs	Semiconductor saturable absorber mirrors
PA	Photoacoustic imaging
MRI	Magnetic resonance imaging
SWeNTCG	Carbon nanotubes product
NaI	Sodium iodide
CNM	Carbon nanomaterials
PDs	Polymethine dyes
Cy3	Cyanin dye
FWHM	Full width half maximum
IL	Initial loss
PDL	Polarization dependent loss
PVA	Polyvinyl alcohol
EDFL	Erbium doped fibre laser
HML	Harmonic mode locking
NPR	Nonlinear polarization rotation
OIS	Fibre Optic Isolator
LD	Laser diode
WDM	Wavelength division multiplexing
PC	Polarization controller
FLF	Fober Lyot filter
IWDM	Integrated a wavelength division multiplexer with built-in optical isolator

PM	Polarization maintaining
NPE	Nonlinear polarization evolution
ND	Number density of state (density of states in the saturable absorber)

Symbols

α	Chiral angle
a	Carbon-carbon bond length
d	Diameter of tube
Io	Initial intensity of incident light
I	Intensity of incident light
T	Transmittance
A	Absorbance
ε	Absorption coefficient
c	Concentration
L	Optical path length through the medium
ϑ_{RBM}	Frequency for vibrational mode
$\alpha(I)$	Absorption coefficient at the at the intensity *I*
α_0	linear absorption coefficients
I_s	Saturation intensity
g (r)	Ion–NMP radial distribution functions
α_{ns}	Nonsaturable absorption
σ_A	Saturable absorber cross-section
F_{sat}	Saturation fluence
τ_A	Recovery time

List of Figures

List of Tables

Chapter 1

1. Introduction

Rapid development of nanomaterial has resulted in the creation of a unique platform for new research and industrial applications. Reducing the size of materials to nanoscale causes new physical and chemical properties to appear which are unavailable in bulk materials. Carbon is a versatile chemical element, which is able to form various allotropes including graphite, diamond, fullerene and carbon nanotube (CNT). Those materials possess a wide range of mechanical, thermal and electronic properties making them important for current and future applications such as in composites, mechanics, solar cells and supercapacitors.

The aim of this research is to develop functionalized CNT and techniques for CNT bundle engineering with the purpose of achieving strong optical properties for applications in ultrafast photonics. The thesis comprises of five chapters. Chapter one gives a brief introduction to state-of-the-art properties of CNT from synthesis through functionalization to applications. In chapter 2, a new method for CNT bundle engineering through the salting out of CNTs in organic solvent in presented. Chapter 3 describes the development of new complexes of CNT-organic dye with enhancement of photoluminescence (PL). Chapter 4 shows how ultrashort pulse lasers can be mode-locked using CNTs. Chapter 5 contains an overall conclusion.

1.1 Carbon Nanotubes

Since the first observation in 1991 by Iijima [1], carbon nanotubes (CNT) have attracted considerable scholarly attention worldwide due to their unique thermal, mechanical and electronic properties. CNT is a one dimensional (1D) allotrope of carbon created by rolling up of graphene sheets and appears in the form of single-walled carbon nanotubes (SWNTs) and multi-walled carbon nanotubes (MWNTs). SWNTs can be semiconducting or metallic and have exceptional electrical and thermal conductivities and massive tensile strength [2]. SWNTs have a cylinder shell with one atom thickness and a small diameter approximately 0.8 – 1.4 nm and the tube length can be many thousands of times longer. In contrast MWNTs have a diameter up to 100nm and up to approximately 3 cm long. Due to the strong optical properties, SWNTs have potential use as near-infrared emitters and detectors, nonlinear optical switches, fluorescence sensors and bio-labels in biomedical applications. The electronic structure of SWNTs depends on the geometrical structure (tube diameter and chiral angle), and chirality (n,m) is used to specify a nanotube structure. A nanotube is referred to as zigzag if α = 0, armchair if α = 30° and chiral where 0 <α< 30°, as shown in Figure 1-1. The diameter of the tube is given by;

$$d = \frac{a}{\pi}\sqrt{n^2 + m^2 + nm} \qquad (1)$$

Where a is the carbon-carbon bond length and a = 0.249 nm [3].

The chiral angle of the CNT α is derived from measurement of n and m as follows;

$$\alpha = \tan^{-1}\left(\frac{\sqrt{3}m}{2n+m}\right) \qquad (2)$$

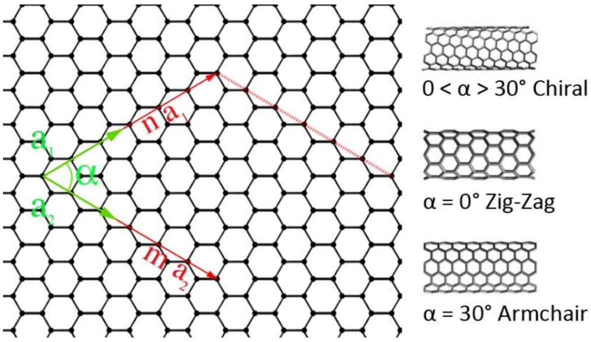

Figure 1-1 Construction of carbon nanotubes.

Semiconducting SWNTs have a direct energy band gap, which depend on tube diameter. Energies of the optical transition of SWNTs can be simply deduced from a Kataura plot [4] (Figure 1-2), showing the strong dependence of SWNT optical properties on chirality (n,m) of the CNT [4].

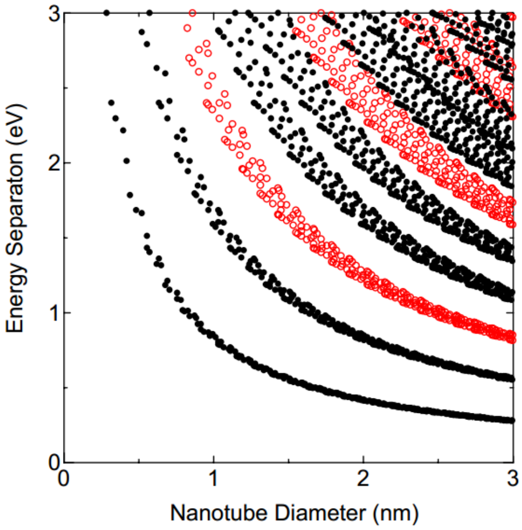

Figure 1-2 Kataura plot of the optical transition energies of single-walled carbon nanotubes. Reproduced with permission from [4].

1.2 Nanotube growth method and characterization

The unique mechanical and electronic properties and promise the potential for applications of both MWNTs and SWNTs have stimulated the search for production of CNTs in bulk amounts and with controllable parameters. The first observation of MWNT was reported in Japan by Prof Iijima in 1991 [1] and only two years later, Iijima and co-workers from the IBM Almaden Laboratory made experimental observation of SWNTs [3]. Due to advancements in various syntheses, and in purification and separation techniques, SWNTs and MWNTs can be currently produced in tonne quantities. Only the most common methods for synthesis of CNTs are reviewed here.

1.2.1 Arc discharge

Arc discharge is the easiest and most common way to produce CNT. A DC electric arc discharge is ignited between a pair of graphite electrodes in an inert gas atmosphere. The formation of MWNTs occurs due to hot gaseous carbon atoms being evaporated from the solid carbon electrodes. The formation of SWNTs requires the presence of a metallic catalyst in the arc system, and this method allows production of CNTs in gramme quantities. However, a complex mixture of carbon-based components is produced by this technique, and further purification is required for separation of CNTs from the soot and residual catalytic metals, present in the crude product.

1.2.2 Laser ablation

A high power laser pulses has been used for evaporation of carbon from a graphite target typically placed in high temperature oven with an argon atmosphere [6]. Both MWNTs and SWNTs can be produced by this technique. As in the case of arc method, the graphite target needs to be placed together with 50:50 catalyst mixtures of cobalt and nickel in order to produce SWNTs. The average nanotube diameter and diameter distribution can be controlled, by varying the growth temperature and size of catalyst particles [3].

Both laser ablation and the arc method produce CNTs in the form of powder and it is not possible to synthesize ordered CNTs on the substrate. Additionally, the laser ablation method requires expensive equipment and significant energy consumption. However the laser ablation SWNTs used in this work, have an extremely narrow diameter distribution with a central tube diameter of

1.186 – 1.789 nm which leads to controllable absorption bands in the 1400 – 2000 nm spectral range [3,7].

1.2.3 Chemical vapour deposition

Chemical vapour deposition (CVD) utilises a decomposition of gaseous carbon compounds over nanoparticle metal catalysts. This method has been used to produce various carbon nano-materials. Typically cobalt and iron catalysts deposited on silica or zeolite act as nucleation sites for initiation of CNT growth. The advantage of CVD is the possibility to grow of isolated nanotubes or a CNTs forest on different substrate in 10-100 gramme quantities.

SWNTs have been directly grown by CVD in a methane atmosphere on catalytically patterned substrates. Both of CoMoCaT and HiPco SWNTs are used in our research because offer strong optical properties in the near IR range (1000 - 1600 nm), a uniform diameter distribution with specific SWNTs chiralities, high purity [8,9] and they are process able into optical composites via simple methods [10]. Typically, HiPCO tubes show a broader diameter distribution when compared with CoMaCat and can be used for photonic applications in a broad spectral range [11].

1.3 Material and Methods for Preparation of SWNTs

Both commercial and in laboratory synthesized SWNTs are used in this research. The choice of tubes was predominantly conditioned by their optical properties in a specific spectral range. Those SWNTs have a strong optical absorption and PL in the range 1000 - 2000 nm, which corresponds to a typical diameter distribution of 0.9 - 1.4 nm. We understand as a “dispersion ability” of those materials, as an ability to disperse SWNTs within specific solvents or water-based solutions. Table 1-1 displays general information on methods of preparation, purity and diameter distribution within initial material [10].

Table 1-1 CNT material details of the properties and sources as used in this research.

CNT Product	Method	Purity	Diameter	Features
SWeNt CG100	CVD	≥70% (carbon as SWNT)	0.7 - 1.3 nm	• High purity • Uniform chiral distribution
SWeNt CG200	CVD	≥90% (carbon as SWNT)	0.7 - 1.4 nm	• High purity • Large diameter • High metallic tube content • High electrical conductivity
HiPco Pure	CVD	<15 wt%	0.8 - 1.2 nm	• Dry powder of nanotubes bundled in ropes
Laser Ablation	LA	Grown in scientific laboratory condition, raw	1 - 1.4 nm	• CNT paper and powder

In order to study the optical and electronic properties of SWNTs, samples need to be firstly dispersed in various solvents and then dispersed in polymer matrixes or deposited onto various substrates. The challenge here is the hydrophobic nature of SWNTs which leads to aggregation of SWNTs in water, whilst organic solvents have tenable same effects on SWNT electronic properties. For example in optics and photonics, SWNT bundles can act as quenchers for PL or can scatter light. Therefore, controlling the formation of large CNT bundles and their size is critically important for photonic applications [12]. The successful dispersion of individual carbon nanotubes and small bundle were achieved by wrapping of polymer or surrounding of surfactant micelles in solvent and water-based.

Researchers typically use ultra-sonication systems as shown in Figure 1-3, using approximately 20 KHz frequency range. In the first moments of exposure to ultrasound the CNT aggregate can be dispersed in the solution through breaking the Van der Waals attraction, dispersing single tubes and small bundles within the solvent. The presence of polymers or surfactant makes it possible to wrap or surround CNT with their molecules.

There are two types of sonication system. Figure 1-3 (a) shows direct sonication, so the waves are generated in a sample through a probe immersed directly into the solution. The power is delivered into the solution without any physical barriers and gives a higher effective energy output into the dispersion as shown in Figure 1-3 (a).

The second method uses indirect sonication. The sample container is immersed in a water bath through which ultrasonic waves are propagated. This second type system (NanoRuptor, Diagenode SA) was used in this study (Figure 1-3 (b)). There are advantages both systems related to the amount of energy, time, and direct contact of ultrasonic tip with dispersion. However, it has been suggested that indirect sonication helps to avoid making modifications and reduces the damage which is observed with direct sonication. Studies by Matarredona, Moor and Islam [13–15] have shown that, sonication time was a parameter determining quality of CNT dispersion, and an enhancement of the CNT suspension can be achieved by using a longer time of sonication procedure. However, in other studies, Yang and Hilding [16,17] observed that dispersion of CNTs mostly depended on sonication energy rather than sonication time.

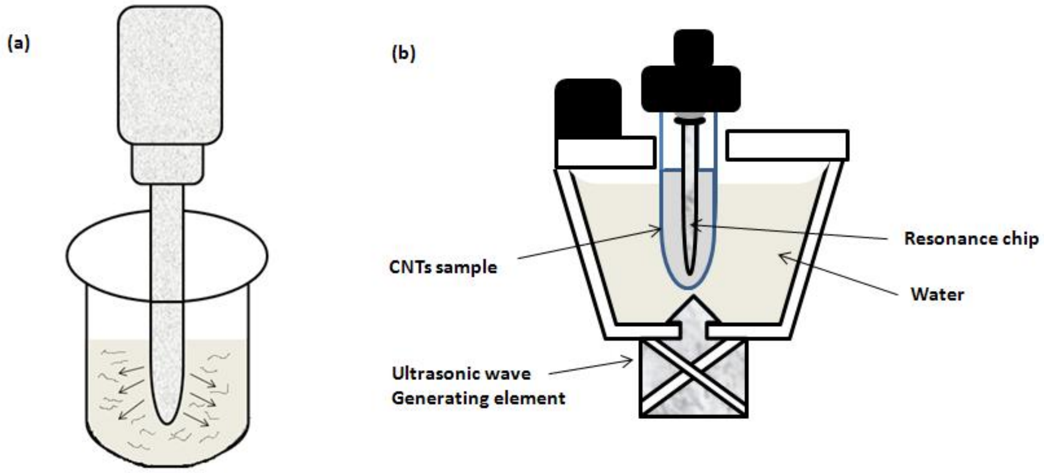

Figure 1-3 Ultrasonication system, (a) direct sonication (b) indirect sonication.

Although sonication allows dispersal of CNTs in various solvents, it is difficult to control the size of CNT bundles in the resulting dispersion. Therefore subsequent centrifugation and filtration is widely used to eliminate large CNT bundles and impurities remaining in solution [18].

SWNTs can be separated by using density differentiation via ultracentrifugation (DGU) as a function of diameter, which was demonstrated for the first time by Arnold and co-workers [18]. This technique depends on differences in response of various densities of material to centripetal force. The result of DGU on SWNTs in solution is a gradient separated by range of diameters. After centrifugation, SWNTs dispersions are separated layer by layer and each layer can be recognized visibly. For further separation of individual SWNT the intensity of ultracentrifugation can be increased [19], by increasing the number of revolutions per minute of rotor (rpm). Figure 1-4 shows samples with different revolution per minute which are started from low to high rpm. Sorting also depends on direction of DGU so it can be repeated multiple times to improve the sorting process. Ultracentrifugation with (Beckman Coulter Optima Max-XP, MLS 50 rotor) was used in this study to separate SWNTs with high quality results.

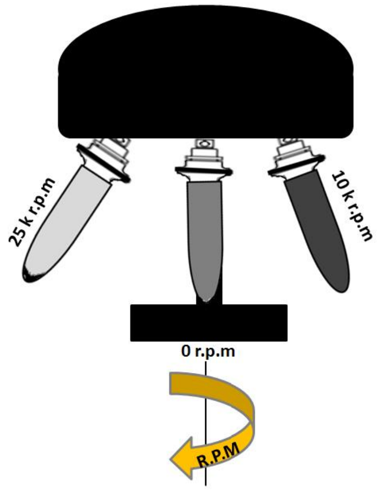

Figure 1-4 Ultracentrifugation holders.

1.4 Functionalizaion of carbon nanotubes

CNTs tend to form bundles or aggregates due to their relatively high surface energy [20]. Bundles of SWNTs as grown typically consist of mixtures of metallic and semiconducting nanotubes. Pure SWNTs, like graphene are strongly hydrophobic [21–24] and this is why pristine SWNTs cannot be dissolved in water directly and require additional surface modification (covalent or non-covalent functionalization) in order to disperse them in aqueous solutions or organic solvents [25,26].

Covalent functionalization modifies the structure of CNTs by chemical interactions. The advantage of covalent functionalization is the possibility of making the tube ends open, and increasing the solubility of these tubes [27]. However, the disadvantage of covalent functionalization is modification of the original structure of CNTs through introducing defects which may strongly affect the physical and electronic property of CNTs [26]. In order to utilise the advanced physical and chemical properties for applications in optoelectronics, researchers need to choose treatments, which will not affect the surface of SWNTs. The solution for this is non-covalent functionalization of SWNTs by chemical interaction with molecules of surfactants or wrapping polymers. The following sections describe those methods.

1.4.1 Surface functionalizaion of carbon nanotube in water

SWNT dispersions in aqueous media have been produced using ionic and nonionic surfactants [28]. Surfactants are chemical substances that tend to lower to the surface tension of liquids they are dissolved in. A surfactant molecule consists of two parts: a tail formed by hydrophobic groups and head part formed by hydrophilic groups. Depending on hydrophilic head polarity, surfactants can be classified as non-ionic, anionic, cationic, and amphoteric [29]. Variation of chemical structures of surfactants can result in formation of different types of aggregates such as spherical or cylindrical micelles or bilayers in water.

Introductions between CNTs and surfactants change the buoyant density by encapsulation of the CNTs (Figure 1-5) depending on tube diameter. The advantages of using surfactants are that nanotubes can disperse at high concentrations, surfactants are cheap and easy to use; and highly stable in water. Importantly, CNT electronic properties are mostly unmodified with surfactants [30].

Since Smalley and colleagues [11] demonstrated the sodium dodecyl sulphate (SDS) as an effective dispersion agent for solubility of SWNTs, many researchers have used a variety of anionic surfactants for dispersion of nanotubes in aqueous systems. Additionally, Smalley’s group demonstrated strong absorption and PL of SWNTs in water with narrow spectral bands corresponding to absorption and emission from single SWNT chiralities [11]. Later and Islam [15] showed that sodium dodecylbenzene sulfonate (SDBS) was even more efficient than SDS. By studying the morphology of the surfactant on CNT surface using atomic force microscopy (AFM), Islam and co-authors showed that SDBS efficiency is caused by the presence of hydrophobic alkyl interaction and π–π interaction between SDBS and SWNTs [15]. Importantly, this technique has increased the resolution of the SWNT band in the absorption spectra [14].

Arnold *et al*. [18] have reported a comparison between two different surfactants, SDS and SDBS with bile salt as sodium cholate (SC), which interact well with the SWNT surface. They demonstrated that SWNTs can be separated by means of tube diameter or by metallic or semiconductor type via density gradient ultracentrifugation (DGU). After centrifugation, SWNTs can be recognized optically in separated layers.

One of the advantages of centrifugation is that it can be repeated multiple times to improve the sorting process. For more separation of individual tubes of SWNTs the number of cycles of ultracentrifugation can be increased [18]. However, the resulting quantity of SWNTs produced is still very small and this prevents wide applications of SWNTs.

Finally, dispersion of CNTs in water has potential for use in biomedical applications and biophysical processing. However, many bio-applications of SWNTs require surfactant to be removed after the dispersion processes because of toxicity issues.

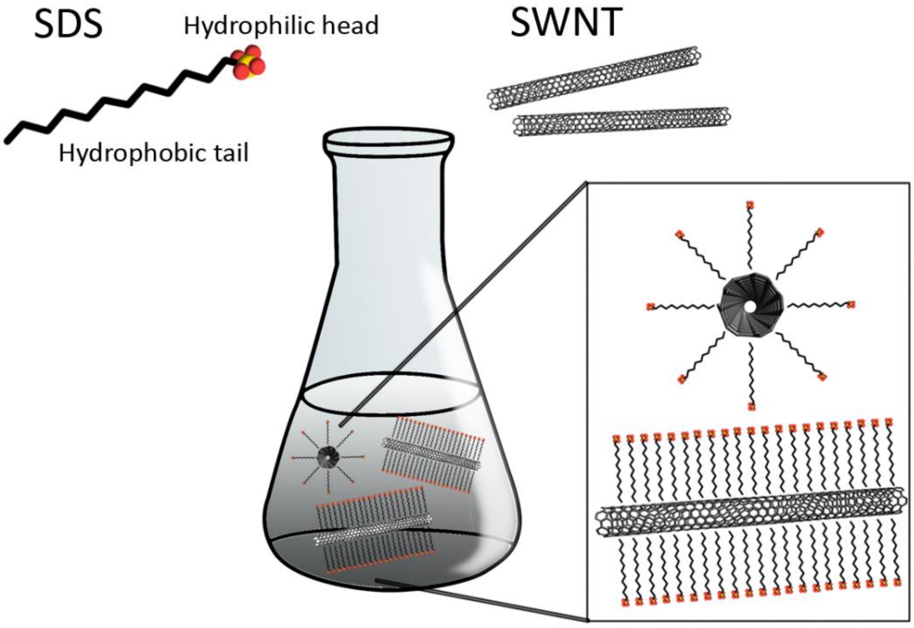

Figure 1-5 Schematic for surfactant (SDS) encapsulation of CNTs.

Polymers, such as polyvinylpyrrolidone (PVP), have been found to act as surfactant for CNTs dispersion in aqueous solution, As it shown in Figure 1-6, polymers wrap around CNTs, and these can remain homogeneous and stable in solution without any precipitation for a long time [31].

For the first time, Zhang *et al*. [32] discovered an ability of DNA molecules to disperse and separate SWNTs. DNA wrapping of nanotube sidewalls is attributed to the π-π interaction between aromatic bases of DNA and SWNTs. This process is promising for applications of CNT in the field of biotechnology [32].

In the research repeated here, the effects of both anionic (such as SDS, SDBS, deoxycholic acid (DOC) taurodeoxycholic acid (TDOC)) and non-ionic surfactants, such as Triton X-100 and PVP polymers were explored dispersing of SWNTs in water.

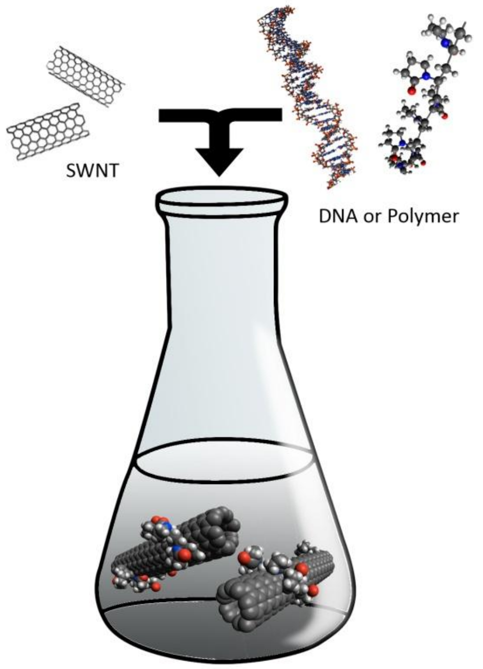

Figure 1-6 Schematic for wrapping polymers or DNA around the CNTs.

1.4.2 Surface functionalizaion of CNTs in organic solvents

The surface functionalization of SWNTs in organic solvents has attracted large attention these days, because some organic solvents can disperse significant amounts of CNTs without any modification of their surface and achieve stable dispersions. This opens up many attractive applications in polymer nano-composites, nano-fibres and electronic applications. Bahr *et al*. used different solvents and different concentrations at room temperature for solubility of the SWNT materials and argued that a type of solvent could have an effect on the dispersion of SWNTs by chemical derivatization. Those results proved that a range of common highly polar solvents such as dimethlformamide (DMF), and NMP are suitable for dispersion of SWNTs [33].

Later, Giordani et al. [22] demonstrated that SWNTs even can be thermodynamically de-bundled at small concentration to achieve isolated SWNTs in NMP solvents. Furthermore, solubilisation of SWNTs is useful for their chemical derivatizaton and demonstration of their photo-physical properties. To confirm the presence of individual nanotubes in N-methylpyrrolidinone the photoluminescence spectroscopy was used, showing that photoluminescence intensity of the bands with diameters distributions of single walled carbon nanotubes within the solvent and with concentration of the SWNTs [22]. These results are in good agreement with the results of Bahr and co-workers [33].

Later, Hasan and colleagues used PVP for the isolation of single walled nanotubes SWNTs in NMP [34]. They used ultrasonic treatment and then vacuum filtration by glass fibre filters to achieve the initial SWNTs dispersion. PVP was used to stabilize single walled nanotubes SWNTs in a liquid environment. The results show significant enhancement of dispersion stability over long periods of time, and high quality optical and electronic properties of the dispersion. They argued that addition of PVP is the major factor in debundling small aggregates of SWNTs, which lead to a drastic increase in intensity of SWNTs photoluminescence (PL). Furthermore, there is less or no effect of nonionic surfactants on stabilization of dispersed SWNTs in NMP. However, the amount of nanotubes dispersed in NMP with a non-ionic surfactant is higher than for SWNTs dispersed in pure NMP but the dispersion is not stable over a period of time [34].

There are several challenges in the development and application of SWNTs for photonic applications, which were a focus of this study

- SWNTs dispersion must be stable over a long period time;
- the possibility of SWNTs bundle engineering is necessary in order to enhance the optical properties of SWNTs
- the creation of novel macromolecular complexes with SWNTs in order to enhanced optical properties
- novel laser applications with SWNTs saturable absorbers.

1.5 Characterisation methods

Absorption spectroscopy, PL spectroscopy, and micro Raman spectroscopy have been used for recognition and characterisation of SWNT. Each individual SWNT shows chirality and small SWNT bundles possess a range of the unique optical properties. The following sections will give a brief overview of characterisation methods used in this research.

1.5.1 Absorption spectroscopy

Since the first demonstration by Kataura and co-authors [4], absorption spectroscopy has been widely used as a tool to identify the presence of isolated SWNTs or SWNT bundles within liquid dispersion or composites. In the simplest case, light transmission through the sample leads to oscillations of electrons under the field of the electro-magnetic wave and attended by reducing of energy of that wave. The process is the absorption of energy of the electromagnetic wave. Part of the absorbed energy is re-emitted as secondary waves generated by oscillating electrons or is transformed into other forms of energy.

An absorption spectrum presents the intensity of absorbed energy by the sample as a function of frequency or wavelength. In general molecules can absorb light in all optical ranges from ultraviolet to far infrared. The absorbance is directly proportional to the light path length and the concentration of absorbing molecules. The ratio between the intensity of incident light (I) passing through the medium to the intensity of light after passing through the medium (Io) is given as percent transmittance (%T), absorbance (A) is given by the equation:

$$A = \log_{10} \mathrm{I}/\mathrm{Io} \qquad (3)$$

Transmittance, T = I / Io

% Transmittance, %T = 100 T

The absorbance is used to determine the concentration by using the Beer Lambert law:

$$A = \alpha\, c\, L \qquad (4)$$

Where α is the absorption coefficient, c is concentration and L the optical path length through the medium.

Figure 1-7 shows a schematic diagram of a double beam spectrophotometer. The light sources are a tungsten, and deuterium lamps to cover the range from ultraviolet through visible light to mid-infrared. A double monochromator and triple detector system (PMT, InGaAs, and PbS) give a capability for testing across the entire range from 175 nm to 3300 nm. The double beam configuration allows to measure both a sample and a reference sample same time, excluding the contribution of polymer matrix, solvent, or glass/silica substrate on the absorption/transmission properties of analysed substance. By controlling the acquisition time and spectrometer’s slits, the highly sensitive spectra with high resolution can be measured with the system.

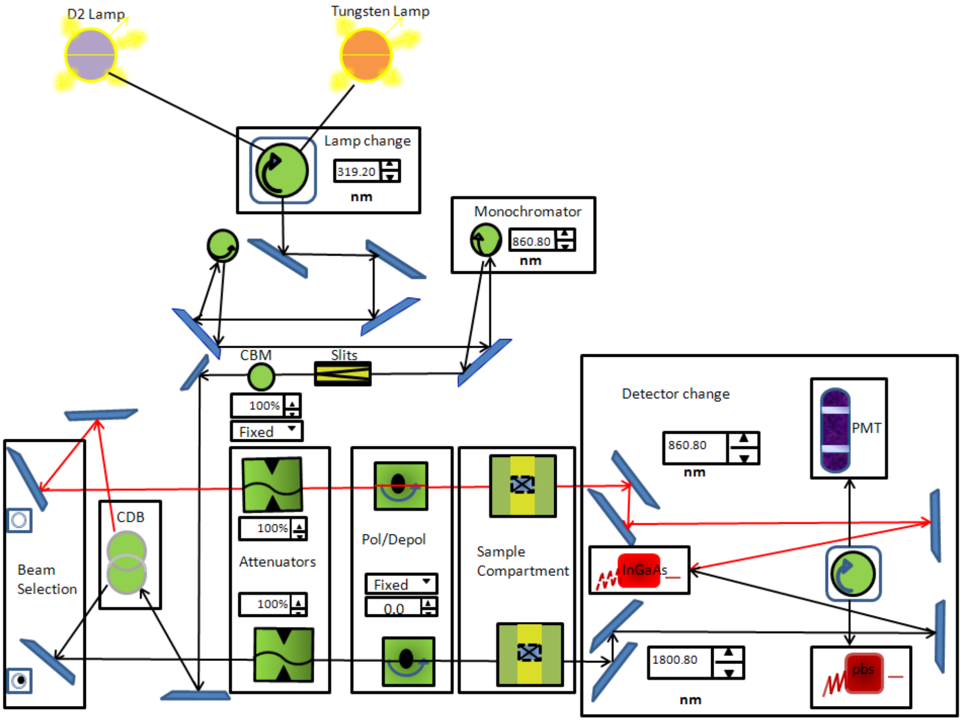

Figure 1-7 Schematic diagram of double-beam spectrophotometer.

Optical absorption spectra of SWNTs in this research were measured using a Perkin Elmer Lambda 1050 UV-NIR spectrometer.

1.5.2 Photoluminescence spectroscopy

Photoluminescence spectroscopy characterizes the phenomenon of spontaneous light emission from gas, liquid or solid matter after electronic absorption of photons (light). Depending on the timing of the emission, the process can be defined as fluorescence (10^{-9} - 10^{-7} s) or phosphorescence (10^{-6} - 10^{3} s). Fluorescence stops almost immediately after excitation finishes, while phosphorescence continues for up to 10^{3} s after termination of electronic excitation (absorption of light). Vibration relaxation occurs when the excited state returns to the electronic ground state. The excess of vibrational energy is transferred to the surrounding matter through collision with other molecules or thermalization of large molecules, as described in Figure 1-8.

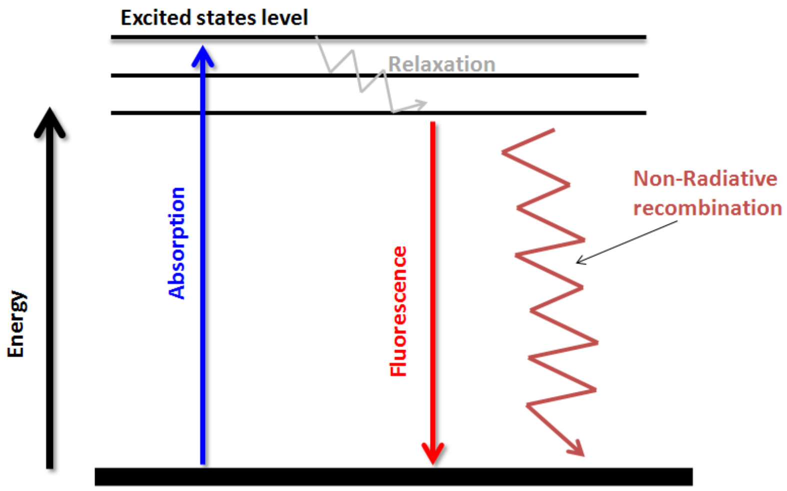

Figure 1-8 Physical processes following absorption of a photon by a molecule.

A schematic of the principles of the Horiba Nano Log excitation–emission spectrofluorometer, which was used in our work, is given in Figure 1-9. This spectrometer is equipped with a light source, a double monochromator for excitation of light, a sample compartment, emission monochromator, (photo multiplier tube) PMT detector and the nitrogen cooled InGaAs array detector. This system allows acquisition of photoluminescence exaction-emission maps, which will be discussed in section 1-6-3.

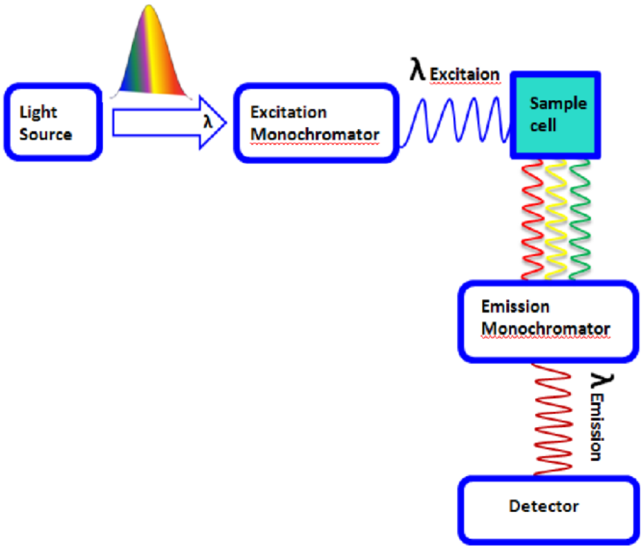

Figure 1-9 Schematic diagram of the principle of PL spectroscopy.

1.5.3 Raman spectroscopy

Raman spectroscopy is a technique used for investigating of vibrational and rotational energy levels of molecules. It is based on the theory of inelastic scattering of light by matter. Figure 1-10 shows a diagram of a Raman spectroscopy system. The experimental technique regimes three stages: a laser-light source, a monochromator coupled with a detector such as charge-coupled devices (CCDs) or other forms of array detector and optical microscopy. The sample is exposed to illumination with monochromatic light, a spectrometer is used to examine light scattered by the sample.

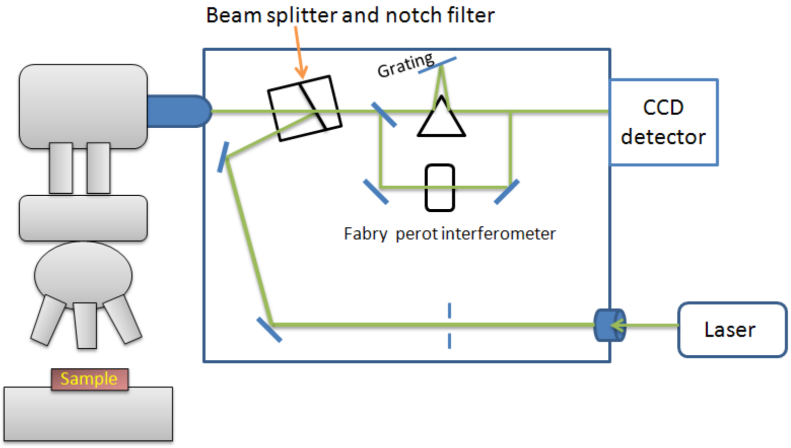

Figure 1-10 Schematic diagram of a Raman spectrometer.

Raman spectroscopy is the best non-destructive method for characterisation of the carbon nano-materials, because it allows to respect their diameters and quality of the samples properties [38].

1.6 CNT for photonics

The strong optical properties of SWNTs offer a huge promise for various applications [12]. Applications such as optical sensors and bio- imaging could be based on photoluminescence and Raman phenomena and ultra-fast optical switches could be based on the nonlinear optical effects. Importantly, SWNT-based photonic devices could be developed in the spectral range of 1000-2000 nm, which completely cover the telecommunications window (1300 – 1600 nm), the therapeutic window (800 -1300 nm) and a range of absorption of many gas molecules (around 1600 nm and

2000 nm) which could lead to many applications in telecommunications and healthcare. In the following section optical and nonlinear optical properties of SWNTs are reviewed.

1.6.1 Optical absorption spectroscopy

Since the first observation of optical absorption from SWNTs by H. Kataura and co-workers [6], the method has attracted considerable attention from researchers due to the simplicity of preparation of samples and of analysis or results. Generally, SWNTs show strong absorption in the ultraviolet through visible to near infrared spectra region. Three groups of transitions are seen, referred to as E_{11} or S_{11} the lowest allowing transition of semiconducting SWNTs, E_{22} or S_{22} the second allowing transition of semiconducting SWNTs, and M_{11} the peak corresponding to metallic SWNTs [11]. The spectral positions of the absorption bands are depicted in Figure 1-11 and the corresponding transitions of semiconducting SWNTs will show in section 1.6.3.

Typically the absorption bands corresponding to both semiconducting and metallic SWNTs are broadened due to a presence of ensemble of SWNTs with different (n,m) chiralties. Thus, the peak position and its width can provide the information on CNT diameter distribution within the sample. The absorption band intensity will give of relative information about the concentration of CNTs with a specific diameter. The ratio of intensities of S_{11} to M_{11} bands will approximate the ratio of metallic and semiconducting carbon nanotubes [35]. Finally, the broadening of absorption bands and their shift will give information on bundling and interaction with other materials such as polymers and surfactants. The important point regarding optical applications of SWNTs is that absorption of SWNTs totally covers the telecommunications window 1300 – 1600 nm [36] (Figure 1-11), and a number of applications have already been demonstrated with SWNTs coupled with fibre optics systems [12,37].

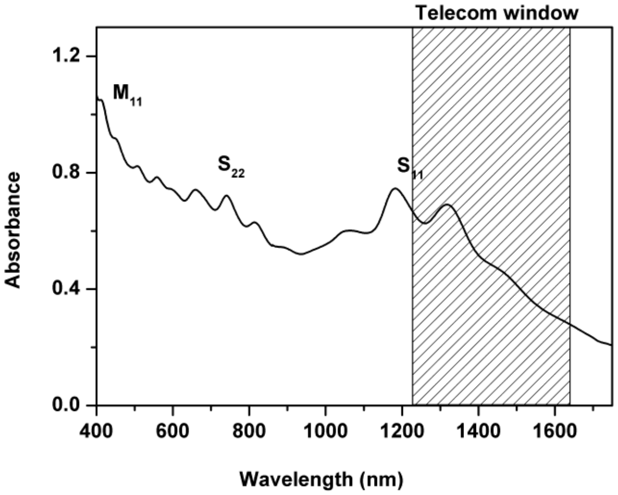

Figure 1-11 Absorption spectrums for SWNTs in telecommunications range.

1.6.2 Raman spectroscopy for photonics

Raman spectroscopy is a powerful and non-destructive technique when applied for detection and characterisation of isolated nanotubes and in bulk samples [38]. It is an essential tool for the identification of the diameter and chirality of individual and bundled SWNTs and is typically used at room temperature and at ambient pressure. Figure 1-12 shows typical Raman spectra for semiconducting SWNTs which consist of 4 major bands: radial breathing mode (RBM), D-band, G-band and G', which are explained as follows.

RBM is a symmetric vibrational mode caused by vibration of C atoms in a radial direction in respect to the SWNT axis. The position of RBM peaks is directly related to the diameter of SWNTs and can be resonantly enhanced at specific laser wavelengths. Furthermore RBM is a unique phonon mode for SWNTs, and therefore it is very useful for determination of the presence of SWNTs within the sample. The diameter of the tube d is shown through the frequency ϑ_{RBM} of the peak as:

$$\vartheta_{RBM} = {}^{A}/_{d} + B \qquad (5)$$

Where, A and B are coefficients, with values strongly dependent on the way SWNTs examined: on the silica dioxide substrate, freestanding powder and in liquid solution [2]. The D-band a feature observed between 1300 and 1400 cm^{-1} in Raman spectra is assigned to disordered graphitic materials and usually connected with the presence of defects (impurities or missing atoms) in CNTs, or molecules linked to CNT side-walls.

The G-band is a group of peaks in the approximate range 1580–1605 cm^{-1}. In case of graphite, the G-band exhibits a single peak at 1582 cm^{-1}, related to tangential mode vibrations of the C atoms. The shape of the G-band differs for metallic and semiconducting tubes. Also the shift of the position of the G-band can be used for interpretation of energy transfer in SWNTs composites.

The G′-band is the frequency of the second order overtone of the defect-induced D-band at around 2600 cm^{-1}. Recently, the G′-band has become very important for characterisation of single and multi-layered graphene.

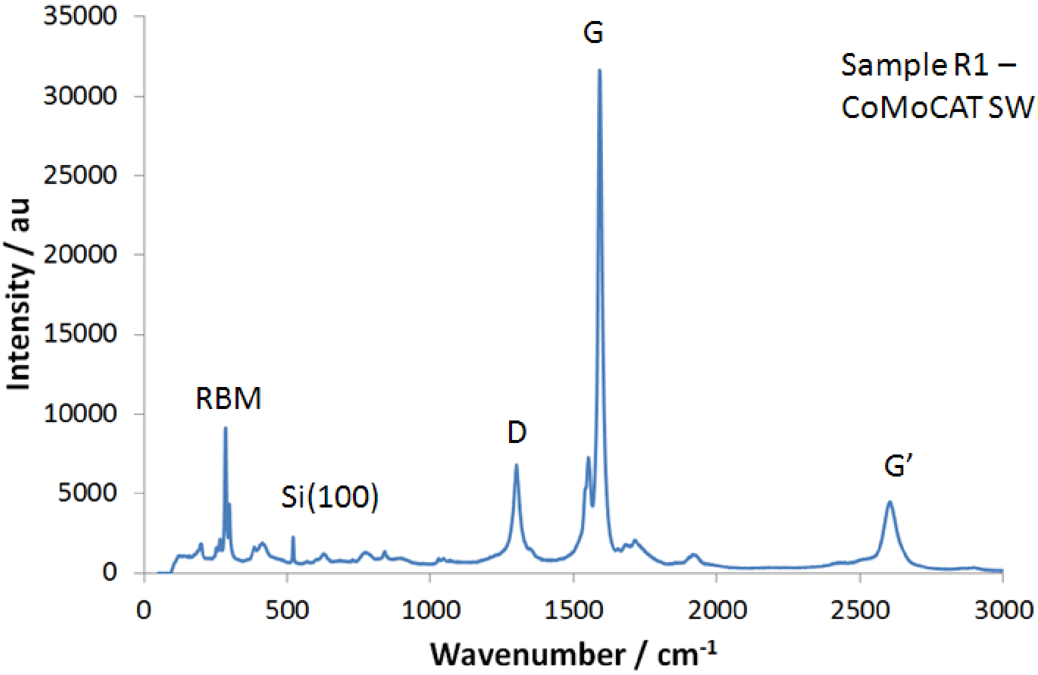

Figure 1-12 Raman spectra for metallic and semiconducting SWNTs.

1.6.3 Photoluminescence spectroscopy of SWNTs

Photoluminescence (PL) has been found useful as on optical technique to investigate the properties of single walled carbon nanotubes SWNTs, because the electronic and optical properties of nanotubes are directly related to the structure of the tubes. That means absorption and emission energies are directly related to nanotube diameter and chirality. Initially, a simple model for PL was proposed as it shown in Figure 1-13 [11]. The photons were absorbed in E_{22} transitions as shown with an upward-pointing arrow. After fast non-radiative relaxation from E_{22} toE_{11}, the fluorescence emission appears from E_{11} energy levels as shown with a downward-pointing arrow in Figure 1-13 [11].

In the first demonstration of SWNTs PL by O'Connell *et al* [39], the SWNTs PL was observed in the near-IR spectral range, which is important for bio-imaging and telecommunications applications. Those researchers succeeded in isolating single SWNTs or small SWNT bundles with a surfactant in aqueous solution. Bachilo *et al* [11] reported fluorescence intensity versus excitation and emission wavelengths for SWNTs which it is suspended in air. They found that the optical transition was related to the diameter and structure of semiconducting-SWNTs. Figure 1-14 shows a PL excitation map for a sample of SWNTs suspended in SDS and deuterium oxide. The bright spots correspond to specific chiralities of SWNTs, and the high intensities PL is shown in red, and low intensities in blue [11].

Their initial conclusion was that PL is quenched by aggregation of the tubes, because the large bundles comprises a metallic SWNT adjacent to a semiconducting tube, causing the efficient quenching of PL [39]. In 2005 the exciton of PL in SWNTs was revealed by using two-photon PL excitation spectroscopy [40] and the exciton of PL in SWNTs is now commonly accepted in nanotubes photonics [2].

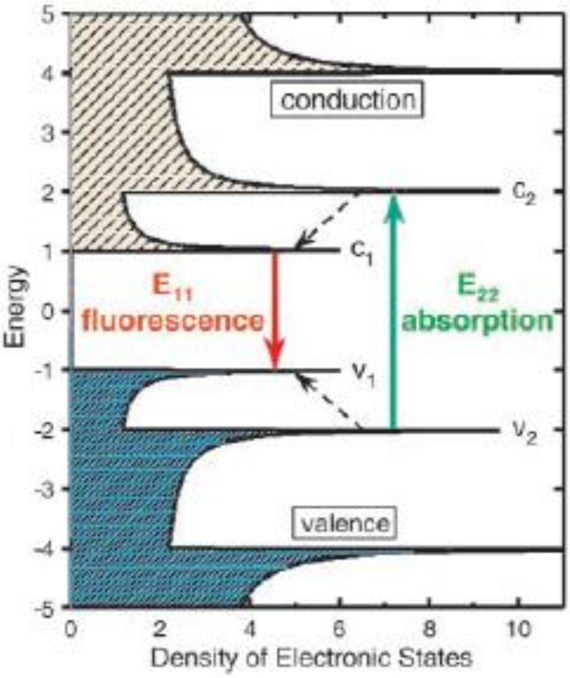

Figure 1-13 Single nanotube structure of density electronic states. [11] Reprinted with permission from AAAS

Moreover, the work of Tan and colleagues investigated excitation energy transfer processes in SWNTs bundles. Importantly, SWNT bundles remain in the water dispersion even after strong ultracentrifugation of the solution. The spectra of absorption and emission broadened, and PL peak intensities reduced, with the ageing of SWNTs solutions. However, new PL features appear on the PL map, which do not coincides with the PL features of known chiralities. Investigations of PL excitation in nanotube bundles show that, there is an exciton energy transfer (EET) between neighbouring semiconducting tubes. The efficiency of EET depends on the SWNT bundle size, and can be observed from optical absorption and emission spectra. The EET appears when a SWNT with a large band gap act as a donor and an adjacent SWNT with smaller diameter acts as an acceptor for electronic excitation. The PL Spectra have resonant features corresponding to different (n,m) chrialities of individual semiconducting SWNTs or to resonant excitation transfer in SWNTs bundles [41].

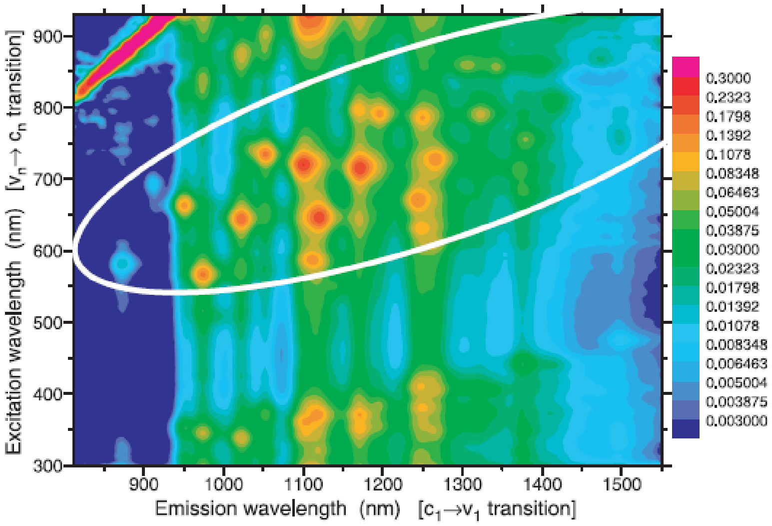

Figure 1-14 Plot of fluorescence intensity. [11] Reprinted with permission from AAAS

Additionally, PL indicates a dielectric screening of the SWNT surface by the surrounding media [42].

There are a number of uncertainties remaining around PL from SWNTs. How can the quantum yield of PL be enhanced; how can EET within the solution be controlled; what contribution SWNTs defects play in PL processes; and how to build the efficient molecular complexes with SWNTs having the enhanced PL. These challenges are addressed in chapters 2 and 3.

1.7 Photonic applications of carbon nanotubes

One dimension (1D) and the single atomic layer structure cause the unique optical properties of SWNTs, which is sensitive to their environment and external surface effects. Since 2002, when PL [39] and sub-picosecond non-radiative recombination dynamics [43,44] from SWNTs were demonstrated, this field has attracted the attention of many research groups world-wide without any signs of saturation [12]. Moreover, graphene application for photonics have been a logical spin-out from nanotube photonics [45].

The SWNTs in suspensions or polymer composites have been used as Saturable Absorbers (SA) for the near-infrared spectral range. Importantly, SWNTs possess ultrafast relaxation and as result it is possible to realise an ultrafast optical switch and loss modulator on this SWNTs - bases. In the simplest case, the saturable absorption behaviour can be described as follows [46]:

$$\alpha(I) = \frac{\alpha_0}{1 + I/I_s} + \alpha_{ns} \qquad (6)$$

Where $\alpha(I)$ and α_0 is dependent on light intensity I and on linear absorption coefficient respectively, I_s saturation intensity and α_{ns} is nonsaturable absorption component.

In this case, laser light is absorbed by SWNTs with a band gap, which resonantly matches the energy of the laser light. As a result of the initial carrier excitation, absorption can saturate and SWNTs remain transparent. Moreover, SWNTs show ultrafast absorption recovery time due to CNT intrinsic electronic properties [36]. Thus, the new absorption and recovery cycle will begin in a picosecond time scale. Additionally, the saturable absorber properties of SWNTs can be significantly enhanced by selection of tubes with proper diameter and by bundle engineering of SWNTs. Saturable absorption in the near IR range (1000 - 2000 nm) can be achieved by selection of tubes with diameter between 0.8 to 1.4 nm [7,12].

Based on these SWNTs properties, saturable absorbers have been used in ultrafast photonics as mode-lockers to generate ultra-short laser pulses and as switching devices in fibre optic telecommunications systems. Fibre, solid-state, and semiconductor lasers have been successfully mode-locked by SWNT saturable absorbers since initial demonstration in 2003. SWNT-based mode lockers usually appear in 3 different types: SWNT dispersions [46], SWNT polymer composites [36] and grown SWNTs forests [47].

In addition SWNTs SA has been used for Amplified Spontaneous Noise suppression [7]. Usually, semiconductor-saturable absorbing mirrors (SESAMs) are used as a mode locker in diode pumped solid state laser systems [48]. The advantages of CNTs as saturable absorbers are first, these are simple and cheap, and second, easer to fabricate and integrate into optical fibres for communication systems than SESAM. Additionally, CNTs may have a number of applications in photonics including nanometre-scale light sources, photodetectors and photovoltaic devices [49].

Finally, SWNTs can be used in near infrared fluorescent imaging due to deep tissue penetration through reduced scattering of photon in the near infrared region (700 – 900 nm) [50]. SWNT bio-imaging probes have even higher sensitivity with Raman imaging. Moreover, SWNTs can be used in other imaging techniques such as Photoacoustic (PA) imaging, Magnetic resonance (MR) imaging and nuclear imaging. The use of SWNTs as on imaging probe with multiple functionalities could make it of great importance in biomedical imaging [52].

Chapter 2

2. SWNTs Bundles Engineering

Liquid dispersions of carbon nanomaterials (CNM), and in particular, CNTs are currently a subject of intensive research due to their wide areas of application. Single walled carbon nanotubes (SWNTs) have many interesting and versatile physical properties. Aqueous dispersions of SWNTs are important for many applications in photonics, biological and environmental sensing, drug delivery, and bioimaging [53]. The aim in this study is to prepare and develop SWNTs in organic solvent, because such solutions offer key advantages such as photoluminescence for fluorescence imaging [50], sensors and biosensors [54]. However, PL is quenched by the presence of metallic SWNTs and increases for isolated tubes and small bundle sizes [39]. Furthermore, organic solutions are starting points for preparation of CNT-based of composites with promise for applications such as conductive polymers, reinforcement composites, and composites with electrical conductivity, on photonic or thermal properties. Subsequently, SWNTs solution and composite are thus suitable for photonic applications as saturable absorbers in passively mode-locked lasers [12] noise suppression filters in telecom systems. Ultrafast absorption recovery has been shown in SWNTs in time range 10 to 100 ps in isolated SWNTs and less than 1 ps in SWNT bundles [7]. Thus, bundle engineering of SWNTs is very important in ultrafast photonics [12] and bio-imaging applications [55,56] due to the advantages of controlling the recovery time with extraordinary promise to use as a saturable absorber in mode locked fibre and solid state lasers, and in biomedical application with time resolved luminescence characterisation.

2.1 Study of liquid dispersion of SWNTs in NMP

The following is a comprehensive study of liquid dispersions of SWNTs (SWeNt CG100)) in organic solvent N-methyl-2-pryrrolidone (NMP). NMP has been demonstrated as an efficient organic solvent for dispersion of single wall carbon nanotubes (SWNT) [57] and the aim of this experiment was to made stable dispersion of pristine CNTs. However, CNT-NMP dispersion contains mixtures of metallic and semiconducting CNTs with a wide range of diameter distributions. Thus, to efficiently exploit the properties of certain CNT chirality, the mixture must be separated to isolate the correct chiral compound. Importantly, Giaordani and co-authors [22] achieved a thermodynamically stable dispersion of SWNTs in NMP solvent by “de-bundling” of SWNTs in pure NMP at a concentration below 0.02 mg/ml [22]. Therefore, a stable dispersion can be achieved in low concentration dispersion to minimize the van der Waals interactions. This limited concentration ratio is a disadvantage for this method.

2.1.1 Experimental methods and Preparation

Purified single wall CNTs (SWeNt CG100) were used as pristine materials in this experiment. CNTs dispersed in NMP at two different concentrations 0.01 mg /ml and 0.0165 mg/ml by ultrasonication for 1 h at 21 kHz and 250 W. Then the dispersion was subjected to ultracentrifugation for 2 h 30 min at 47 000 rpm at 17 ^{0}C.

2.1.2 Results and Discussion

NMP has a high potential to solubilize SWNTs and graphene individually in organic solutions [58,59]. SWNT-NMP solutions show strong optical properties, and the distribution of the diameters of SWNTs included in the SWNT-NMP solution can be measured by optical absorption spectra. Figure 2-1 shows semiconducting SWNTs with diameters 0.7-1.3 nm and the absorption features around 950-1400 nm correspond to the S_{11} excitonic transitions of the chrialities (6,5),(7,5),(7,6), (8,6), (8,7) and (9,7) while the isolate tube and features around 550-750 nm correspond to the S_{22} excitonic transitions. The metallic SWNTs can be found in M_{11} which has exciton transition around 400-550 nm.

Furthermore, the optical spectra contained SWNTs having (6,5), (7,5), and (7,6) indices, each chirality corresponding to a given SWNT species with a specific diameter. As shown in the Figure 2-1, comparing the optical absorption spectra of the SWNT-NMP dispersion using two different concentrations, considerably different absorption spectra are obtained depending on concentrations of SWNTs in the solution and there is an immediate effect of high concentration on the optical absorption. The spectrum for both samples still show strong absorption at 1000-1300 nm, which is due to the presence of SWNTs with diameter distribution 0.7-1.3 nm [4]. The absorption spectra have the NMP solvent background subtracted

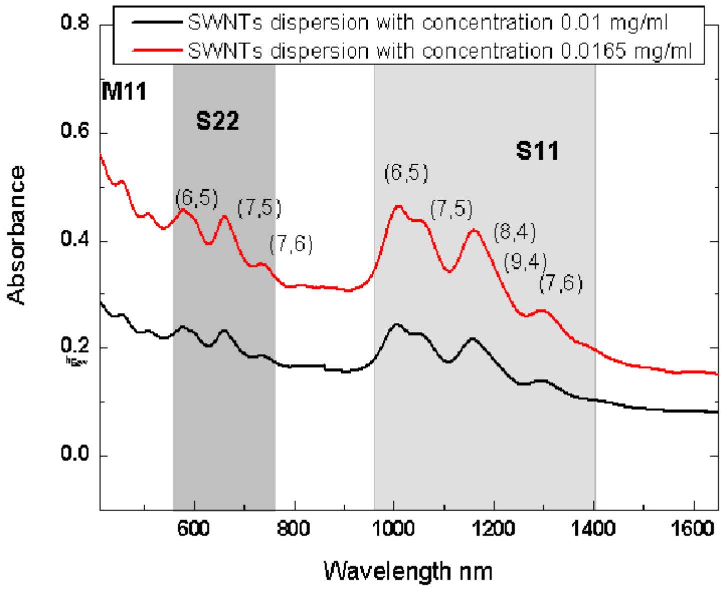

Figure 2-1 Absorption spectra of SWNT-NMP dispersion at different concentrations, with excitonic transitions highlighted (M_{11}, S_{11} and S_{22}).

Figure 2-2 shows a typical PLE map of individually isolated semiconducting or small bundle SWNTs in dispersion. Several peaks can be clearly seen. The major PL peaks is seen at around 400-800 nm excitation and 950 – 1350 nm emission range. This range covers most of (CoMoCAT 100) SWNTs, which was used as the material for preparation of SWNTs solution in this experiment. Also the PL shows the chiralities present in the sample solution such as (6,5), (7, 5),(8,4), (7,3), (8,3) and (7, 6). The peaks intensities are plotted as a function of emission and excitation energies.

Additionally, PL gives information whether the tubes in solution are isolated or bundled [41] and indicates a dielectric screening of the SWNT surface by surrounded media [42]. The PL emission in this spectral range is due to the presence of isolated semiconducting SWNTs of different chiralities or from small SWNT bundles. The PL map of pure CNTs–NMP solution shows strong and high photoluminescence (PL) signal intensities. In addition, the sample with high concentration of SWNTs shows high PL intensity for isolated tubes and small bundle.

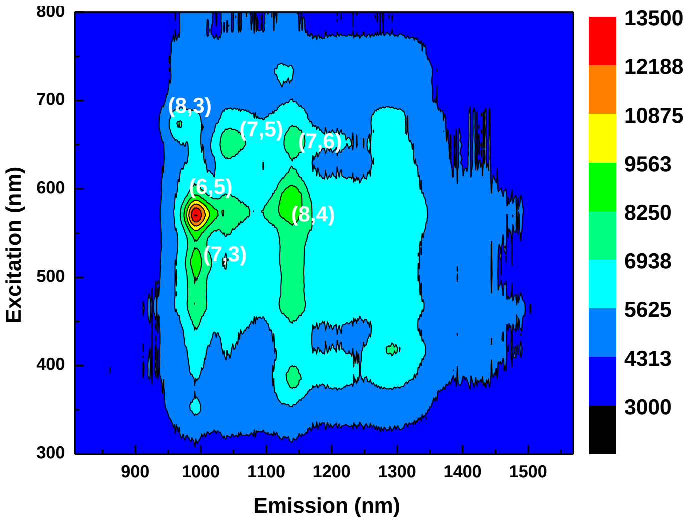

Figure 2-2 Photoluminescence map of the SWNT-NMP solution.

The PL intensity measurements for the stability study are taken at 570 nm excitation. Figure 2-3 shows the intensities of the bands indicating the presence of SWNTs predominantly including (6,5), (7,5), (8,4) and small bundles (8,7) and (9,7). The peak for individual tubes is narrow whereas those for small bundles are broad. Comparison between intensity of the peaks for isolated tubes (6,5) at different SWNTs concentrations indicates that the sample with high SWNT concentration emits at higher intensity than the sample with low SWNT concentration. Furthermore, there is no difference between the peaks intensities for small bundle.

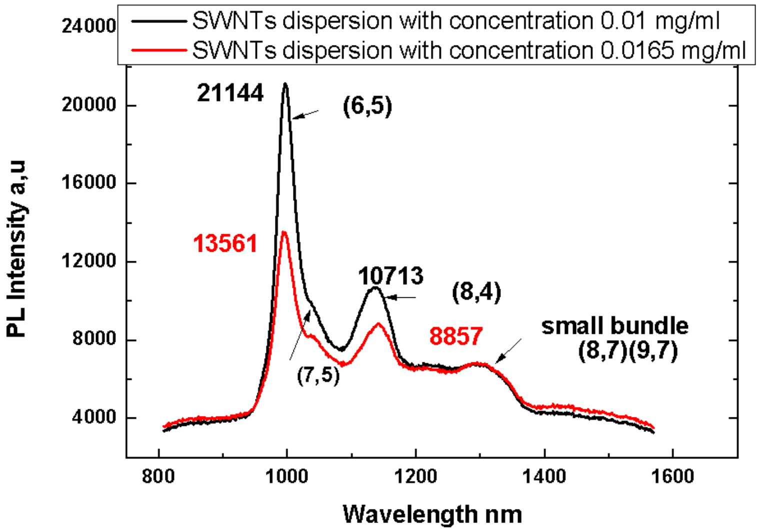

Figure 2-3 PL spectra of the SWNTs dispersion at 0.0165 mg/ml and 0.01 mg/ml concentrations at excitation wavelength 570 nm.

2.2 CNT-NMP-PVP

To prepare stable dispersions of SWNTs with different concentration ratio in NMP it was necessary to add additional agents. Polymers can efficiently be used as dispersing agents for SWNTs in both aqueous [60] and non-aqueous media [61]. In this study SWNTs-NMP dispersion with addition PVP polymer was achieved at low and high concentrations. The result shows that PL intensity increased comparable with the pure SWNTs–NMP at same concentration. Moreover, PVP polymer makes SWNT–NMP solutions more stable without any visible aggregation and homogeneous dispersion is maintained for a long time [34].

The purpose of this dispersion is for use as a stable solution which will subsequently be mixed with sodium iodide, which will be discussed in section 2-4.

2.2.1 Experimental methods and Preparation

Two samples were prepared at the same initial concentration of CNT-NMP (0.014 mg/ml), and then two different quantities of PVP, 6 mg and 33 mg respectively which was added to each sample before ultrasonic treatment. Both samples were sonicated for 1 h at 21 kHz and 250 W. After the ultrasonic treatment, the samples were subjected to ultracentrifugation for 2 h 30 min at 47 000 rpm at 17 ^{0}C .

2.2.2 Results and Discussion

The presence of isolated SWNTs or small bundles were determined by PL mapping. Figure 2-4 shows maps of the SWNTs dispersed by PVP polymer in NMP solvent, fig 2-4 (a) PL shows map for the sample with low concentration of PVP (6 mg), and Figure 2-4 (b) is shows the PL map for the sample with high concentration of PVP (33 mg). There is a small difference in the PL intensities in the (a) and (b) maps, even through the initial SWNTs concentrations are the same in both of them. It is difficult to control the finial concentration of SWNTs in the dispersion, due to the centrifugation process [18]. PVP polymer is thought to wrap around the SWNTs [34], and increases is the concentration of PVP polymer is thought to favour single SWNTs over bundles, due to the wrapping of polymer around tubes make to keep the surface of the tube more isolated with the surface of other tubes, and this assist to do not de-bundle again. For this reason the PL intensity in the Figure 2-4 (b) is higher than the PL intensity in the Figure (a), and there is more isolated tubes in the solution. Furthermore, the solution with PVP polymer is more stable than SWNT dispersion in pure NMP.

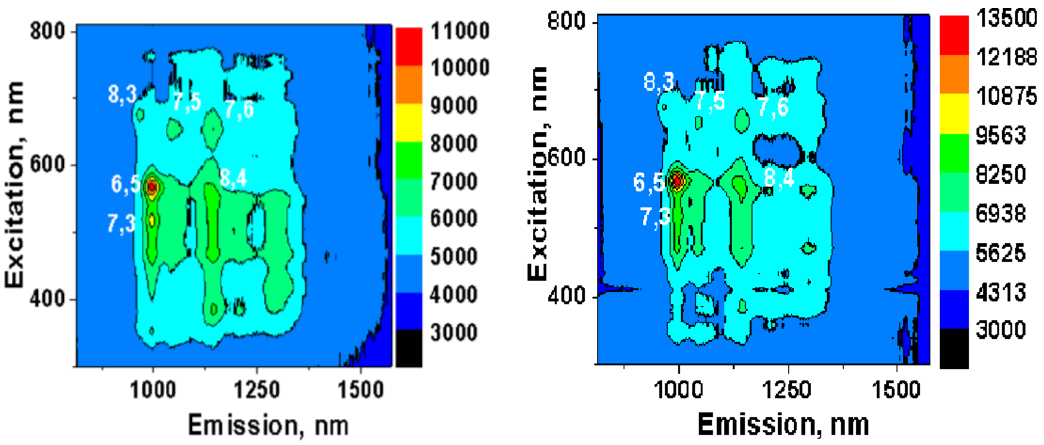

Figure 2-4 PL maps for SWNTs-NMP (a) with 6mg of PVP, (b) with 33mg of PVP.

Figure 2-5 shows representative absorption spectra for SWNT dispersions with 6 mg and 33 mg PVP in NMP. No affects of PVP concentration were observed on absorbance for both of them. Furthermore the distributions of diameters of SWNTs are the same (profile or position). The concentration of SWNT in solution for both samples were the same, and this is supporting the explanation above which is the solution with 33mg of PVP contains more isolated tubes.

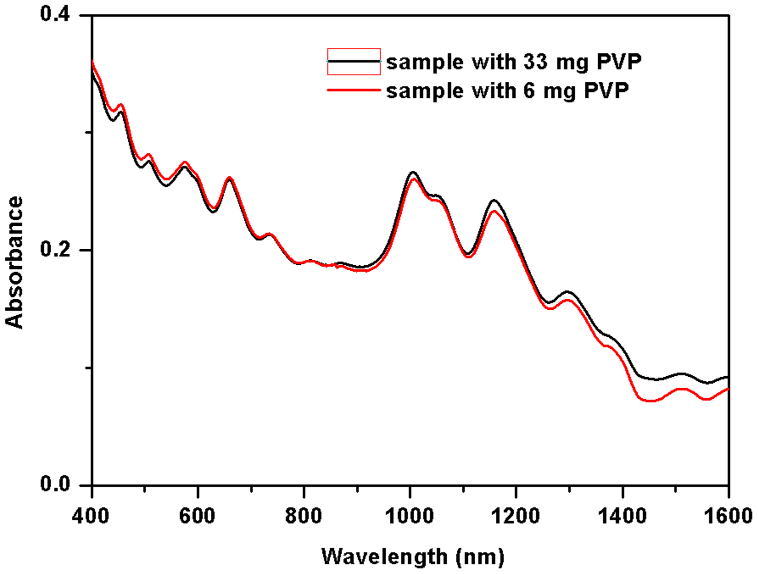

Figure 2-5 Optical absorption spectra of SWNTs dispersion in NMP with addition of PVP at 6 mg and 33 mg.

2.3 CNT-NMP-NaI (salt)

Sodium Sodium iodide (NaI) is a crystalline salt with white colour. It is soluble in NMP up to 0.2M [62,68]. We studied NaI effects on CNT-NMP dispersions. The reason for choosing NMP were, first, NMP is a highly polar solvent and secondly, NaI salt has good solubility in NMP. Therefore, the NMP molecules strongly interact with the dissolved ions due to the electrostatic charge-dipole interactions. The molecular-scale mechanisms of ion interactions with the nanotube surface were investigated and it was shown that the microscopic ion–surface interactions affect stability of CNT dispersions in NMP. Finally, a possibility for controlling the size of the SWNT bundles in NMP solution was demonstrated by the addition of NaI salt at different concentrations.

2.3.1 Experimental methods and Preparation

We dispersed CNTs in NMP at a concentration of 0.013 mg/ml with the same process as in the section 2-3-1, sonication treatment and ultrcentrifugation. The resulting CNT dispersion was divided into 4 samples which were numbered 0, 1, 2, and 3 correspondingly. Sample 0 was used as a control sample, without salt. Different amounts of NaI were added to the other 3 samples to achieve different molar concentrations of salts in the samples: sample 1 with 0.06 mM of NaI; sample 2 with 0.11 mM of NaI; sample 3 with 0.17 mM of NaI. Addition of salts caused an immediate formation of bundles, which we removed after storing the samples for 24 h by 1 h ultracentrifugation at 47 000 rpm.

2.3.2 Results and Discussion

The changes in the CNT dispersions in response to addition of different amounts of salt were investigated by using photoluminescence (PL) spectroscopy and optical absorption spectroscopy as well as by visual inspection of the samples. Addition of salt into the CNT–NMP dispersions results in sedimentation of CNTs. The nanotubes self-assemble into bundles, which later form CNT aggregates in the samples that are visible to the naked eye. This effect occurs for all salt concentrations in this study, as illustrated in Figure 2-6 (a). Figure 2-6 (a) shows photographs of four samples, the first one on the left for control sample 0, pure CNT–NMP dispersion, and it is visibly clear. In the three other samples of CNT–NMP dispersion with added different salt concentrations, the samples start to aggregate after adding salt, with different ratio of aggregate corresponding with increase in the salt concentration. The size of aggregation in sample 3 is more than in sample 2, and sample 1 with a low concentration of salt (0.06 mM) is less aggregated in comparison samples 2 and 3.

Figure 2-6 (b) shows the photoluminescence (PL) map of the control CNT–NMP dispersion sample (no salt), and shows the presence of SWNTs of different chiralities as mentioned before in section 2-1-2, Figure 2-2.

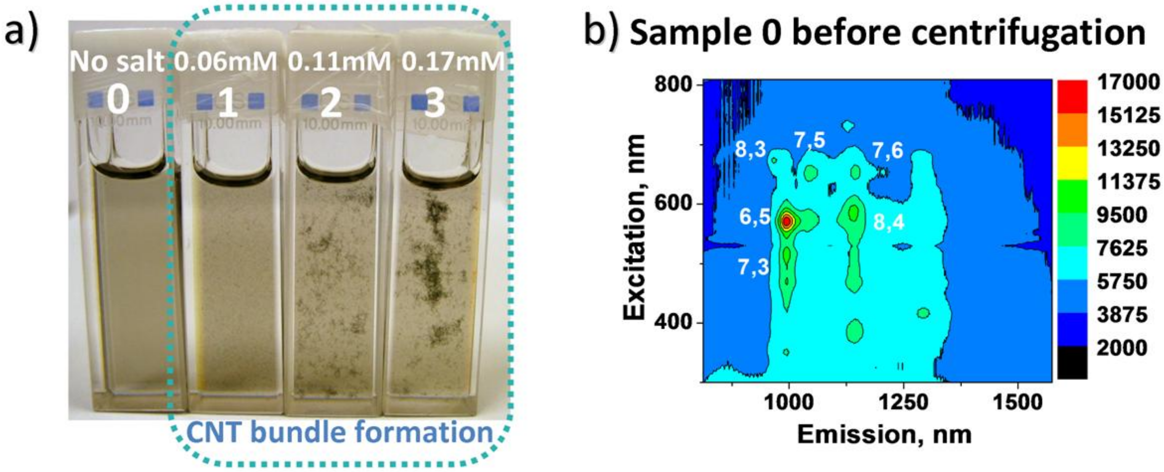

Figure 2-6 (a) Photographs of the samples containing the CNT-NMP dispersions with different amounts of added salts, sample 1 (0.06 mM), sample 2 (0.11 mM) and sample 3 (0.17 mM) respectively, (b) PL map of the control sample [63].

PL intensities and optical absorbance of CNTs were investigated after centrifugation of the dispersions. Figure 2-7 (a) shows a PL map of the CNT–NMP dispersion sample at 0.17 mM concentration of NaI salt after centrifugation (sample 3). The map shows that isolated CNTs and small CNT bundles remain in the dispersion. However, the overall PL intensity decreased significantly in sample 3 with 0.17 mM sodium iodide compared to the control sample both before (Figure 2-6 (b)) and after centrifugation (Figure 2-7 (b)). The map of sample 3 is very similar to the PL map of the control sample before centrifugation showing only a minor decrease in the overall intensity as compared to the PL map of sample 0 before centrifugation (Figure 2-6 (b)).

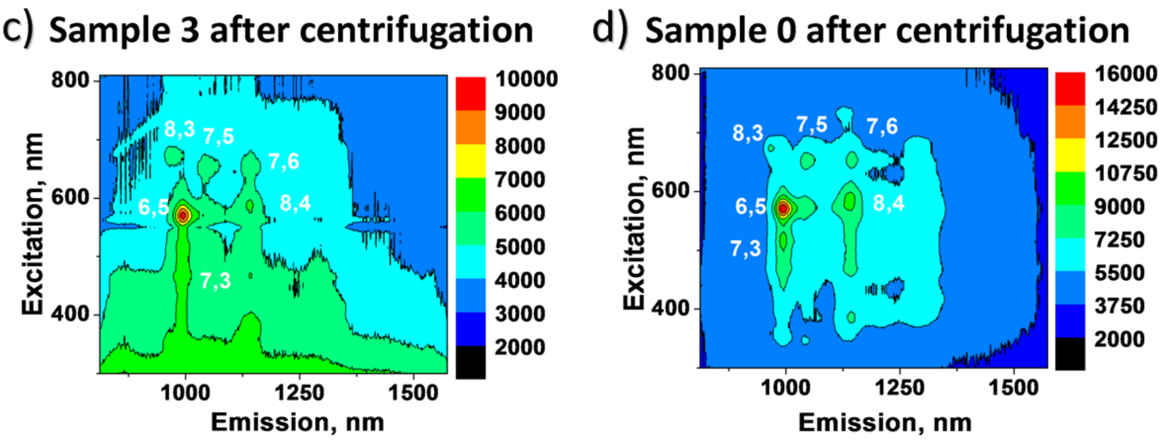

Figure 2-7 Samples after ultracentrifugation (a) PL map of sample 3 with 0.17 mM salt addition , (b) map of the control sample (sample 0) after centrifugation [63].

The decrease in PL intensity and optical absorbance correlates with the salt concentration in the samples, as illustrated in Figure 2-8 (a). The Figure shows that larger concentrations of salt cause a larger decrease in the intensity. These changes in spectral intensities were attributed to a significant decrease in concentration of isolated nanotubes and small CNT bundles in these dispersions after centrifugation. PL intensity measurements for the stability study are taken at 570 nm excitation, showing that the addition of NaI salt stimulates CNT self-assembly into larger bundles (see Figure 2-6 (a)). In contrast, centrifugation of the initial (control) dispersion makes a much smaller effect on the PL intensity and optical absorbance of CNTs, indicating a high stability of the control dispersion. This serves as an additional confirmation that the observed self-assembly of CNTs is stimulated by salt rather than by aging of the CNT dispersions. Figure 2-8 (b) shows the absorbance spectra for the CNT-NMP dispersions and the dispersions with different salt concentrations before and after an additional centrifugation. For NaI concentrations (0.06, 0.11 and 0.17 mM) and after addition centrifugation the spectra show the absorption intensities decreased with increasing the salt concentrations. Moreover, in the case of the control sample (no salt) the additional centrifugation almost does not affect. Similar to the PL plot, the addition of salts leads to a corresponding decrease in the intensity of the spectra. The decrease in intensity correlates with the increase of the salt concentration. The lines with symbols indicate spectra measured before centrifugation.

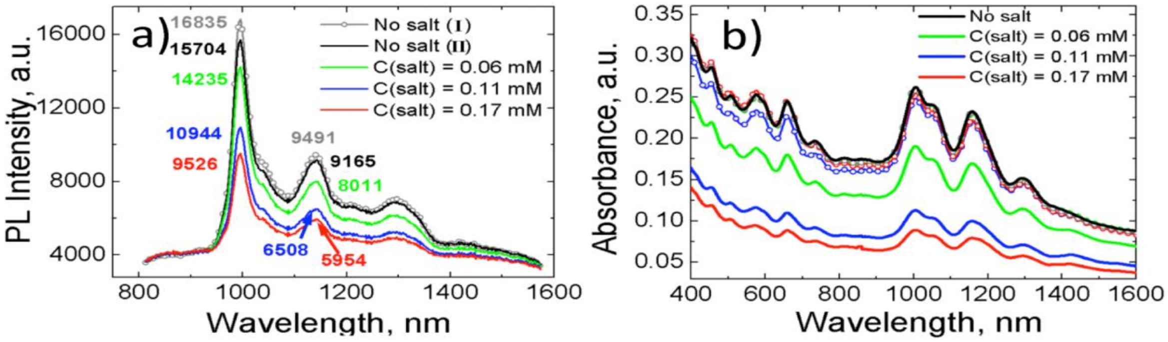

Figure 2-8 (a) Photoluminescence (PL) spectra at the excitation length 570 nm for different samples with and without salts. (b) Absorbance spectra for the all samples before and after second centrifugation [63].

We assume that it is reasonable to extrapolate qualitative explanations of the effect from water to NMP solutions. Indeed, similar to water, NMP is a highly polar solvent where the solvent molecules strongly interact with dissolved ions due to the charge–dipole interactions and thus form distinctive ion solvation shells [64]. Therefore, ions in the CNT–NMP dispersion tend to interact mostly with the polar NMP molecules rather than with the CNTs non-polar surface. Hence it is thought the ions in the vicinity of the CNT surface have fewer NMP molecules to interact with compared to the ions in bulk solution, because of the satirical restraints caused by the surface. When contacting the CNTs surface, ions undergo partial desolvation that should be energetically unfavorable in a highly polar solvent like water or NMP [65].

2.3.3 Modelling

We assume that the concentration of nanotubes within the sample correlates with the intensity of PL bands and optical absorbance for the corresponding nanotube chiralities. That allows us to make quantitative analysis of the changes in the dispersions upon additions of salt. The mechanisms of interactions between CNT species in organic solvents were investigated by molecular dynamics (MD) simulations. We describe our findings on molecular mechanisms of ion and NMP interactions with the CNT surface. We performed molecular dynamics (MD) simulations of a single wall CNT with (8,6) and (6,5) chiralities dissolved in 0.15M NaI NMP solution to reveal the basic molecular mechanisms of ion interactions with the carbon nanotube surfaces. Salt concentrations higher than in the experiments were used to collect good simulation statistics at reasonable computational cost (we were able to put many ion pairs into a relatively small simulation box). However, to prove that the trends obtained for higher concentrations can be extrapolated to lower salt concentrations, we also investigated a CNT with (8,6) chirality dissolved in 0.01 M NaI solution in NMP. In simulations we could not explore concentrations lower than 10 mM, because this would require much larger simulation boxes that would lead to impractically large computational expenses. To reveal ion distribution at the CNT (8,6) surface at 0.01 M NaI concentration we performed a series of 304 small simulations. We present only the computational details for the systems with CNT (8,6) and CNT (6,5) dissolved in 0.15M NaI solutions. We used the Gromacs 4.5 software.39 Segments of CNTs were placed in rectangular boxes (7.50 × 7.50 × 5.19 nm^3) and (7.25 × 7.25 × 4.07 nm^3) in the case of (8,6) and (6,5) CNT chiralities, correspondingly. The CNTs were oriented along the Z axis. Then, 1600 (1200) NMP molecules, 27 (19) Na^+ ions and 27 (19) I^- ions were placed inside the box with the help of Packmol program in the case of (CNT (8,6) CNT (6,5)) [66]. The initial configuration was first optimized by energy minimization [67], and then the density of the system was equilibrated during a 0.2 ns simulation in the NPT-ensemble. Then we performed simulations for 60 and 50 ns in the NVT-ensemble at 300 K for CNT (8,6) and CNT (6,5) correspondingly. Next, to enhance statistics and to estimate the errors in the calculated preferential interaction coefficients and the free energy changes, we performed 10 replica simulations for each CNT starting from different initial coordinates. The initial configurations for the replica runs were collected by taking coordinates of the system each 3 ns and 5 ns from the initial simulations starting from 30 and 0 ns for the systems with CNT (8,6) and CNT (6,5), respectively. Each replica was first simulated for 0.2 ns at elevated temperature (450 K) and then annealed to 300 K during 0.1 ns of simulation time in the NVT ensemble. The production simulation times for each replica were 15.9 and 20.7 ns for systems with CNT (8,6) and CNT (6,5), respectively. Coordinates of the system were sampled each 0.3 ps (for the initial runs) and 0.4 ps (for replica simulations) for further analysis. We employed the fully atomistic OPLS-AA force field [68,69]. Which has been thoroughly tested for NMP and similar organic solvents in refs. [70–72]. For sodium iodide, we used the recent set of ion arameters developed consistently with the general framework of the OPLS force field [69]. We used the Particle-Mesh Ewald method to evaluate the electrostatic interactions [73]. To analyze molecular mechanisms of ion solvation in NMP, we performed an additional simulation of NaI solution in bulk NMP (without the CNT) using similar simulation setup to the one described above.

The results of analysis of the simulation data on sodium iodide salt effects on CNT dispersions in NMP are described in this section.

1- Ion solvation in the bulk NaI NMP solution.

In our simulations we observe that ions dissolved in NMP have distinct solvation shells, as expected, because NMP is a high polar solvent. Therefore, the NMP molecules strongly interact with the dissolved ions due to the electrostatic charge-dipole interactions. Both of the ion–NMP radial distribution functions g(r) shows a peak (Figure 2-9).

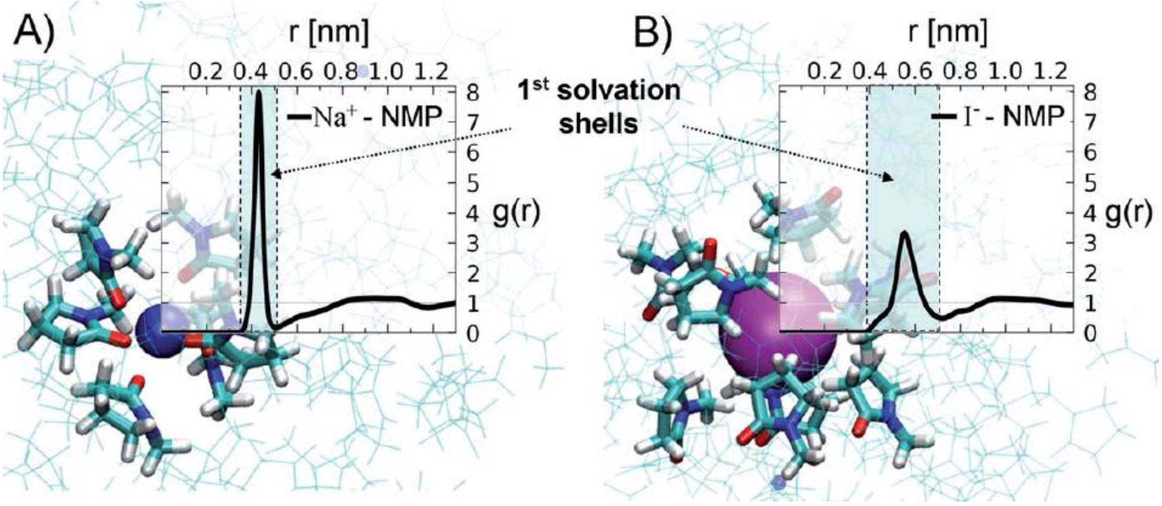

Figure 2-9 Ion-NMP (center of mass) radial distribution functions, g(r), in NaI–NMP solution combined with corresponding simulation snapshots: (A) sodium ion (shown as a blue sphere), B) iodide ion (shown as a magenta sphere) [74].

Both of the ion–NMP radial distribution functions show a peak (at r = 0.42 and r = 0.55 nm for Na^+ and I^-, respectively) followed by a hollow (at r = 0.50 and r = 0.70 nm for Na^+ and I^-, respectively), indicating formation of the first solvation shells around the ions.48 The boundaries of the ion solvation shell were estimated as the region with non-zero ion – NMP radial distribution function ending at the first distinct minimum on the corresponding function. The structures of the solvation shells of the ions are different: the negatively charged NMP oxygen atoms are strongly attracted to the positively charged sodium ions (see the Figure 2-9 A) from another side, the oxygen atoms are placed outwards from the negatively charged iodide ions (see the Figure 2-9 B). In general, similar to the mechanisms of ion solvation in water [75,76] there is a strong asymmetry in sodium and iodide solvation in NMP. As illustrated by the high peak on Na^+ – NMP g(r) (Figure 2–9), the sodium ion solvation shell is very dense because the ion is relatively small and, consequently, has a large surface charge density [77]. Therefore, the Na^+ ions strongly coordinate polar solvent molecules around them that resulted in the height of the first peak on Na^+ – NMP radial distribution function to be about 8.0. On the other hand, the iodide ion solvation shell is much more diffuse because of the larger size of the I^- ion and, consequently, its smaller surface charge density than that of the Na^+ ion [77].

As a result, the height of the first peak on I^- – NMP radial distribution function is much smaller than that on the Na^+ – NMP g(r) (it is slightly above 3.0). The position of the first maximum on the I^- – NMP g(r) is also shifted compared to the Na^+ – NMP g(r) (from 0.42 to 0.55 nm). This is because of two main reasons: (i) I^- (r = 0.220 nm) has a larger radius compared to Na^+ (r = 0.102 nm) [78]; (ii) as discussed above, the I^- – NMP interactions are weaker than the Na^+ – NMP interactions.

2- Ions behavior at the CNT surface in CNT–NMP dispersion.

Results of MD simulations indicated two major effects, which take place during ion interactions with the CNT surface. First ions have to become partially desolvated to make direct contacts with the CNT surface, as shown in Figure 2-10. The MD simulations show that upon approaching the CNT surface the sodium ions have to release one NMP molecule and the iodide ions have to release two NMP molecules from their solvation shells, there is a significant decrease of the solvation number of ions at the CNT surface, see Figure 2-10 A. The partial desolvation of ions also means that the strong ion–NMP dipole interactions are substituted by the much weaker van der Waals interactions of ions with the non-polar CNT surface. That leads to large energy costs for desolvation of ions and, overall, makes the direct contacts of ions with the CNT surface to be energetically unfavorable.

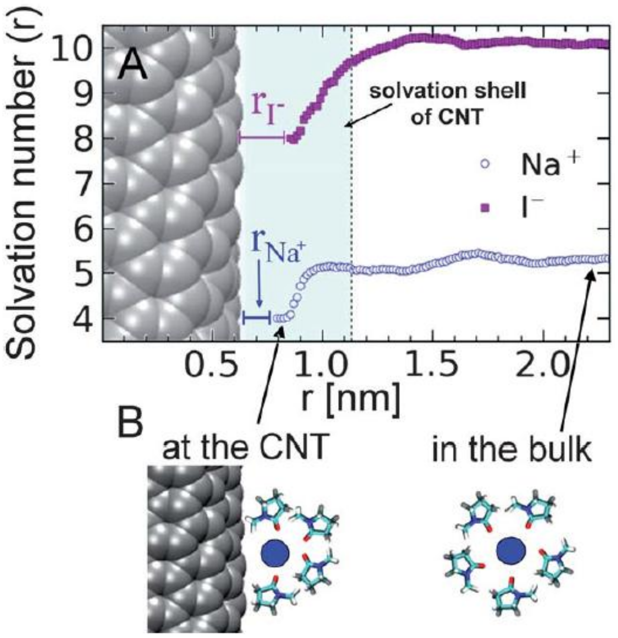

Figure 2-10 (A) Solvation number of ions (the number of NMP molecules in the first solvation shell of the ions) as a function of distance from CNT with (8,6) chirality. (B) Schematic representation of the partial desolvation of the ions upon direct contact with the CNT surface [74]**.**

Secondly, it appears that to approach the CNT surface, ions have to penetrate a very dense layer of NMP molecules in the first CNT solvation shell, as shown in Figure 2-11. It is profile with two distinct high peaks in the vicinity of the CNT surface. This NMP enrichment area is followed by a deep hollow at about r = 1.1 nm. Thus, during the formation of ion–CNT direct contacts, not only the ions have to be partially desolvated (as shown on Figure 2-10), but also the CNT has to release some NMP molecules from its solvation shell.

This further increases the energetic barrier for the formation of ion – CNT direct contacts.

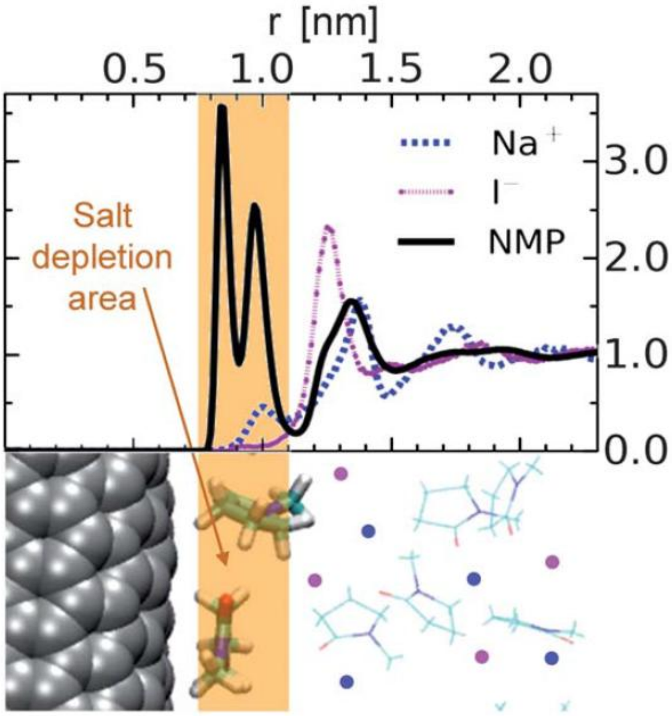

Figure 2-11 Radial density profiles of ions and NMP molecules (center of mass) at the CNT [74]**.**

From the simulation and experimental data on sodium iodide salt effects on CNT dispersions in NMP, the observation and conclusions can be summarized as follows. The NMP solution is a highly polar solution with strong ion-solvent interaction. These bonds must be overcome in order for salts to come in to direct contact with the CNT surface. It is particularly unfavourable from an energetic point of view since the ions must overcome their strong ion-solvent interaction and become partially desolvated. Furthermore the ions must conquer the prominent and dense solvation shell of the CNT in order to make direct contact, which poses yet another obstacle for the ions.

On the other hand, the interactions between the ions and the CNT surface depend on the salt depletion area which is formed around the CNT. The width of the salt depletion area corresponds to the width of the first solvation shell of CNT in NMP, which means the concentration of ions is much less in this area than in the bulk solution.

However, at higher concentrations of salts, the CNT-NMP dispersions become thermodynamically less stable resulting in the increase of solvophobicity of the CNTs in the CNT-NMP dispersions. The increase of the CNT solvophobicity can be observed through the increase of salt concentration and the increased aggregation of CNTs (Figure 2-6 (a)). This is confirmed by the MD simulations [74]. The salting-out effect appears to lead to an efficient, safe and inexpensive method of bundle engineering of the CNTs in non-aqueous media.

2.4 CNT-NMP-PVP-NaI (salt)

Nanotechnological applications of CNTs are related to the selective separation of CNT chiralities, which it is a great challenge. In general there is no efficient method yet for SWNT separation. Recently, a salt addition to the SWNT dispersion has been shown to be a method that might serve as an tool for chirality separation of CNTs [79,80]. SWNTs-NMP solutions with addition of PVP are more stable, as explained in section 2-2. When SWNTs-NMP-PVP is dispersed with addition of NaI salt at different concentrations, the resulting solutions show excellent stability with respect to re-aggregation of the nanotubes.

In this work the salt (NaI) effects on CNT–NMP-PVP dispersions were studied. PVP was chosen because it is possible to increase concentration of SWNTs to at least 0.28 mg/ml in the bulk NMP solution and the dispersion may stay stable for few weeks [34]. Moreover, PVP polymer wrapped around the carbon tubes which it is thought to make the solution thermodynamically more stable.

2.4.1 Experimental methods and Preparation

CNTs were dispersed in NMP as in a section 2-2-1 and 33mg PVP polymer was added. Then the resulting CNT dispersion was divided into 5 samples which were numbered as sample 0, 1, 2, 3 and 4 correspondingly. Sample 0 was again used as a control sample (without salt). Four different salt concentrations were added to the other samples: 0.065, 0.130, 0.190 and 0.500 mM. The final concentrations of the salt in the samples were prepared as follows. Concentrated salt solution in NMP was added to each sample with a calibrated micropipette. All samples were shaken at 300 rpm for 10 minutes. Due to the small volume of the added drops of the concentrated salt solution the dilution effect on the whole sample was not taken into account. The final salt concentrations were 0.065, 0.13, 0.19 and 0.5 mM, corresponding to the samples 1, 2, 3, and 4.

2.4.2 Results and Discussion

Figure 2-12 shows photographs of all samples. Sample 0 (without salt) was used as a control, and sample 1 was observed to be stable without any aggregations. Formation of CNT bundles was observed by visual inspection of samples 2 to 4, and the photographs show the effect of interaction between the salt and polymer in de-bundling SWNT aggregates.

Figure 2-12 also illustrates the stabilizing effect of sodium iodide at low concentration. The remaining samples have formed CNT bundles with addition of sodium iodide at higher concentration. That means the ratio between the sodium iodide concentration and SWNTs solution in sample 1 is under the threshold conditions and the sample remained thermodynamically stable.

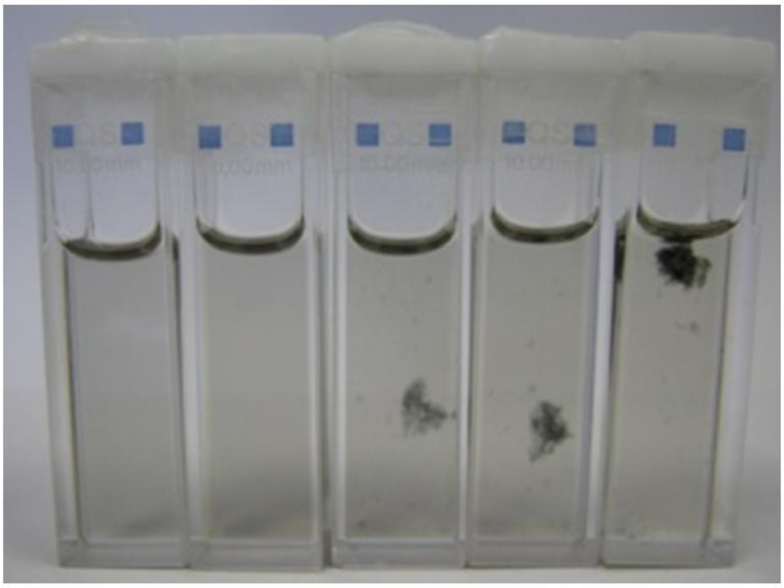

Figure 2-12 Photographs of SWNTs dispersion in (left to right) a control sample (without salt) and the samples 1,2,3 and 4, 0.065 mM, 0.130 mM, 0.190mM, and 0.500 mM sodium iodide respectively.

Nanotube aggregation increased in samples 2 to 4 with increasing salt concentration. However, when the salt concentration increased, the negative ions around tubes increased and this stretches out the polymer. It may be that the main molecular mechanisms of ion interactions with the nanotube surface changed with different salt concentrations than those used in section 2-3, because the PVP polymer wrapped around the tubes makes the tube more stable with respect to the effect of external influences. Also it could be that energy is transferred from polymer to tubes, and achieve tubes which is more thermodynamically stable [34]. That is evident from the PL map shown in Figure 2-13. The intensity of the PL bands increased with additions of salt. That means it might be the same interaction energy between the salt and polymer being transferred to the carbon tubes, which led to increased PL intensity in sample 1. Figure 2-13 (a) shows the PL map for control sample without salt and Figure 2-13 (b) the increased intensity for sample 2. Figure 2-13 (c) shows the reduction of the average PL intensity in sample 4 compare with control sample (0).

Therefore, faster aggregation is expected in sample 4 than in the other samples. However, experimental results from the SWNTs-NMP-PVP dispersion with added sodium iodide indicates that salting-out happens after adding salt to the SWNTs-NMP-PVP dispersion, as described in section 2-3. This means the interaction between the sodium iodide and SWNTS-NMP-PVP solution is different, and hence the PVP causes as effect in this interaction.

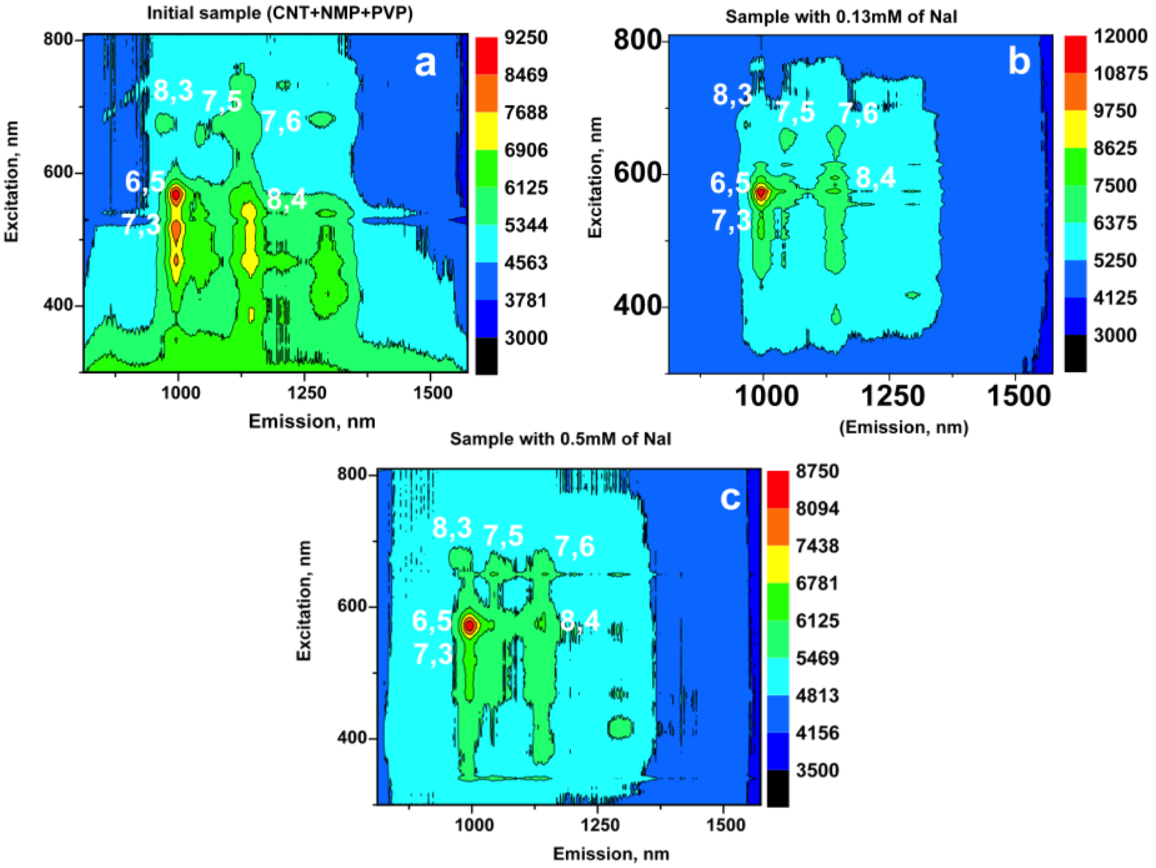

Figure 2-13 (a) PL map of control sample without salt addition, (b) sample 2 with 0.130 mM sodium iodide and (c) PL map of the sample 4 with 0.500 mM sodium iodide.

Figure 2-14 shows PL intensity measurements for a stability study taken at 570 nm excitation. It can be clearly seen that the intensities of PL increased for samples 1, 2 and 3 but for sample 4 the intensity was reduced with increased the salt concentration.

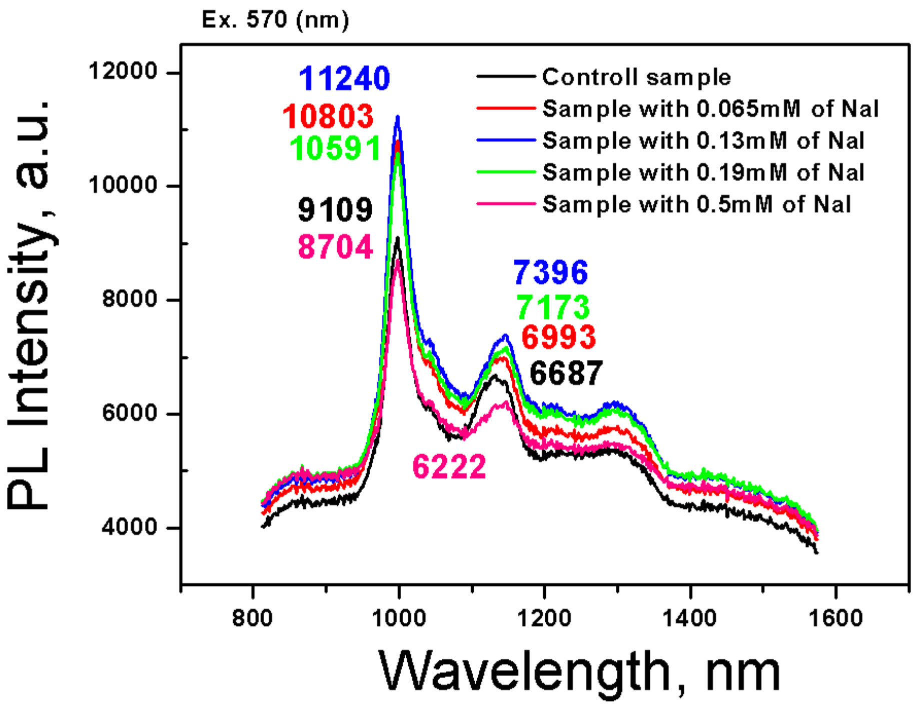

Figure 2-14 Spectra from excitation at 570 nm for samples 0, 1, 2, 3 and 4 with and without salts.

Optical absorption spectra for samples 1 to 4 with different concentrations of sodium iodide and sample 0, the control sample, are shown in Figure 2-15. The spectra clearly show electronic transitions in the VIS-NIR region, that is, absorption peaks resulting from the first and second interband transitions of semiconducting SWNTs (S_{11} and S_{22}) for all samples, even the control. The absorption intensities are nearly same for all samples, which show that the concentrations are nearly same for all samples.

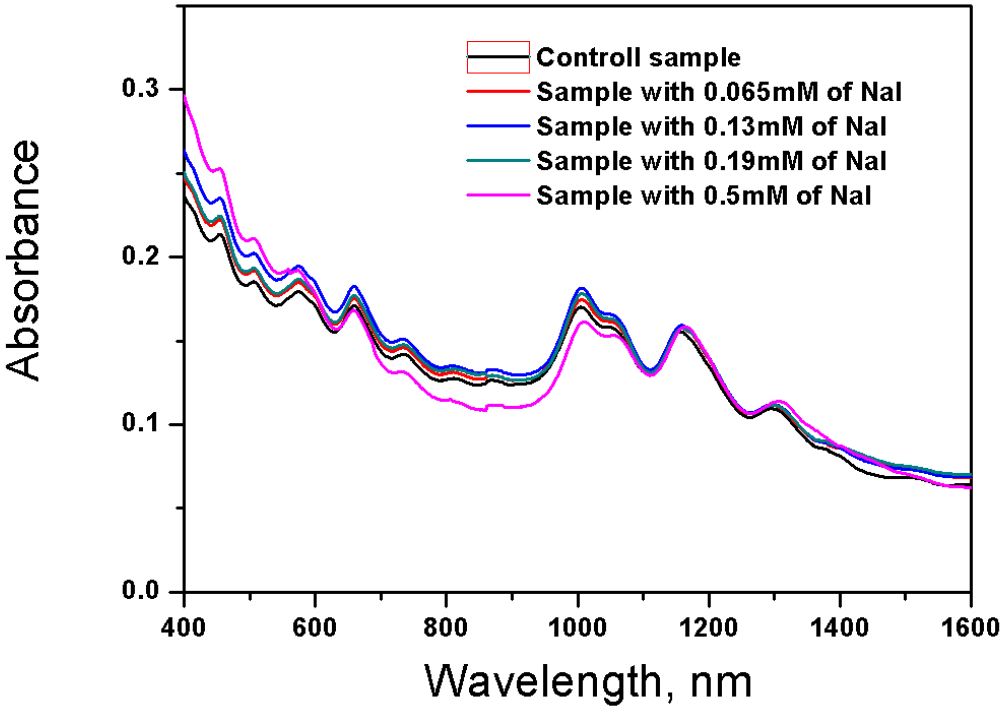

Figure 2-15 Optical absorption spectra of all samples 0 to 4.

In this study it has been shown that the SWNTs-NMP-PVP solution with additions sodium iodide can show very promising properties, comparable with the results in case of SWNTs-NMP with sodium iodide but without PVP. Figure 2-16 shows the threshold of concentration dependence of PL intensities for tubes (6,5) of solution mixtures (SWNTs-NMP-PVP) with added sodium iodide. The PL intensities tend to increase with increasing the concentrations of salt until the threshold, which can be related to the unique process which makes these SWNT-NMP-PVP solutions thermodynamically unstable.

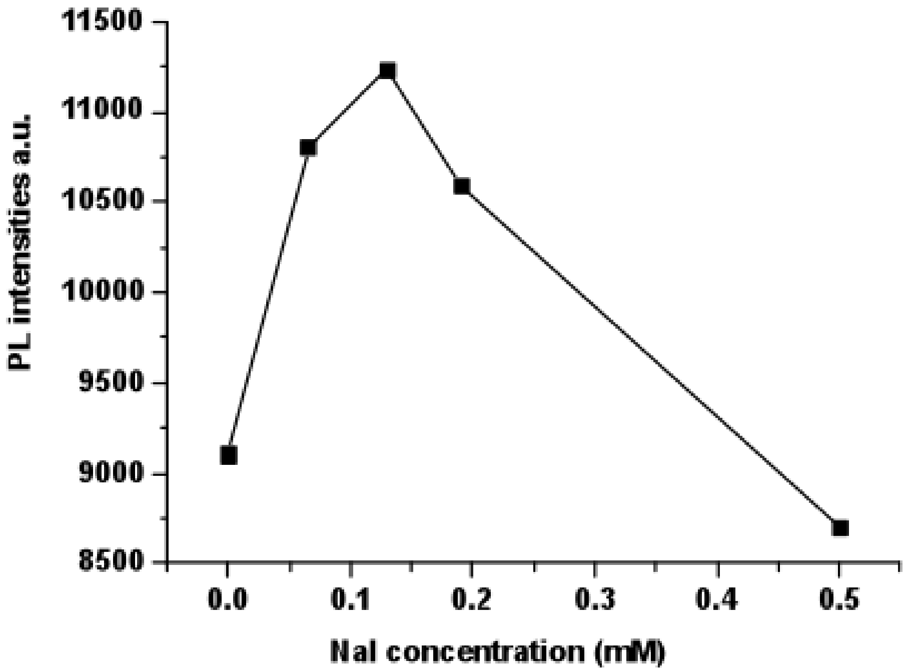

Figure 2-16 Concentration dependence of PL intensities for tubes (6,5). PL intensity increases to a peak in the solution of sample 2, with 0.13 mM sodium iodide.

CNT-NMP-PVP dispersions with addition of sodium iodide have been studied, with results as follows; first, as mentioned Section 2-3, the NMP solution is a highly polar solution with strong ion-solvent interaction. Polymers carrying a charge can be integrated with groups of ions in polar solvents such as NMP, and the ion groups can be separated, and charges may be departure from polymer chains, releasing counterions into the solution. Counterions are ions that accompany a charge to maintain electrical neutrality. Condensed counterions decrease with increase polymer concentration, due to polymer chains interpenetrating, where the polymer becomes bunched in on itself which lead to a higher concentration of the counterion in solution. However, in a good conditions the solvent condensed counterions could be high [81]. The mechanism for ion conduction is not yet understood enough for solid polymers and it is still unclear. Second, sodium iodide with CNT-NMP was also described in Section 2-3. Third, PVP:NaI, in the case of PVP polymer has a carbon bond with oxygen which is a strong electron donor, and may interact with sodium ions. PVP also has a carbon bond with nitrogen which can be attracted to iodide ions. Ravi and co-workers [82] have used PVP with Potassium perchlorate to increase conductivity with an increase in salt concentration. Figure 2-17 shows the effect of sodium iodide on the polymer, which tends otherwise to occur as a random coil, and ions lead to stretching out of the polymer.

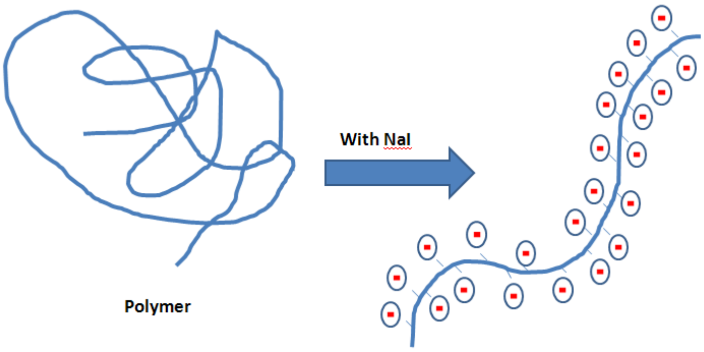

Figure 2-17 Schematic of interaction ion with polymer.

An increase in salt concentration is known to lead to an increased number of adsorbed counterions around the polymer skeleton, which means the net charge fraction of the polymer decreases with increasing salt concentration [83]. That means the polymer may be stretched out by sodium iodide.

In addition, there is a threshold value for interaction between polymer and salt. The number of repeats of the polymer chain should be larger than the degree of ionization, which depends on the length and radius of the polymer and on the concentration-dependence of the chain size for partially charged chains with a monomer with fractional charges. This happened with sample 1 (0.065 mM) and sample 2 (0.130 mM), where it is assumed the quantities of ions, and the concentration of sodium iodide in the solution were not sufficient to stretch out the polymer around tubes, and the polymer was still wrapped around tubes. That was confirmed by PL, as the intensities of PL in sample 1 was still increased compared with the control sample, and the PL intensity was maximal in sample 2 (Figure 2-14), which started to aggregate, as seen in the photograph Figure 2-12, third from left. However, in the case of sample 3 (0.190 mM) and sample 4 (0.500 mM) the quantities of ions, and the concentration of sodium iodide in the solution are enough to cover the whole chain of PVP polymer, to stretch out the polymer around tubes. Salting out was observed for the tubes, and PL intensities decreased abruptly for those samples (Figure 2-14).

In conclusion, an ion interaction with the surfaces of carbon nanotubes dispersion in NMP solvent was investigated. Small salt concentrations of sodium iodide salts are capable of salting out carbon nanotubes from their dispersions. The effect of salt addition increases with an increase of the salt concentration. The CNT–NMP dispersions become thermodynamically less stable at higher concentrations of salts. These findings provide new access for CNT bundles engineering in nano-science.

Chapter 3

3. Photoluminescence enhancement of carbon nanotube using polymethine dye complexes

Dye is a material which can be involved in a transfer of energy from the dye molecule to SWNTs. Enhancement of PL intensity and transfer of energy has been described in this chapter, with selectivity to SWNTs, by addition of dyes. CNTs with one dimension have remarkable multifunctional application potential in electronics, reinforced composite materials, chemical and biological sensing, scanning probe microscopy and in many more areas [12,50,84–87]. Chemically functionalized CNT might be designed for advanced tasks, including light-harvesting devices, sensors, drug delivery and energy storage [50,86–91].

While some of these applications still remain a far-off aim, others are actually very close to practical realization [91] such as hydrogen storage. However, CNT could be a potential industrial pollutant in the near future due to the growth of nanotechnology, with total mass production of CNT exceeding the thousands of tons annually [91]. These is only fragmentary knowledge about their toxicity [12,89,90]. CNTs could get into the environment during production, application, and disposal, and the ambient risk posed by CNT must be controlled. Therefore, we need to be well equipped for rapid detection of CNT, to prevent contamination of the human bodies and the wider environment in the case of technological catastrophes.

Among known techniques of chemical sensing, one of the most promising is the photoluminescence (PL) method, due to its high sensitivity, rapid detection and simplicity. The most efficient mechanism for PL sensing can be achieved through an enhancement of the emission in the presence of the compound to be detected [92,93]. The quantum yield of PL emission of CNT is low [12,50,84–87], and PL quenches with both bundling of the tubes [41, 79] and interaction with some analytes [54,95,96]. The ‘brightening’ of CNT PL has been pursued for various photonic applications, and has been achieved through encapsulation of organic materials inside the tubes[97,98], covalent incorporation of sp^3 defects [99], embedding luminescent local states(100), admixture of an electrolyte [101], and non covalent attachment of π-conjugated organic molecules [102–104]. The merits of non-covalent attachment of organic molecules are that unique intrinsic features of the tubes are prepared whilst novel advances associated with the organic conjugates may also be conferred [86,89].

Among the variety of organic conjugated compounds, the polymethine dyes (PDs), organic molecules containing a polymethine chain of different length and enormously variable end groups, can be easily modified and tuned towards a desirable opto-electronic task. PDs are advanced photonic materials which have applications as spectral sensitizers (105), light harvesters (106) and ‘laser’ dyes with large optical non-linearity [107–109].

The effects of some other dyes have been studied: Cyanine dyes, Cy3 and astraphloxin, affect emission from CNTs in a very dramatic way [110,111]. PDs are known to attach non-covalently to CNTs, which produces a significant PL amplification of CNT emission by energy transfer [98]. In this experiment a series of polymethine dyes were tested to observe the effect. Most of the dyes showed slightly quenched fluorescence in the presence of CNTs with no influence on NIR emission of CNT. The results of these studies are reported in this chapter.

3.1 Energy Transfer

SWNT solutions contain isolated semiconducting SWNTs and metallic tubes. Furthermore, there are bundles of different sizes and containing combinations of semiconducting or metallic tubes. Assuming a random chirality distribution, two-thirds semiconducting nanotubes and one-third metallic would be expected [11]. Semiconducting SWNTs have a band gap which depends on the tube diameter, and nanotube fluorescence is related to the electronic band structure. In PL, electron excitation occurs through absorption of light at higher energies, which is subsequently emitted during electron relaxation at lower energies. Exciton energy transfer (EET) happens between tubes assembled in bundles consisting of only semiconducting nanotubes with different diameters of tubes. Excitons can be transformed from larger band gap donor tubes to smaller band gap acceptor tubes amongst SWNTs. This interaction depends on the distance between donor and acceptor semiconducting nanotubes [41]. However, PL can be quenched, in large bundles or in metallic nanotubes, due to the nonradiative property of metallic tubes. Moreover, the PL quenching effect dramatically increases with increase in bundle size.

Exciton recombination, one of the possible intraband relaxation processes, can be either radiative or nonradiative. Figure 3-1 shows the mechanism of (a) the radiative process between excitation of large gap donors exposed to light and the emission from small gap acceptors, showing a high transfer efficiency process in bundles. In Figure 3-1 (b) the light is absorbed by metallic tubes, which are nonradiative, so the metallic nanotubes can strongly quench luminescence from semiconducting SWNTs due to the nonexistent band gap. The presence of large bundles with large tube diameters may also absorb and quench luminescence instead of emitting.

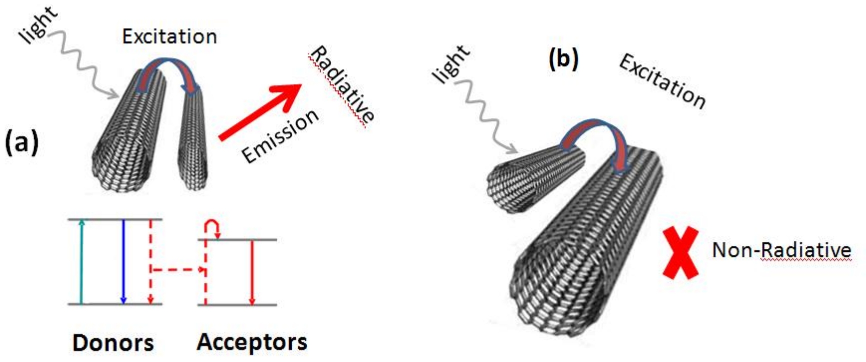

Figure 3-1 Schematic of (a) radiative and (b) nonradiative energy transfer in SWNTs bundles.

Forster resonance energy transfer (FRET) is a process of transfer of energy between two different molecules via a nonradiative path, which is not mediated by photon emission. Transfer of energy occurs between a donor and a nearby acceptor molecule. The process is involves a donor in an excited electronic state, which then may transfer the excitation energy to a nearby acceptor molecule in a nonradiative way through dipole-dipole interactions. This process is highly distance dependent within several nano meters, due to spectral overlap between the donor emission and acceptor absorption spectra, shown in Figure 3-2.

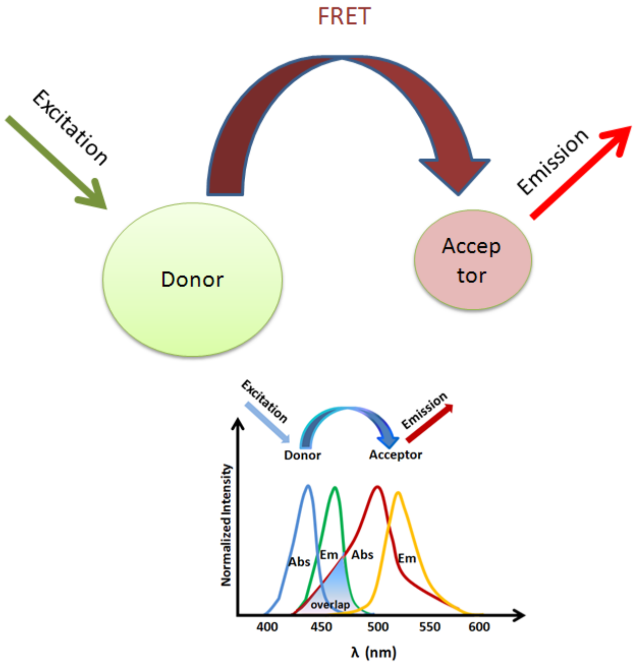

Figure 3-2 Schematic of donor-acceptor spectral overlap region.

3.2 Polymethine dyes

Cyanines have many uses as fluorescent dyes. Pure organic dyes not only are easier to prepare but also have low costs. Dye-sensitized systems have been extensively studied as having promise for photoelectric conversion. Recently, researchers have succeeded in synthesizing a series of hemicyanine and cyanine dyes and it has been found that these dyes could perform excellent spectral sensitization by reasonable design [112]. In order to enrich the research field of cyanine dyes for CNTs and gain more information on the structure, property relationships have been developed in this work, indicating that pure organic dyes would be a promising type of sensitizer for SWNTs. Cyanine dyes have intense and broad absorption bands in the visible and near-infrared regions. Moreover, there are many applications for these dyes in industry, particularly in biomedical imaging, depending on the structure of the dyes. The molecular structure of cyanine polymethine dyes, Cy3 and astraphloxin, differs only by presence of a long alkyl chain (hexanoic acid) in the Cy3 side group compared to Astraphloxin as shown in Figure 3-3. The long alkyl chain may alter an interaction of the dye with CNT as well as interaction between dye molecules [111,113].

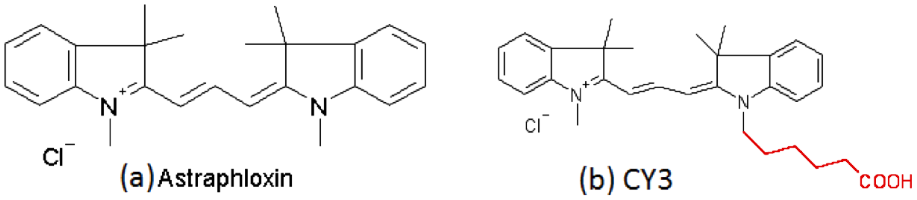

Figure 3-3 Molecular structures of selected cyanine dyes: (a) Astraphloxin and (b) Cy3.

A series of newly synthesized and well known PDs for rapid recognition of CNT were tested when covered by ionic and non-ionic surfactants in water. Enhancement of PL from the chiral (semiconductor) tubes functionalized by astraphloxin dye was demonstrated, as shown in Figure 3-4. Functionalization occurs through coulomb coupling of positively charged astraphloxin molecules (Figure 3-5) to anionic surfactants (sodium dodecyl-benzene sulfonate (SDBS), sodium dodecylsulfate (SDS), sodium deoxycholate (SDOC) and sodium taurodeoxycholate (STDOC)) covering CNT and forming micelles. The astraphloxin attached to the micelle interacts with CNT by weak π-π complexation resulting in quenching of the emission of the dye and enhancement of CNT PL up to 6 times. Excitation-emission PL mapping in spectral ranges of the dye and CNT allowed experimental demonstration that only PD molecules stacked in CNT micelles contributes to PL amplification of CNT (Figure 3-4). The reference systems with neutral surfactants (Triton-X

100, polyvinylpyrrolidone) or negatively charged astraphloxines with sulfonated groups were unable to create complexes with CNT. Physicochemical modelling of the complexation process is reported which fully supports by the complementary study of the reference systems. The ability to tune π-conjugated systems of PDs allows alteration of the energy levels in the studied complexes. An efficient light harvesting system is thus demonstrated with great potential to boost future photonic applications.

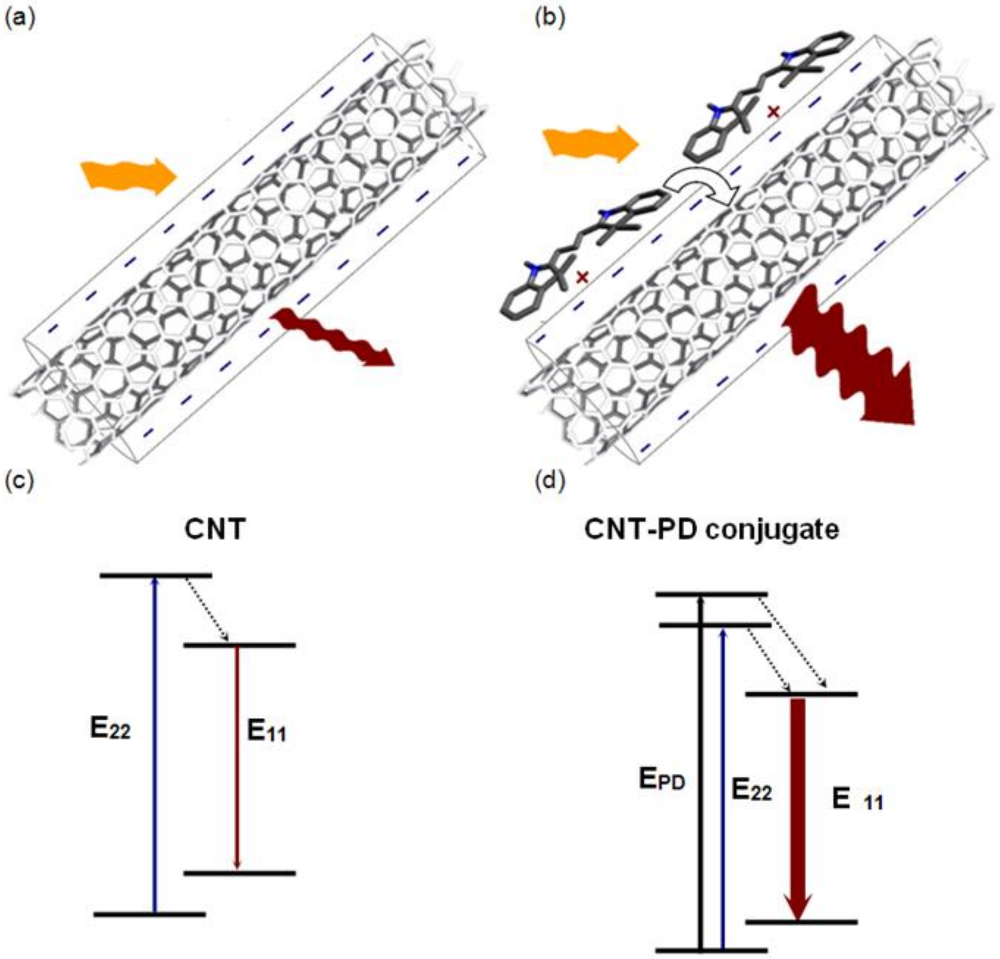

Figure 3-4 Schematic diagram of energy transfer in studied complexes. (a) The micelle is formed around CNT by anionic surfactants (SDBS, SDS, SDOC, and STDOC); (b) coulomb attraction attaches positively charged astraphloxin to anionic CNT micelle. A non-covalent conjugation of PD – CNT emerges with enhanced PL emission from CNT. (c) The CNT has characteristic exciton energy levels of PL excitation E_{22} and emission E_{11}; (d) a visible range excitation of the dye molecules attached to the tubes transfers to CNT PL levels (E_{11}) in NIR range.

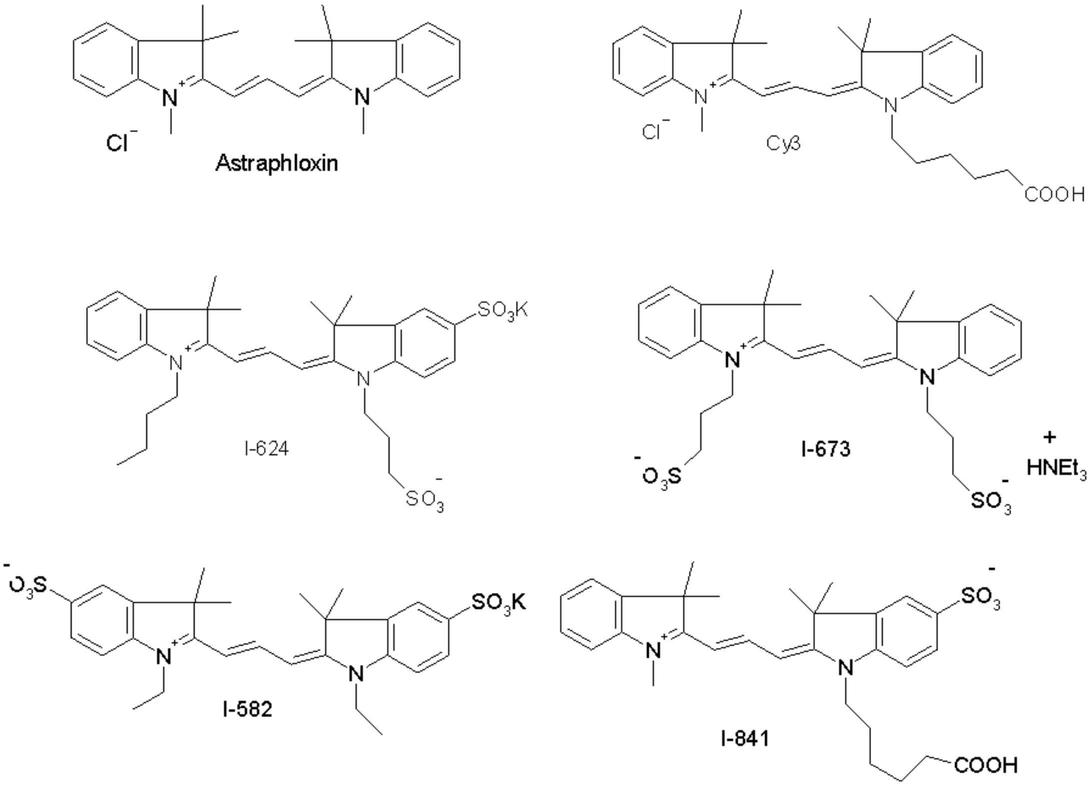

Figure 3-5 Molecular structures of selected PD. Positively charged: (top, left) astraphloxin and (top, right) Cy3; and negatively charged anionic analogues of astraphloxin (I-624, I-673, I582) and Cy3 (I-841).

One of the most efficient surfactants for dispersing CNT is SDBS, an anionic compound, providing a stable micelles solution with debundled tubes (15). Most of the studied PD had slightly quenched PL in the presence of CNT with no influence on NIR emission of CNT. However, astraphloxin and Cy3, an astraphloxin analogue with a long alkyl chain (Figure 3-5), affected emission from CNT in dramatic way by significant amplification of CNT PL. Cyanine terminal groups connected with the polymethine chain constitute the astraphloxin molecule, which has uncompensated positive charge at one of nitrogens. In Figure 3-5 we demonstrated a tremendously small part of engineering variety of this molecule, which can serve as a diverse model system for CNT functionalization and promising unit in future practical applications.

3.3 Experimental methods and Preparation

1.24 mg SNWTs (CoMoCAT-100) were dispersed in 20ml DI water with the presence of 6.5mg sodium dodecylbenzene sulphonate (SDBS). First the dispersion was exposed to ultrasonication for 1 h at 21 kHz and 250 W. Second the dispersion was subjected to ultracentrifugation for 2 h 30 min at 47 k r.p.m at 17 °C, in order to remove the aggregate phase. A series of polymethine dyes summarized in Figure 3-3 were supplied from the Institute of Organic Chemistry (NASU, Ukraine).

The concentration of CNT in all mixtures used in the experiments was similar; approximately 80 % of the neat solution of CNT was used and 20% of the solution of the dye to make a certain ratio of components. Mixtures with the following concentrations (in mg/ml) of dyes were studied: 0.0005, 0.0010, 0.0020, 0.0040, and 0.0080 mg/ml. The PL data for high concentrations of the dyes (above 0.008 mg/ml) was not included in the discussion because of the effect of PL emission re-absorbance.

3.4 Results and Discussion

3.4.1 Shift in absorption spectra of SWNTs dispersion.

Absorption spectra for mixtures of astraphloxin or Cy3 with CNT show a peak shift related to dye absorption depending on the concentration of the dye, as shown in Figure 3-6 (a) and (b). The peak at 540 nm for neat astraphloxin solution shifts to 554 nm for a concentration of the dye at 0.0010 mg/ml in the mixture Figure 3-6 (a). For Cy3, having a maximum at 543 nm in neat solution, the peak also shifted to 554 nm for the lowest concentrations of the dye in the mixture Figure 3-6 (b).

Thus, the absorbance peak of the dye monomers (540 nm for astraphloxin and 543 nm for Cy3) vanishes in the mixtures at the low concentration of the dyes. An increase of the concentration recovers the peak from dye monomers Figure 3-6 (a) curves 4 and 5. The mixtures with high concentration of the dyes have absorption spectra that could be fitted as a superposition of components: one for monomers of the dye, second for the dye interacting with CNT, and third for CNT itself.

The spectra of the mixtures with high concentration of astraphloxin can be well fitted by these components taking into account a further red shift of the peak for the dye interacting with CNT. For example, at an astraphloxin concentration of 0.0040 mg/ml the peak has to move 6 nm from 554 to 560 nm. In this way, we evidence is demonstrated for J-aggregation of astraphloxin on CNT. The spectra of mixtures with Cy3 are perfectly fitted, with no shift at higher concentrations, vindicating the suggestion that Cy3 interacts with CNT without aggregation between dye molecules. It should be noted that neat solutions of the dyes, as well as mixtures of Cy3 with CNT, are stable for weeks with no aggregates formed, whereas overnight (or longer) aged mixtures of astraphloxin with CNT contain small shiny crystals (particles) as well as dye deposited on the walls of the containers.

The explicit red shift of the peaks can be explained by an interaction of the dyes with CNT. One can suggest a formation of J-aggregates of the dyes in the vicinity of the tubes [106], as we clearly observe an emergence of red shifted peak. However, the astraphloxin-CNT mixtures can be shown to have dependence of the shifted peak on the dye concentration further evidencing a J-aggregation of astraphloxin molecules with CNT. Moreover, in the studied mixtures, a threshold in the appearance of the dye monomers is shown at high concentrations (see curves 5 in Fig. 3-6 (a) and (b), which evidences saturation of the dye aggregation on CNTs. It appears that the dye covers the CNT surface in a single layer only. A similar effect of single layer formation was shown in system of CNT non-covalently covered by porphyrin molecules [103].

The interaction of the dyes with CNT is evidenced by the absorbance data in the region of transparency of the dyes (600 -1400 nm), where the peaks of CNT absorbance were analyzed in the above mixtures. For example, a CNT peak with the maximum at 655 nm does not alter its position, whereas peaks at 994 and 1024 nm shift to the long wavelength side by 5 nm (to 999 and 1029 nm, respectively). The peaks are shifted for by same position regardless of dye concentration.

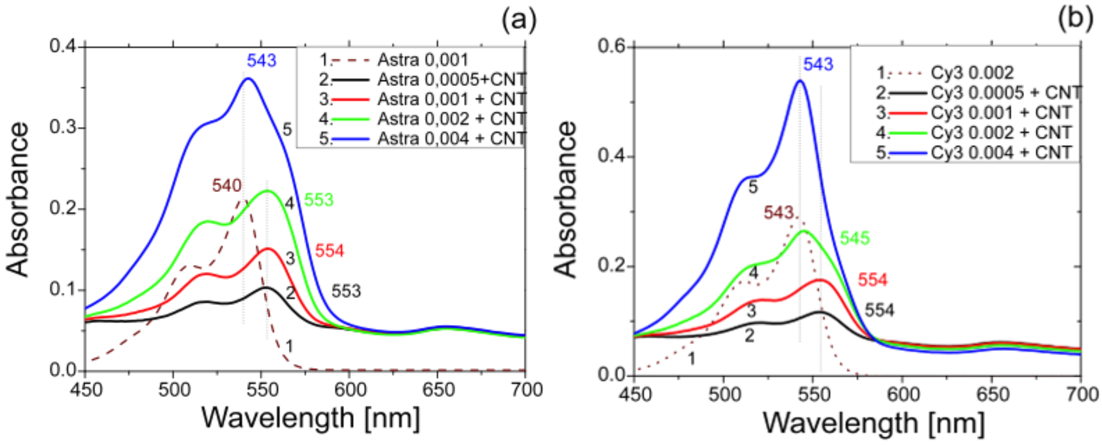

Figure 3-6 Absorption spectra of (a) astraphloxin and (b) Cy3 in water. The peak for neat dye solution, (a) 540 nm and (b) 543 nm shift with addition of CNTs at low concentration (spectrum 2 a and b) but at high concentration (spectrum 5 a and b) show recovery of dye monomer peaks in addition to dye-CNT shift peaks at 543 nm and a third component from non-complexed CNT emission.

3.4.2 PL enhancement

Figure 3-7 (a) and (b) shows PL for mixtures of CNT with dye in the visible range of 500-700 nm. Quenching of the dyes emission is shown a as a result of the admixture of CNT. Thus, the observed quenching of PL may be explained by non-radiative transmission of the excitation energy from the dyes to CNT with further emission from CNT excitonic levels (E_{11}). A red shift of approximately 11 nm from 556 nm to 567 nm, for astraphloxin and approximately 5 nm from 557 nm to 562 nm for Cy3 is observed in the maxima for excitation and emission for the mixtures. This is shown in Figure 3-7 (c) and (d).

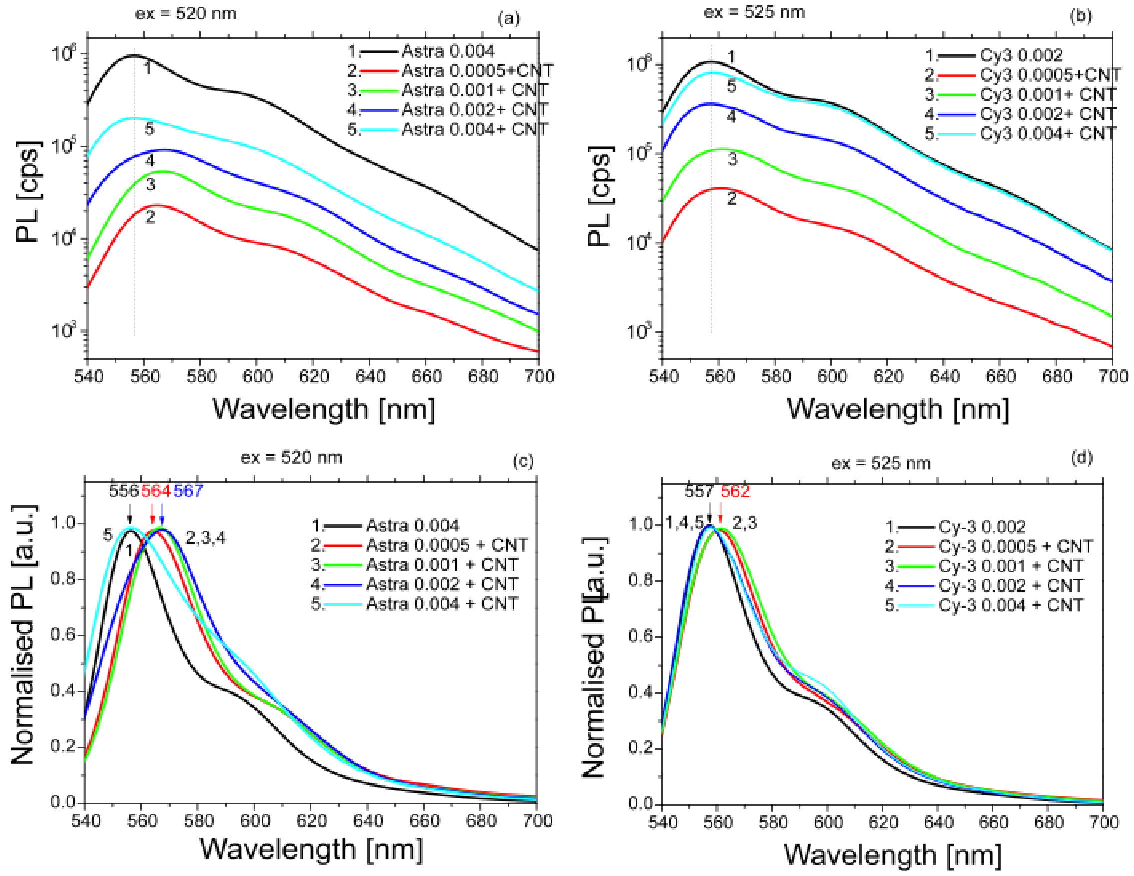

Figure 3-7 PL emission for mixtures CNT with dye at various concentration (a) and (b), and normalised PL emission from mixture of CNT with dye at various concentration showing a red shift of approximately 11 nm for Astraphlaxin (c) and 5 nm for Cy3(d).

In the NIR range, maps of excitation-emission of PL, EPL maps, where the X axis is wavelength of PL emission, λ_{EM}, and the Y axis is the wavelength of PL excitation, λ_{EX}, were measured for neat CNT and mixtures of CNT with various concentrations of the dyes. The EPL map data showed a rise in PL intensity from the tubes (PL amplification) in the range of the dye excitation as in Figure 3-8. Particularly, the maximum of excitation did not coincide with the maximum of the absorbance of the dye monomers (540 and 543 nm for astraphloxin and Cy3, responsibly). However, it coincides with the absorption maximum for dyes interacting with CNT (maximum at λ_{EX} = 555 nm accompanied by a vibration peak at 520 nm).

The resonant energy transfer (RET) process from dyes, donors, dye molecules attached to CNT, acceptors, is the most obvious reason for the effect explained by dipole-dipole interactions between the molecules. Dye monomers present in the mixtures at high concentration do not appear to contribute to energy transfer to CNT. It means that the short range Dexter-type energy transfer is the more likely, in comparison with a Förster mechanism of RET, where energy can be transferred for distances up to 90 Å [114].

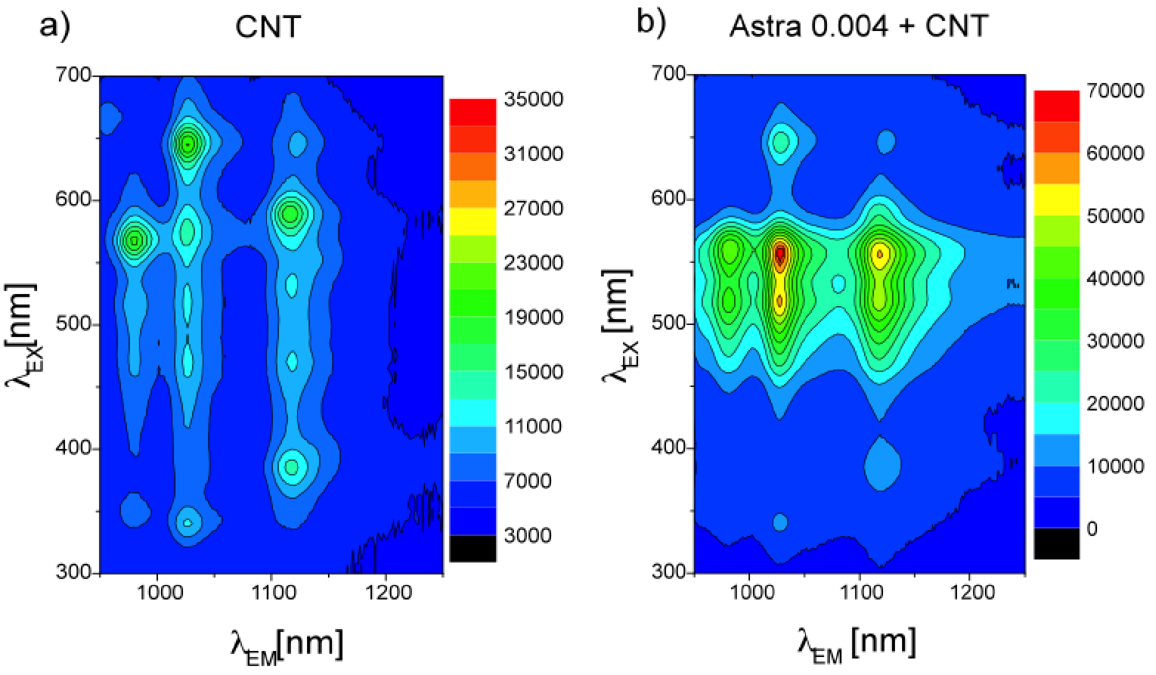

Figure 3-8 EPL maps of (a) neat CNT and (b) mixture of CNT with astraphloxin (0.004 mg/ml) in water solutions of SDBS. High PL intensities are depicted in red whereas low intensities are shown in blue. It should be noted that the PL intensities in part (a) are twice lower than that in part (b).

The enhancement in the PL peaks in the NIR range were observed as having a maximum at an excitation at 555 nm, as shown in Figures 3-9 (a) and (b).

3.4.3 Enhancement intensities of PL for SWNT dispersions are dependent on dye concentrations

To demonstrate the amplification more explicitly, PL emission spectra at excitation of 555 nm were extracted from the EPL maps as shown in Figure 3-9 (a) and (b). For astraphloxin, the maximal amplification amounting to six times is achieved at 0.004 mg/ml concentration, whereas, for Cy3, the highest amplification is four times, which is reached at Cy3 concentration of 0.002 mg/ml. In addition, the Cy3 molecule is heavier than astraphloxin one, and molar concentrations for the maximal amplification differs ($M^{[astraphloxin]}$ = 393 g/mol; $M^{[Cy3]}$ = 493 g/mol; $C_M^{[astraphloxin]} = 1x10^{-5}$ mol/l; $C_M^{[Cy3]} = 4x10^{-6}$ mol/l). This means that more astraphloxin molecules can contribute to energy transfer due to more regularity in the attachment to CNT. The tendency of astraphloxin to form J-aggregates has to be taken into account. Cy3 has a long alkyl chain, which interferes with the ordered alignment of molecules on the tubes and limits the total number of molecules able to attach to CNT.

The different dependences of PL, in the visible range (emission from dyes) and in the NIR range (emission from CNT), on the concentration of dyes in the mixtures are depicted below Figure 3-9 (c) and (d). The NIR emission tends to saturate at astraphloxin concentrations of 0.004 mg/ml of has a maximum at 0.002 mg/ml, whereas, PL in the visible range increases until the phenomenon of re-absorbance of the emission begins to prevent the effect at approximately concentrations of 0.008-0.010 mg/ml. The PL saturation or appearance of the maximum in NIR range means that the amount of the dye molecules able to attach the CNT has reached a limit. A further increase of the concentration of the dye results in the presence of free molecules of the dye that do not interact with CNT, as seen by recovery of the dye monomer peak.

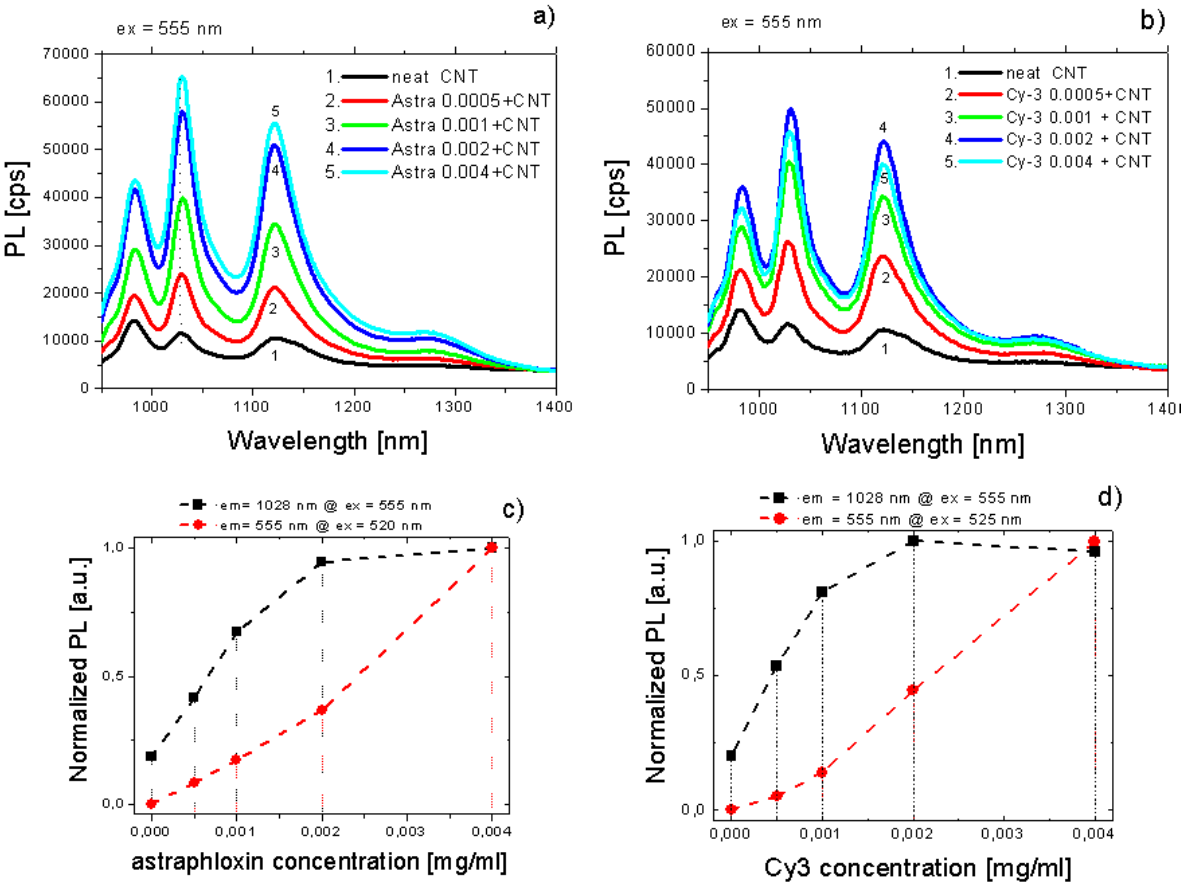

Figure 3-9 (a,b) PL spectra of neat CNT (1) and mixture (2-5) of CNT with astraphloxin (a) or Cy3 (b) dye (2 - 0.0005 mg/ml, 3 - 0.0010 mg/ml, 4 - 0.002 mg/ml, 5 – 0.0040 mg/ml). (c,d) Concentration dependence of PL for mixtures of CNT with astraphloxin (c) or Cy3 (d) dye at (λEX = 555 nm; λEM = 1028 nm) (squares, black) and (λEX = 520-525 nm; λEM = 555 nm) (circles, red).

3.4.4 SWNT dispersions with different surfactant and dye

A series of CNT dispersions with ionic surfactants (SDBS, SDS, SDOC, STDOC) were tested for interaction with astraphloxin as a step towards engineering molecular complexes with enhanced PL. Comparison of absorption spectra for neat solution of astraphloxin and mixtures with different CNT showed the emergence of new absorbance peaks for the mixtures in the range of 550 to 600 nm Figure 3-10 (a). A new explicit peak at 576 nm appears in absorption spectra of the mixtures with CNT dispersed by SDOC and STDOC, whereas the spectra of the mixtures with CNT dispersed by SDBS and SDS have a shoulder in that range. At the excitation corresponding to the new absorbance peak, a PL enhancement from CNT levels (E_{11}) can be observed for all mixtures made with anionic surfactants (Table 3-1). The maximum enhancement of PL is observed for the mixtures of astraphloxin with CNT dispersed by SDBS (Table 3-2). The maximum of excitation for PL enhancement shifts from λ_{EX} = 555 nm for SDBS to λ_{EX} = 565 nm for SDS, and to λ_{EX} = 570 for SDOC and STDOC. It should be mentioned that the mixtures of CNT dispersed by non-ionic surfactants showed no new peaks of absorbance or PL.

PL spectra show the different effect of the dyes on each type of CNT chirality revealing a selectivity of sensing for CNT of various diameters. First, the enhancement of PL strongly depends on chirality of CNT (see Table 3-1). The highest PL amplification was observed for (7,5) chirality of CNT. For SDOC and STDOC, the small tubes with chirality (6,5) did not show any PL amplification, whereas (7,5) and (8,4) CNT 'brightened' in a few times. Second, a shift of λ_{EM} was observed for CNT peaks in the mixtures strongly dependent on surfactant and chirality of CNT (see table 3-1 for details). Particular attention is drawn to CNT dispersed by STDOC, where λ_{EM} for chirality (6,5) is red shifted by 3 nm, and chiralities of (7,5) and (8,4) show a shift in λ_{EM} amounting to 11 and 12 nm respectively. This is interpreted as evidence that astraphloxin molecules are more likely to attach with CNTs having chirality of (7,5) and (8,4), because a greater shift in λ_{EM} is observed.

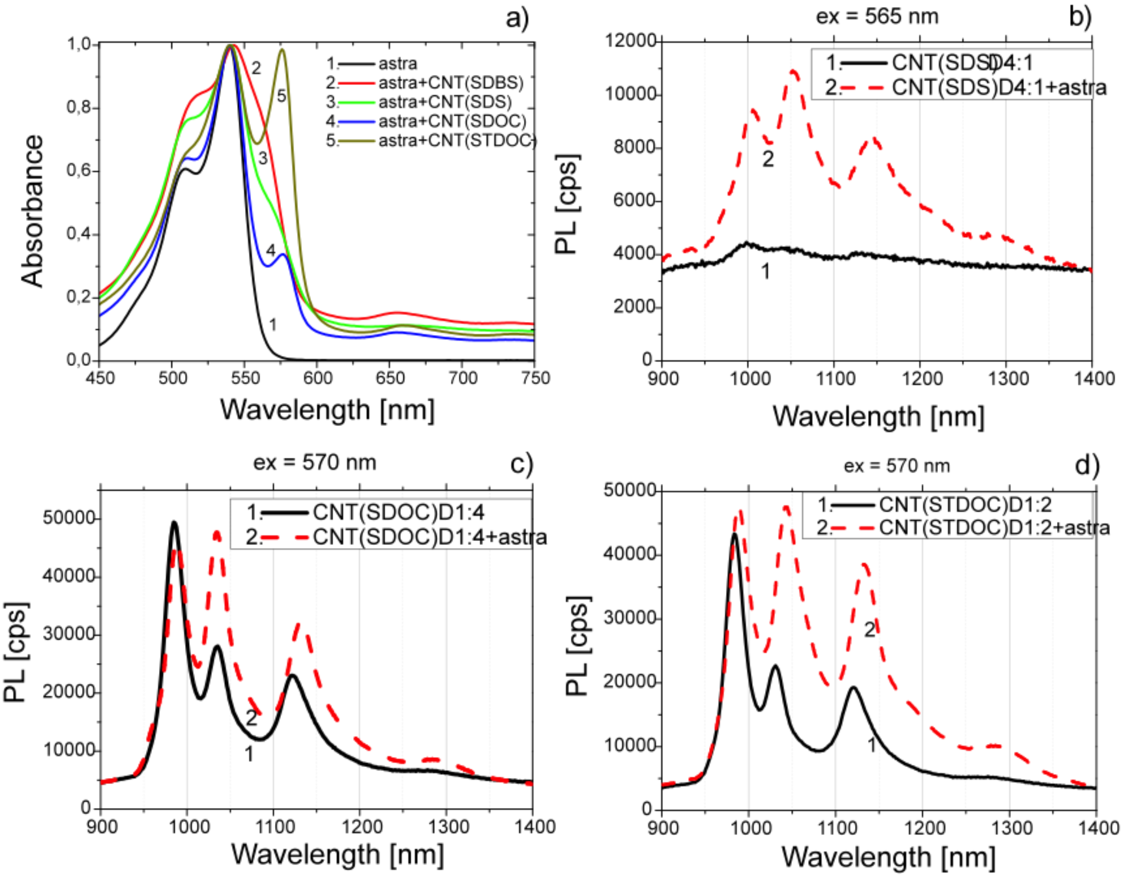

Figure 3-10 (a) Absorption spectra of water solutions for (1) neat astraphloxin and (2-5) mixtures of astraphloxin with CNT dispersed by various surfactants: SDBS, SDS, SDOC and STDOC. All spectra normalized on maximum at 540 nm, and have astraphloxin at a concentration of 0.004 mg/ml. (b-d) PL spectra of neat CNT and mixture of astraphloxin with CNT dispersions by (b) SDS, (c) SDOC, and (d) STDOC.

Table 3-1 PL peak positions for solutions of semiconductor CNT (CoMoCAT) in aqueas solution with different surfactants and astraphloxin at 0.004 mg/ml.

Parameters of CNT with chirality of	(6,5)	(7,5)	(8,4)
Diameter, [nm]	0.75	0.83	0.84
$(\lambda_{EX}$; $\lambda_{EM})$ [nm ; nm]			
CNT (SDBS)	(570 ; 982)	(650 ; 1028)	(590 ; 1121)
CNT (SDBS)+astraphloxin	(555 ; 983)	(555 ; 1030)	(555 ; 1121)
CNT (SDS)	(570 ; 1000)	(650 ; 1046)	(590 ; 1130)
CNT (SDS)+astraphloxin	(565 ; 1004)	(565 ; 1050)	(565 ; 1144)
CNT (SDOC)	(570 ; 985)	(650 ; 1034)	(590 ; 1121)
CNT (SDOC)+astraphloxin	(570 ; 988)	(570 ; 1034)	(570 ; 1131)
CNT (STDOC)	(570 ; 985)	(650 ; 1032)	(590 ; 1121)
CNT (STDOC)+astraphloxin	(570 ; 988)	(570 ; 1043)	(580 ; 1133)
CNT (Triton-X 100)	(570 ; 983)	(650 ; 1033)	(590 ; 1123)
CNT (Triton-X 100)+astraphloxin	(570 ; 989)	(650 ; 1037)	(590 ; 1126)
CNT (PVP)	(575 ; 1004)	(655 ; 1055)	(590 ; 1142)
CNT (PVP)+astraphloxin	(575 ; 1004)	(655 ; 1055)	(590 ; 1142)

Table 3-2 PL amplification or decrease in the NIR range for astraphloxin with CNT dispersed by various surfactants.

Parameters of CNT with chirality of	(6,5)	(7,5)	(8,4)	(9,5)/(8,7)
Diameter, [nm]	0.75	0.83	0.84	0.98 / 1.03
Maximum relative increase of the PL at ex = 555 nm for				
astraphloxin at 0.004 mg/ml + CNT (SDBS)	3.1 (λ_{EM}=983nm)	6.0 (λ_{EM}=1030nm)	5.2 (λ_{EM}=1121nm)	2.4 (λ_{EM} ~1270nm)
Cy3 at 0.002 mg/ml + CNT (SDBS)	2.6 (λ_{EM}=983nm)	4.1 (λ_{EM}=1030nm)	4.0 (λ_{EM}=1121nm)	1.9 (λ_{EM} ~1270nm)
astraphloxin at 0.004 mg/ml + CNT (Triton)	0.6 (λ_{EM}=989nm)	0.6 (λ_{EM}=1037nm)	0.6 (λ_{EM}=1126nm)	0.8 (λ_{EM}=1290nm)
astraphloxin at 0.004 mg/ml + CNT (PVP)	0.6 (λ_{EM}=1004nm)	0.7 (λ_{EM}=1055nm)	0.6 (λ_{EM}=1142nm)	0.9 (λ_{EM}=1290nm)
Maximum relative increase of the PL at ex = 565 nm for				
astraphloxin at 0.004 mg/ml + CNT (SDS)	2.2 (λ_{EM}=1004nm)	2.7 (λ_{EM}=1050nm)	2.1 (λ_{EM}=1144nm)	1.3 (λ_{EM} ~1290nm)
Maximum relative increase of the PL at ex = 570 nm for				
astraphloxin at 0.004 mg/ml + CNT (SDOC)	0.9 (λ_{EM}=988nm)	1.7 (λ_{EM}=1034nm)	1.4 (λ_{EM}=1131nm)	1.3 (λ_{EM} ~1285nm)
astraphloxin at 0.004 mg/ml + CNT (STDOC)	1.2 (λ_{EM}~988nm)	3.0 (λ_{EM}=1043nm)	2.4 (λ_{EM}=1133nm)	2.0 (λ_{EM} ~1285nm)

Another logical step was to test astraphloxin molecules substituted with different anionic groups from these depicted in Figure 3-5: I-624, I-673, I582, and I-841. An aim of this test was to exploit dyes with similar molecular structure but having negative instead of positive charge. In absorption and PL spectra, mixtures of the anionic dyes with CNT result in superposition of two compounds without new features. Thus, we show that the negatively charged astraphloxin analogues do not transfer energy to CNT, regardless of the anionic or neutral nature of surfactants used. This helps explain the nature of interaction between the molecules.

To confirm that the changes observed in the above systems are an effect of interaction of the dyes with CNT, two-component systems of the mixture consisting of the dye and surfactant were studied. No shifts of absorbance or PL peaks were observed after admixture of surfactant to neat solutions of the dyes. No PL features appeared in the NIR range of spectra. Thus the shift of the peaks, significant PL quenching in visible range and the amplification in NIR range, is explained by interaction of CNT with the dye molecules.

The non-radiative energy transfer process from the dyes aggregated to CNT is the most obvious explanation of the effect of PL amplification. The coulomb attraction between positively charged astraphloxins and negatively charged surfactants is thought to be responsible for the aggregation of dyes on CNT micelles. So far as CNT and polymethine dyes are pi-electron systems, the most likely way to explain the interaction between CNT and the investigated dyes is as a stack interaction, as shown in a series of papers [103,115,116]. The interaction between CNTs and dye molecules separated by surfactant molecules should decrease, but cannot be negligible.

In conclusion, macromolecular complexes PDs-CNT provide a novel ways for functionalization of carbon nanomaterials extending its remarkable multifunctional application. The nanotubes emission in the range of dye excitation was enhanced. Through the Coulomb force attracts the polymethine dye to carbon nanotube covered by ionic surfactant in water, so excitation of the dyes can be transferred to the tubes. A strong amplification of the emission from carbon nanotube energy levels in near-infrared range was observed.

Chapter 4

4. CNT Saturable Absorbers for mode locking of fibre lasers

SWNTs are the subject of extensive studies for use in photonic devices, due to the fact that semiconducting SWNTs are direct band gap materials that can be used to generate light. Additionally, the strong nonlinear optical properties of CNTs, including their ultra-fast non-radiative decay rates, allow light switching and shaping applications in the important for modern telecommunication near-IR spectral range. Thus, carbon nanotubes have been a subject of intensive studies by researchers in telecommunication and laser fields in order to demonstrate the integration ability of SWNT materials with standard fibre optics components. So far, a number of ultra-short pulse generations have been achieved in fibre lasers of 1000-2000 nm spectral range with a passive mode-locking technique using SWNTs as saturable absorbers.

4.1 Saturable Absorbers for mode locking of fibre lasers

The field of mode-locked fibre lasers (MLFL) has attracted significant interest worldwide since the early 1990s due to existing and promising applications in telecommunication, material processing, bio-medical treatment and so on. All-fibre MLLs benefit from maintenance-free operation, cost-efficiency, and easy fabrication process. The fabrication of ultra-fast MLFL is straight forward, does not require “clean room” facilities and photolithography, and, therefore, greatly decreases the cost and power consumption of production compared to SESAM. Currently such versatile laser sources primarily generate coherent light in the spectral range of 1000 - 2000 nm which can be expanded into the visible and mid-IR spectral ranges by using higher harmonics for generation, differential frequency techniques, and by excitation in the super continuum.

In order to achieve ultra-short pulse generation with MLFL, researchers need to apply mode-locking techniques which allow modulating gains and losses in the laser cavity. Initially, Kerr nonlinearities were used for these purposes, and later on artificial nonlinearity due to polarisation rotation was adopted. Although those techniques offer ultra-short pulse generation with pulse width down to tens of femtoseconds, the lasers are highly demanding in terms of laser cavity design, and environmental stability. The mode-locking of fibre lasers based on materials with saturable absorption properties gives a much simple laser design, potential for self-started regimes, and excellent stability of generated pulses.

In a simplified approximation, a saturable absorber can be considered as a two level quantum system [117,118]. For weak incident light, the material absorbs light in a linear regime according to the Beer-Lambert law [105]. A high intensity light with resonance energy close to the material's band gap energy will induce large changes in absorption and refractive index [106]. The high power light fills the excited states with carriers (Pauli blocking) and depletes the ground state, causing a decrease in absorption coefficient for light subsequently received [106]. The saturable absorption is given by [106,45]:

$$\alpha(I) = \frac{\alpha_0}{1 + I/I_s} + \alpha_{ns} \qquad (6)$$

Where $\alpha(I)$ is the absorption coefficient at intensity I, α_0 is the linear absorption coefficient, I_s the saturation intensity, and α_{ns} is a nonsaturable absorption component. The saturation intensity is defined as follows [119] :

$$I_s = h\nu/\sigma_A\tau_A = F_{sat}/\tau_A \qquad (7)$$

$$\sigma A = \alpha_0/ND \qquad (8)$$

Where σ_A is the saturable absorber's cross-section, *N*D is the density of states in the saturable absorber, and F_{sat} is the saturation fluence and τ_A is the recovery time.

The important saturable absorber parameters are the nonsaturable losses α_{ns}, saturation intensity I_s, recovery time τ_A and the modulation depth ΔT [107]. Which all parameters are directly related to the material properties of the SA. The modulation depth is a maximum absorption (or reflectivity) change between low and high incident pulse fluence [117]. It should be noted that the formed pulse of a saturable absorber is inversely proportional to the modulation depth of that SA, and thus a higher modulation depth will lead to shorter pulse duration [105].

The four major classes of saturable absorption materials existing for the spectral range of 1000 - 2000 nm are: organic laser dyes, semiconducting quantum dots (PbS, PbSe, etc), and super-lattices based on semiconducting quantum wires and carbon nanomaterials (SWNTs and graphene). Firstly, laser organic dyes have been used as saturable absorbers in the near IR spectral range, and later have been expanded into the telecoms spectral range. However, there is an issue with stability of the material and also the application of micro-cuvette device, which make them almost impossible to use in the fibre laser field. Then MLFL development significantly progressed by introduction saturable absorbers based on III-V binary and ternary semiconductors in form of multiple quantum wells (MQW), grown by molecular beam epitaxy (MBE) or metal organic vapour phase epitaxy (MOVPE) [118,120]. For reduction of recovery time, a significant amount of carrier trapping defects need to be introduced, which can be achieved by low temperature MBE growth of the MQW saturable absorber, or alternatively by utilizing post-growth ion implantation [106,108]. However there are several drawbacks in the use of MQW saturable absorbers in fibre lasers. Devices are mostly grown as laser mirrors, hence they are called semiconductor-saturable absorber mirrors (SESAMs). Such devices are well-suited to the cavity of solid-state lasers [108], while for utilization in fibre optics systems, advanced packaging by means of fibre circulators, fibre focusers or collimators is required [121,122] .

Saturable absorbers for passive mode locking in the wavelength range of 1.3 – 1.5 nm are still a challenge. SESAM, quantum dots (QD) and quantum wells (QW) are running successfully as passive mode locked at range 1 – 1.3 nm [123].

QD based-SESAMs have demanded increasing interest because of the achievement of novel SESAMs with tunable optical properties, which are possible to attain due to the strong localization of wave function leading to an atom-like density of states. Rafailov *et al*. [124] demonstrated stable mode-locking with fast recovery and achieving shorter pulse durations by using a QD saturable absorber.

Although the operational range of SESAMS has been expanded in recent years, there are several technical issues which remain. First, the bandwidth of SESAMs is very narrow, limiting the laser generation range to about 100 nm. SESAMs also have a low power damage threshold and typically need to be replaced after 5000 hours of operation in the cavity.

Very recently, PbS/Se material was used as a saturable absorber, offering huge promise for photonics. However the research is only at an initial stage with major challenges around stability of the material.

SWNTs have been utilised as an efficient saturable absorber for fibre and solid state lasers since the first demonstration in 2003. This is due to the large fraction of semiconducting tubes typically presented within the initial fraction of SWNTS. Importantly, the tube's diameter is proportional to the energy band gap. Thus SWNTs can be synthesized or sorted by means of diameter with the optical properties needed for specific applications. Moreover, the heterogeneity of material, disadvantageous in many electronic applications, gives an opportunity to generate sub picosecond pulses in very broad spectral ranges, which mostly limited by gain spectral profile of active media. Initially, it is necessary to have a high linear absorbance at the wavelength of incident light, which could be achieved by increasing the nanotube concentration within the saturable absorber. This will lead to increase in the modulation depth of SWNT saturable absorbers. However, a high concentration of SWNTs within a composite causes nanotube bundles formation, and hence an increase of scattering losses [125]. The composite surface reflection, absorption of the polymer matrix, SWNTs impurities, and the surfactant at the wavelength of use are other factors contributing to non-saturable absorption [6].

Finally, the excitonic nature of the energy transitions of SWNTs, together with fast relaxation in SWNTs bundles define a sub-picosecond recovery time for SWNTs saturable absorbers. The overall level of nonlinear absorption effects ranging from several per cent up to 30% depending on fabrication techniques.

SWNTs are usually integrated into fibre laser cavities through optically driven deposition of CNTs onto the fibre face from the SWNTs dispersion, or from a liquid polymer's composition or by sandwiching SWNT composite films in fibre connectors. The first method has certain disadvantages such as the dominant distribution of tubes around fibre core, which leads to variations in the thickness of the SWNT layer from the centre to the edge. This will significantly contribute to overall non-saturable losses. The saturable absorber in the form of SWNTs-polymer composite thin film offers a number of advantages such as controllable concentration and size of SWNTs bundles, and the thickness of the film. Also, various optically transparent polymer matrixes (such as PVA, polycarbonate, and polyimide) will offer low saturable absorption in various spectral ranges. Such composites can be simply integrated into fibre cavity by attachment to a fibre face or the surface of a D-shaped fibre with optical adhesive.

Importantly, many efforts have been directed towards evaluation of graphene saturable absorbers in similar configurations to SWNT lasers. However, the lack of stability in generation means SWNTs are still the primary choice in saturable absorption applications.

In the current chapter, advanced mode-locking regimes in Yb, Er, Tm fibre lasers are demonstrated (1000 - 1900 nm) with well-designed saturable absorbers based on SWNTs with diameter from 0.8 to 1.4 nm.

4.2 CNT saturable absorber as mode- locker for ultrafast lasers

Laser mode locking by saturable absorbers (SA) based on SWNT [50] has recently attracted a great deal of attention. An important advantage offered by SWNT-based SAs compared to semiconductor-based saturable absorber mirrors (SESAM) is in their substantially simpler and cost efficient fabrication technology [126]. In addition, over the last few years SWNTs have become more accessible and now feature diverse parameters. This stimulates research aimed both at [1] identification of the most efficient types of SWNT and the methods of their synthesis, development of optimal matrices or substrates for fabrication of SWNT-based SAs, and [2] finding the optimal operational conditions for application of SWNTs as SAs [12,127–139].

SWNTs in liquid solution as a mode locker have been little studied [12]. So far, only Dimethylformamide (DMF) solution [47] and poly-methyl-methacrylate (PMMA) [140] have been investigated for fibre laser mode locking. Il'chev *et al*. demonstrated SWNT in heavy water for erbium glass laser mode locking [141]. Although Martinez *et al*. achieved a robust design with an in-fibre microfluidic device [47], SWNT in DMF solvent may show undesired properties resulting in agglomeration of CNTs which may lead to unstable laser mode locking. In case of [140], a specialty hollow core fibre has been demonstrated for accommodating CNT to achieve an in-fibre mode locking regime. Nevertheless, the introduction of specialty fibre may create issues such as low robustness and high cost packaging. In this experiment described here a fibre laser mode locked by CNT dissolved in NMP solvent with a filled in-fibre micro-chamber is proposed and demonstrated. SWNTs dispersion can also be stabilized by additions of polymer such as polystyrene-block-polybutadiene-block-poly (methyl methacrylate) (SBM) triblock terpolymer. Such techniques play a key role in the achievement of a saturable absorber with predefined ultrafast recovery time, low saturation intensities, and non-saturable losses.

Furthermore, numerous mode-locking techniques have been developed and ultrafast pulse generation has been achieved in a wide range of wavelength bands, and SWNT-SA thin films have expanded various laser configurations.

4.3 Experimental methods and preparation

4.3.1 SWNT solution as mode- locker for ultrafast lasers

We used purified HiPco SWNTs for the preparation of the SWNT solution. The 1.14 mg of HiPco SWNTs were placed in 10 ml of NMP solvent and sonicated for one hour at 21 kHz and 250 W. In order to obtain homogeneous samples of SWNT in NMP solvent, the resulted dispersion was subjected to ultracentrifugation. 1.66 mg of SBM polymer was added to 10 ml SWNT-NMP dispersion. The SBM polymer works as a stabilizer for the dispersion. For the SWNT saturable absorber preparation with surfactant, the HiPco SWNTs were ultra-sonicated for 1 h at 170 W in NMP with the presence of Triton X-100 non-ionic surfactant. As a normal procedure for preparation SWNTs dispersion and to remove residual bundles, the dispersion was placed in centrifugation at 30 k rpm for 2 hrs.

Figure 4-1, shows the optical absorption spectra of the SWNTs -NMP dispersion with and without SBM. There is no immediate effect of SBM addition on optical absorption. However, there is a significant drop in the band intensities of samples without SBM after 1 week, while the band intensities of sample with SBM do not show any degradation in optical properties. It may be that SBM works as an efficient wrapping agent preventing the aggregation of SWNT, which is observed for samples without SBM. The multi-peak absorption in the spectral range 1000 - 1600 nm corresponds to absorption of semiconducting SWNTs with diameters ranging from 0.8 to 1.3 nm. The intensities of the bands indicate the presence of SWNTs of specific chiralities at different concentration. Although the most intense bands are centred at approximately 1200 nm and 1300 nm, the spectrum also shows strong absorption at approximately 1550 nm, which is due to the presence of SWNTs with diameters around 1.2 nm, which will be responsible for the strong saturable absorption allowing mode-locking of the fibre laser.

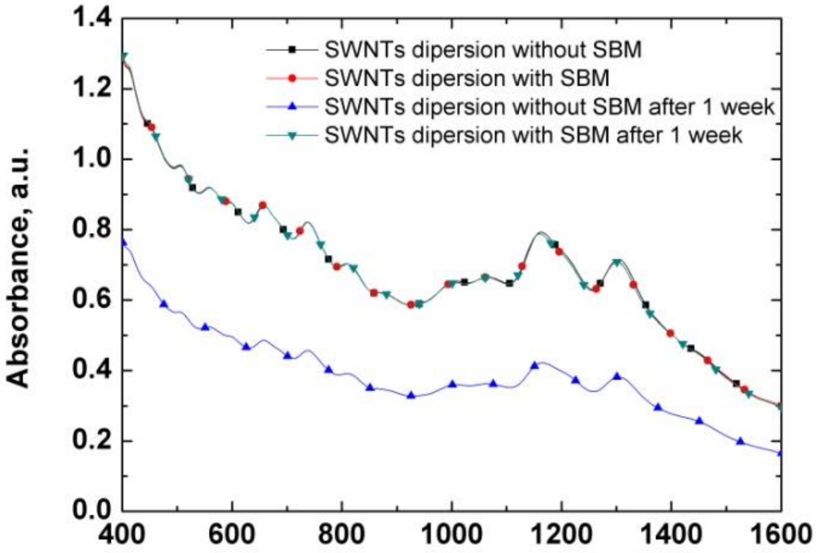

Figure 4-1 Absorption spectra for SWNT-NMP dispersion with and without SBM polymer.

To verify that the band at approximately 1550 nm represents SWNTs with diameters around 0.8 to 1.3 nm the solution was investigated by PL excitation–emission spectroscopy. The PL map in Figure 4-2 shows a number of resonance features broadly distributed between 950 and 1600 nm. The PL emission in this spectral range is due to the presence of isolated semiconducting SWNTs of different chiralities or from small SWNTs bundles [39,41]. A chirality assignment (n,m) of specific tubes was performed. The result is shown in the section 4.4.1 and confirms the presence of a large fraction of semiconducting SWNTs.

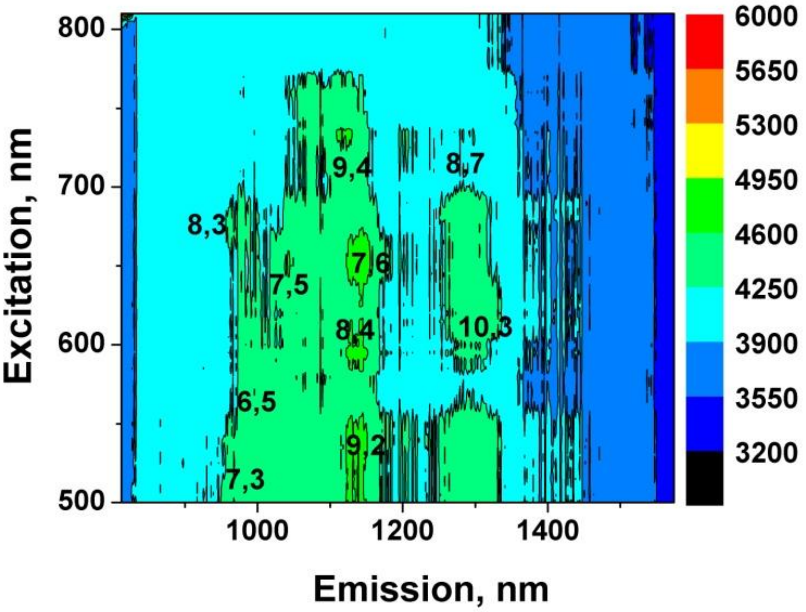

Figure 4-2 Photoluminescence map of the SWNT solution with SBM polymer.

Finally, the resulting SWNTs dispersion with SBM polymer or with surfactant was placed into the fibre micro-channel with 25 μm diameter, which is shown in Figure 4-3. The fabrication of the in-fibre micro-chamber was carried out through femtosecond laser micromachining followed by selective chemical etching of the modified area.

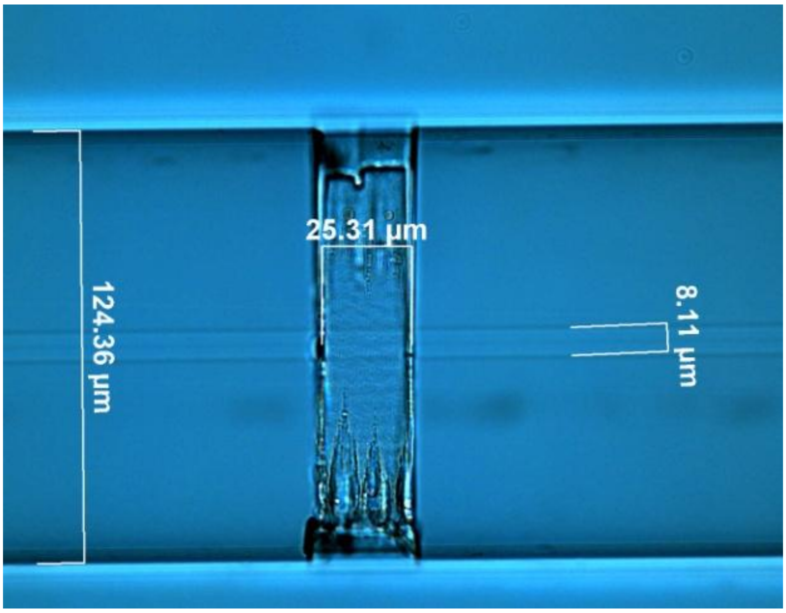

Figure 4-3 Microscopic pictures of the femto-second machined in-fibre micro-chamber in a standard SMF 28 fibre.

Figure 4-4 illustrates the schematic configuration of the CNT mode locked EDFL. The laser cavity contains approximately 1 m of highly doped Erbium fibre (EDF) as the gain medium (80 dB/m nominal absorption at 1530 nm), A 976 nm diode laser is used to pump the EDF through a 980 nm/1550 nm wavelength division multiplexer (WDM), two polarization independent fibre pigtailed isolators are employed to ensure single direction oscillation of the fibre laser operation, an in-line polarization controller (PC) is used to optimise the mode locking conditions. The total length of laser cavity with extra single mode fibre (SMF) is approximately 88 m and a 50:50 coupler is employed to couple out 50% of the laser light. An optical spectrum analyser (ANDO AQ6317B), an autocorrelator (Pulsecheck) and an oscilloscope (Tektronix) were used to study the laser characteristics.

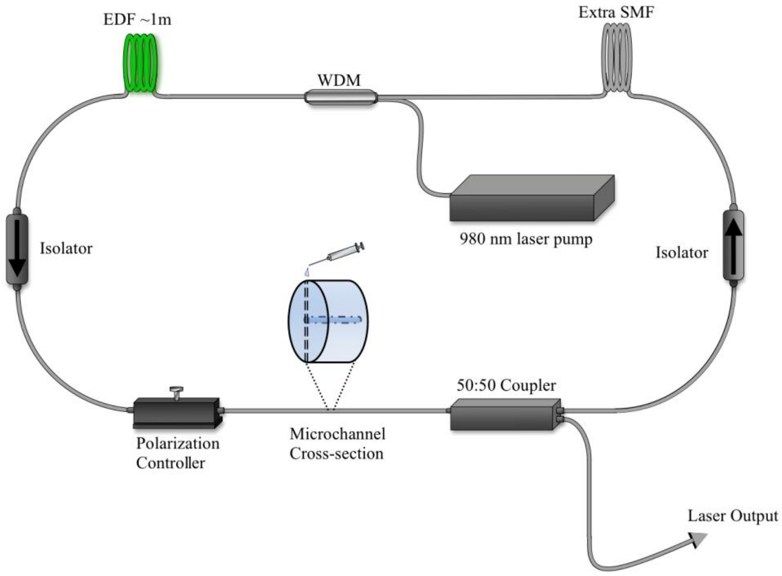

Figure 4-4 Schematic illustration of the proposed CNT mode locked EDFL.

4.3.2 SWNT composites as mode- locker for ultrafast lasers

Laser mode locking by saturable absorbers (SA) based on SWNT [50] has recently attracted a great deal of attention. An important advantage offered by SWNT-based SAs compared to semiconductor-based saturable absorber mirrors (SESAM) is in their substantially simpler and cost efficient fabrication technology [126]. In addition, over the last few years SWNTs have become more accessible and now feature diverse parameters. This stimulates research aimed both at [1] identification of the most efficient types of SWNT and the methods of their synthesis, development of optimal matrices or substrates for fabrication of SWNT-based SAs, and [2] finding the optimal operational conditions for application of SWNTs as SAs [12,127–139]. Furthermore, numerous mode-locking techniques have been developed and ultrafast pulse generation has been achieved in a wide range of wavelength bands, and SWNT-SA thin films have expanded various laser configurations.

Efficient absorption of CNTs at a specific wavelength is determined by the band gap of the specific chiralities of semiconducting single wall CNTS. To achieve efficient saturable absorption, it has been shown that the peak wavelength of the SWNT absorption spectrum should coincide with the wavelength to be used [142]. The wavelength of the absorption peak of SWNTs is controllable as a function of tube diameter [4,5]. Different kinds of SWNTs have been used (see table 1-1). SWNTs were dispersed in water by surfactant assisted sonication and the large SWNT bundles were removed by filtration through a glass microfibre filter or by being subjected to ultracentifugation for one hour at 25 k r.p.m at 17 °C. Several grams of PVA powder was added to water and dissolved. Then both resulting SWNTs dispersions were mixed at a ratio of 3:1 with the PVA solution. The prepared suspension was poured into a petri dish and the water gradually evaporated over the period of one week. The black film formed was removed from the petri dish and hence a freestanding film was obtained. By altering the concentrations of SWNT and PVA in water, the thickness and absorbance of the SWNT-PVA film were controlled. The resulting dispersion was used to produce a SWNT- composite with polyvinyl alcohol (PVA) polymer [142].

CNT PVA film saturable absorbers were used under name F-CNT PVA and C-CNT PVA for the filtration and centrifugation processed CNTs respectively. The resultant film thicknesses were 85 μm and 75 μm for C-CNT PVA and F-CNT PVA respectively. The performance of the saturable absorbers is characterized by the absorption spectrum as shown in Figure 4-5, which shows that the F-CNT PVA has higher absorption than the C-CNT PVA sample. This means that the concentration of CNTs is much higher in the F-CNT PVA sample than in the C-CNT PVA sample. As both CNT PVA samples are prepared with random orientation of CNTs, they are expected to have very low polarization dependency. Pronounced absorption at 1.5 μm can be seen in the absorption spectrum for both samples.

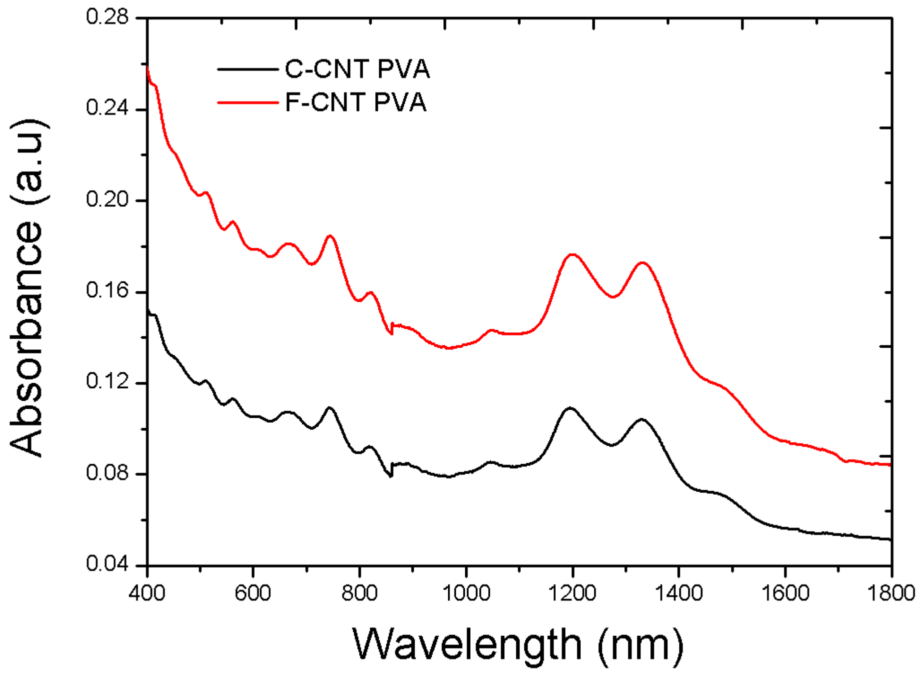

Figure 4-5 Absorption spectrum of the CNT-PVA sample [143].

Figure 4-6 illustrates the schematic configuration of the CNT mode locked EDFL. The EDFL constitutes approximately 80 cm of highly doped erbium fibre (EDF Er80-8/125 from Liekki) as the active medium, which has a nominal absorption coefficient of 80 dB/m at 1530 nm. One fibre pigtailed isolator (OIS) is employed to ensure single direction oscillation of the laser, so the laser is forward pumped through a grating stabilized 980 nm laser diode (LD) using a 980 nm/1550 nm wavelength division multiplexing (WDM) with a maximum output power of 500 mW. One set of commercial diode laser driver and controller (from Thorlabs) is employed to stabilize the performance of the pump. 50% light is coupled out the laser cavity via a standard fused fibre coupler. An in-line polarization controller (PC) is employed to optimize the intracavity birefringence of the laser cavity. The CNT mode locker was incorporated into the laser cavity via the popular sandwiched structure using two standard fibre connector ferrules, and an index matching gel (n = 1.452) was applied between the ferrules to minimize transmission loss. This pre-packaged saturable absorber is then connected into the laser cavity via fusion splicing to maintain the all fibre configuration. The total length of the laser cavity is approximately 8.4 m. This corresponds to a fundamental repetition rate of approximately 24.66 MHz and roundtrip time of approximately 40.55 ns [143].

The overall cavity dispersion is estimated to be approximately +16.8 ps/nm/km indicating an anomalous dispersion regime and respective soliton pulse formation. The output beam is characterized via a low noise photodetector (Newfocus 1 GHz), a high speed sampling oscilloscope (LeCroy Wavepro7Zi, 40 Gb/s sampling rate) and an electrical spectrum analyzer (HP8652). The pulse duration is measured by a commercial optical autocorrelator (APE PulseCheck) without any amplification and an optical spectrum analyzer (ANDO AQ6317B) is used to record the optical spectra with 0.05 nm resolution.

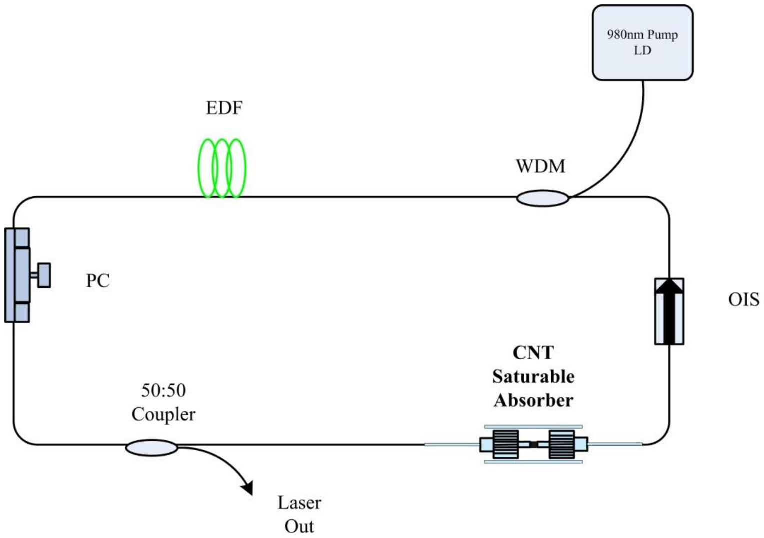

Figure 4-6 Schematic configuration of the CNT PVA based HML EDFL [143].

4.4 Results and Discussion

4.4.1 SWNT-polymer-NMP mode locked fibre lasers

A possible application of SWNTs-SBM-NMP solution as a passive mode locker in Erbium doped fibre lasers was investigated. Figure 4-7 (a) shows the optical spectrum of the mode locked fibre laser with clear Kelly sidebands indicating soliton pulse formation. This is mainly from anomalous dispersion cavity, which can support soliton pulse propagation. The central wavelength of the spectrum is approximately 1571 nm. Figure 4-7 (b) shows the measured autocorrelation trace of output pulse with a full width at half maximum (FWHM) of approximately 3.93 ps, indicating a pulse duration of approximately 2.55 ps.

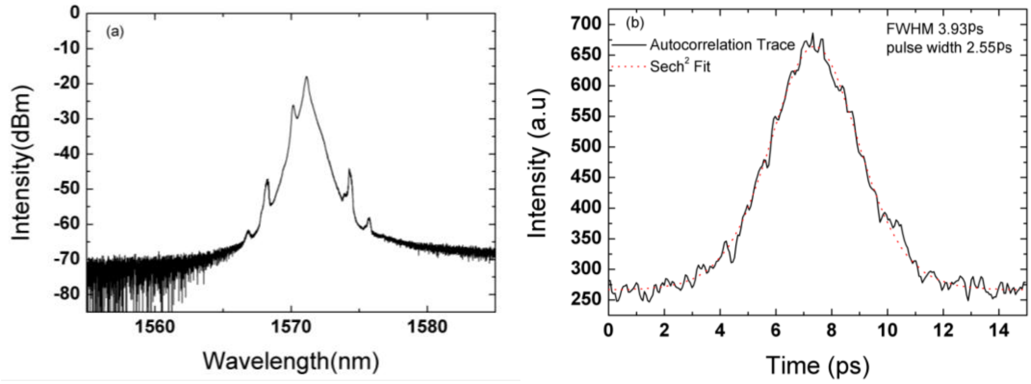

Figure 4-7 (a) Output optical spectrum, (b) Autocorrelation trace.

A typical mode locked pulse train was observed from the oscilloscope as shown in Figure 4-8. This also shows that the laser operates at its fundamental repetition rate of approximately 2.3MHz with a pulse interval of approximately 428 ns. Therefore, a SWNTs-SBM NMP solution facilitated ultrafast mode locked fibre laser with pico-second output pulse duration has been demonstrated. However, the laser based on a mode-locker with SWNT-SBM-NMP dispersion provides shorter pulses compared with one previously described employing a dispersion of SWNT-Triton X 100-NMP dispersion as a mode-locker, generated pulses with duration 5 ps [144]. Furthermore, the output power of the laser in this experiment was approximately 37 mW, which is much higher than using a conventional saturable absorber such as a semiconductor saturable absorbing mirror (SESAM) or CNT embedded polymer matrix.

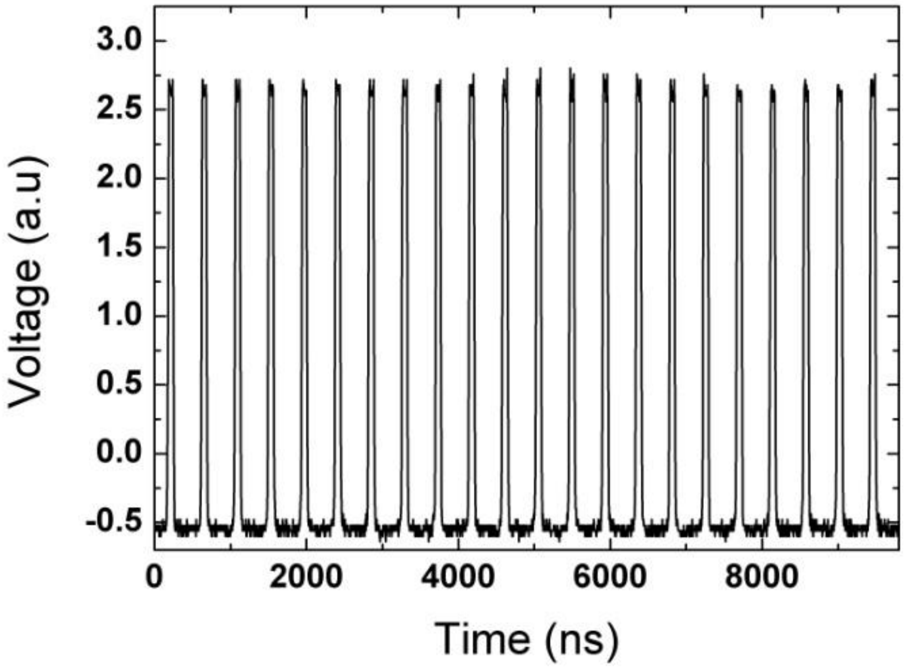

Figure 4-8 A typical output pulse train with approximately 2.3MHz repetition rate.

4.4.2 Polarization insensitive in-fibre mode-locker based on CNT-NMP

This type of low loss saturable absorber shows stable generation of a soliton pulse while maintaining capability to dissipate heat hence leading to stable high energy pulse generation. One important property of this type of mode locker is polarization insensitivity. Previously, a tapered fibre based polarization insensitive mode locker had been reported [48] for polarization insensitive mode locking. However, the in-fibre micro-chamber based saturable absorber has advantages which could preserve the mechanical strength, geometry, and polarization insensitivity. The presence of metallic tubes amongst SWNTs bundles is important for realization of the ultrafast absorption recovery (<1 ps), because in bundles containing both metallic and semiconducting SWNTs, non-radiative relaxation is achieved by charge tunneling from semiconducting to metallic tubes [44].

The absorption spectrum of CNT solution subtracted from the absorption of pure NMP is shown in Figure 4-9. It shows the typical multi-peak structure between 1000 and 1600 nm, which corresponds to the absorption of semiconducting SWNTs with a diameter distribution between 0.8 and 1.3 nm. No obvious agglomeration of CNTs has been observed even during observation over several months.

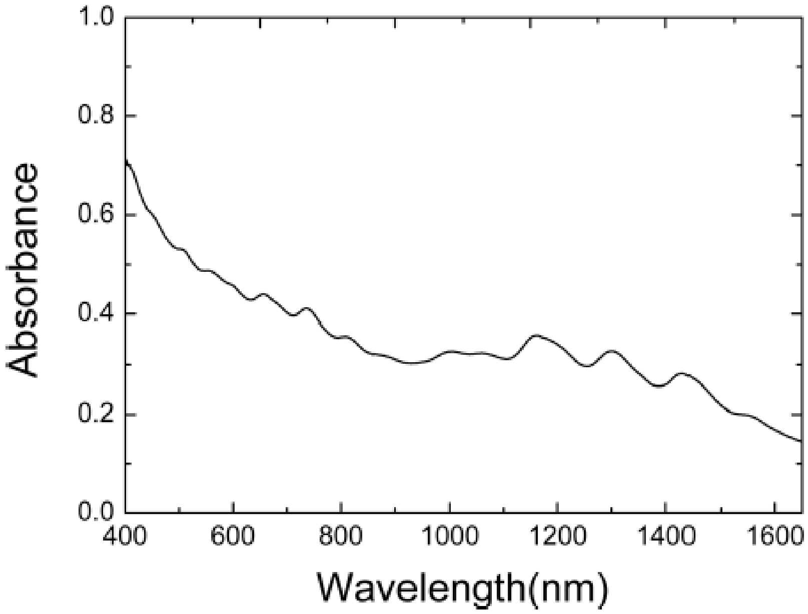

Figure 4-9 Absorption spectrum of the CNT-NMP saturable absorber measured by a wide band spectrometer [145].

Figure 4-10 shows the measured insertion loss (IL) and polarization dependent loss (PDL) of the micro-chamber with and without the CNT NMP solvent. The micro-chamber exposed in the air shows an approximately 3 dB insertion loss. The oscillation appeared across the spectrum range from the Fabry-Perot effect produced by the two edges of the micro channel shown in Figure 4-3. When the CNT-NMP solvent is inserted onto in the micro channel, it is clearly seen that the insertion loss has decreased to approximately 0.5 dB with alleviation of the Fabry-Perot effect. This is due to the refractive index matching the induction of the solvent. It further indicates a low loss saturable absorber.

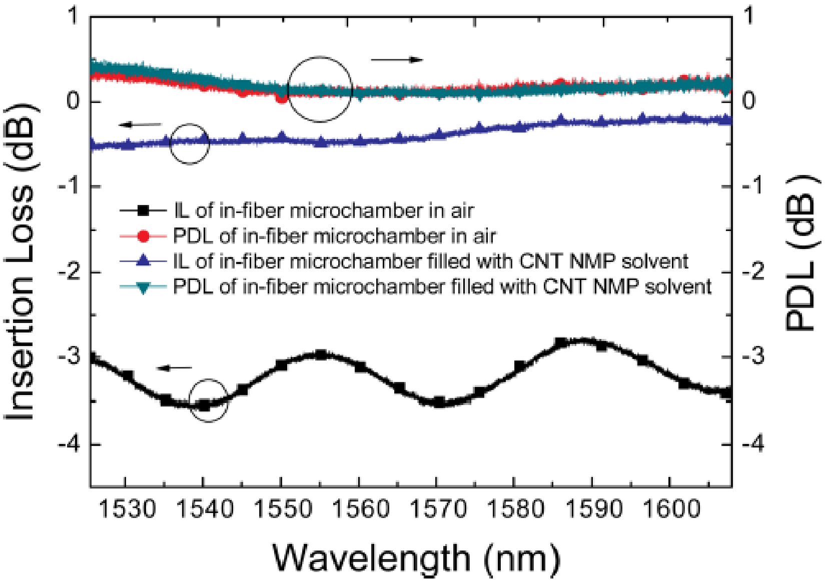

Figure 4-10 Measured IL and PDL of the in-fibre micro channel when it exposed to the air and filled with CNT NMP solvent [145].

Figure 4-10 also shows the PDL of the device, which is less than 0.5 dB across the whole wavelength range from 1520 nm to 1600 nm. This proves that the saturable absorber is polarization insensitive. Figure 4-11 shows a typical output optical spectrum of the EDFL centered at approximately 1564 nm with a spectral bandwidth at a full width half maximum (FWHM) of approximately 0.24 nm. The Kelly side bands indicate fundamental soliton shape of the output pulses.

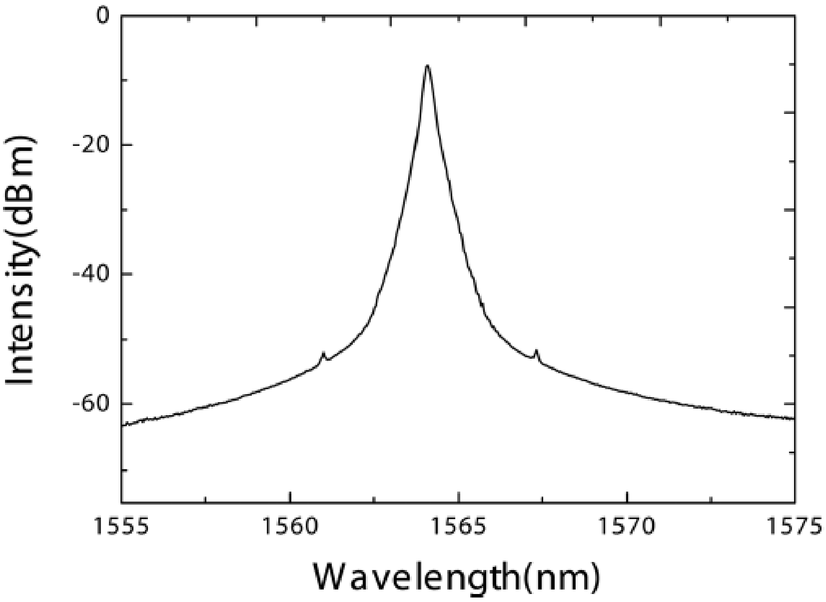

Figure 4-11 Output optical spectrum with pronounced Kelly side bands indicating soliton pulse shape [145].

The output pulses were then directly fed through a commercial autocorrelator without any pre-amplification. The measured autocorrelation trace corresponding to the pulse duration of approximately 3.37 ps is shown in Figure 4-12.

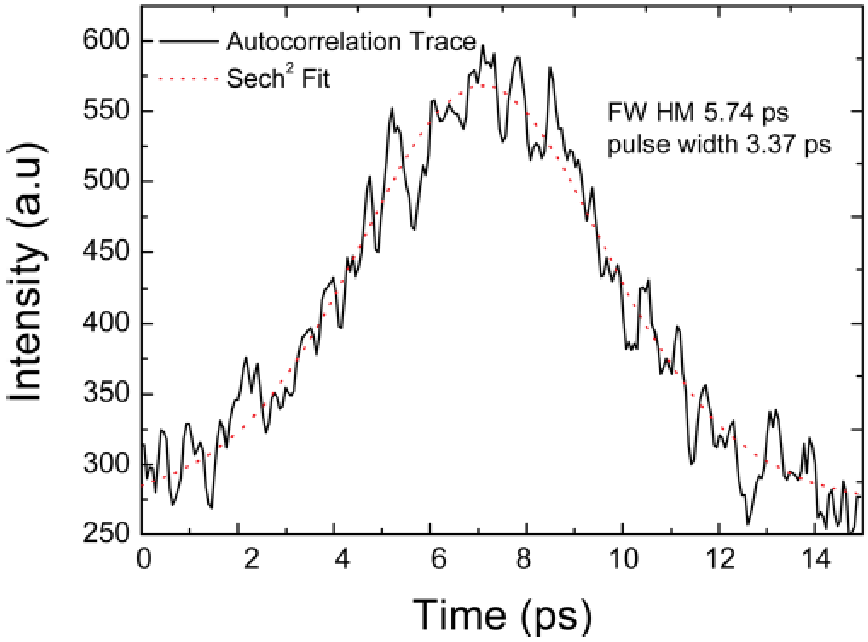

Figure 4-12 Measured autocorrelation trace of the output pulse showing pulse duration of ~3.37 ps [145].

A typical pulse train is shown in Figure 4-13 with approximately 428 ns interval between the two adjacent pulses, giving a repetition rate of approximately 2.3 MHz. The EDFL is pumped at approximately 300 mW which allows approximately 29 mW output power corresponding to an energy of approximately 12.4 nJ. It should be noted that this is a much higher level than the fibre laser mode locked by a solid format CNT previously reported [48].

The result further confirms that CNT solvent is feasible for a high energy mode locked fibre laser [47]. It was also found that CNTs dispersed in NMP solvent are not apt to agglomerate, as samples are still able to mode lock fibre lasers after several months.

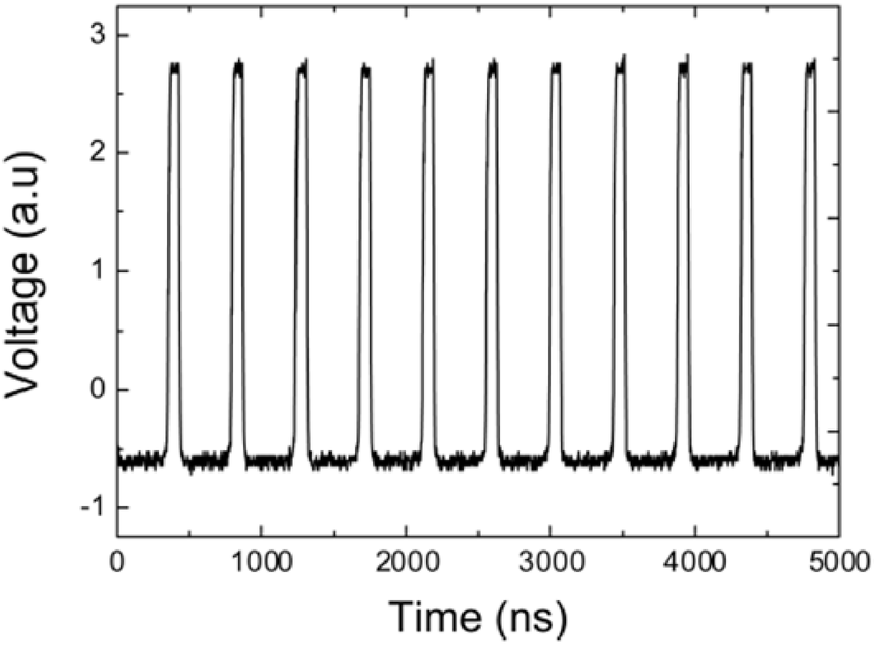

Figure 4-13 A typical pulse train of the EDFL with a repetition rate of approximately 2.3MHz showing a pulse interval of approximately 420 ns [145].

The mode locker fibre laser was operated for more than 24 hours in laboratory conditions, with no obvious fluctuations observed for either the optical spectrum or pulse duration. However, one major issue for such kind of saturable absorber is the evaporation of NMP and moisture adsorption in the solvent. Therefore, in a case where the saturable absorber has to be exposed to air for a long time, (weeks or months) the evaporation and moisture adsorption would be able to affect the thermodynamic equilibrium in the solvent, resulting in CNT aggregation. Hence, this may induce significant scattering loss in the laser cavity which would be detrimental to the laser mode locking. It may be that with proper packaging, a highly stable high energy mode locked fibre laser made from CNT in NMP solvent will have many applications in the future.

4.4.3 Passively harmonic mode locked erbium doped fibre soliton laser with carbon nanotubes based saturable absorber

Recently, SWNTs have attracted a lot of attention due to their high optical nonlinearity and fast recovery time as a saturable absorber in a mode locked erbium doped fibre laser (EDFL) [43,127,146]. Since then, various techniques and configuration have been investigated as CNT mode lockers in EDFL. CNTs embedded in various kinds of polymer matrix as a mode locker have been extensively studied [12,36,147–152] including high power [153], wavelength tunable [154] and pulse duration tunable [155] lasers. Passive mode locking has been extensively used and studied to generate ultra-short pulses in fibre lasers. To generate high repetition rate pulses in mode locked fibre lasers, one could employ either a short cavity (which could be centimeter scale) or harmonic mode locking (HML). Although a short cavity fibre laser would provide robust design and compact configuration, those do rely on a short piece of high gain fibre which inherently limits the output power of the laser and makes them cumbersome to manipulate. HML, however, removes the difficulty in dealing with centimetre scale fibber devices while maintaining a high repetition rate performance. A 10 GHz repetition rate soliton fibre laser was demonstrated based on HML through nonlinear amplifying loop mirror [156]. Nonlinear polarization rotation (NPR) based HML soliton fibre lasers have been demonstrated showing a sub-picosecond timing jitter around the 500 MHz repetition rate [157,158]. A hybrid SA-based HML fibre laser has also been studied indicating the possibility of hundreds of HML orders at a GHz rate [159].

A stable 2.6 GHz HML fibre laser using a short piece of high gain fibre with a semiconductor saturable Bragg reflector has also been reported [160]. A 3 GHz HML double cladding fibre laser with 54 mW output power has been demonstrated recently using NPR [161]. This investigation of a CNT-PVA film based HML of an EDFL uses the direct contact method. Based on the different preparation procedure of the CNT-PVA samples, we have evaluated the performance of filtrated and centrifugated CNT-PVA film in an EDFL for passive HML. The demonstrated laser is able to show stable operation at its 10th harmonic, a 245 MHz repetition rate, with an output power of approximately 12 mW. In particular, the filtration-prepared CNT sampled mode locked EDFL shows a relatively low timing jitter of below 10 ps at almost all harmonic orders. We have also characterized the time bandwidth products (TBP) of the laser with both samples at all harmonic orders showing pulse chirp properties.

The laser behavior with the F-CNT PVA saturable absorber was examined first. The laser mode locking self-started at a pump power of approximately 42.5 mW with a fundamental repetition rate of approximately 24.66 MHz regardless its initial polarization status. The higher threshold compared to some previous results may be due to the high gain fibre and higher output coupling ratio [162,163]. As pump power is increased, the laser repetition rate continues to increase with multiple integers of the fundamental frequency indicating HML. At lower harmonic orders (2nd & 3rd), stable pulsing can be found by simply increasing the pump power.

For harmonic orders greater than 3, stable pulsing may be achieved by tuning the PC. Figure 4-14 (a) shows the evolution of the optical spectrum of the laser output from the fundamental frequency to the 9th order HML with a bandwidth around approximately 4 nm and central wavelength of approximately 1563 nm. The characteristic Kelly side bands can be observed throughout the increase of pump power indicating soliton pulse shaping for all orders of HML. Timing jitter is a critical parameter for HML fibre lasers. In order to characterize the timing jitter, a method similar to previous researchers [164] was used to perform the measurement. A 3 dB coupler was used to feed 50% of the laser output to another identical photodetector that connected into the second channel of the oscilloscope as a data clock. The timing jitter was then calculated by the built-in program of the oscilloscope. The measured timing jitter at 221 MHz, 9th harmonic order was approximately 4.8 ps. The 9th HML laser was stable at this pump power without any noticeable degradation of performance under laboratory conditions for several minutes. Figure 4-14 (b) plots the timing jitter and output energy against the harmonic order. In Figure 4-14 (b), one can see that the timing jitter is below 10 ps for all harmonic orders while the output pulse energies are from 35 to 56 pJ which is higher than the energies previously reported [33,34]. Figure 4-14 (c) shows pulse duration and time bandwidth product (TBP) as a function of the harmonic order. It is shown in Figure 4-14 (c) that at all harmonic orders, the pulses are slightly chirped with a pulse duration of approximately 1 ps. Figure 4-14 (d) shows the radio frequency (RF) spectrum of the 9th order HML laser pulses with 221 MHz repetition rate at 141 mW pump power. In the RF spectrum, the background noise (SNR) was suppressed by 68 dB while the supermode suppression (SMSR) ratio was approximately 40 dB. The measured pulse duration was approximately 0.877 ps with an average output power of approximately 12.38 mW. This output power is an order of magnitude higher than the previous result [162]. The 3 dB bandwidth of the output optical spectrum is approximately 3.89 nm indicating a TBP of approximately 0.41 of the output pulses. This value is slightly higher than the theoretical transform-limited value of 0.32 for soliton pulses, which shows that the pulse is chirped. For all orders of HML, the measured SMSR from RF spectra are between 30 dB and 40 dB. At 156 mW pump power, the laser can operate at its 11th HML but with a higher timing jitter approximately 27 ps. It has been observed that multiple pulsing instability occurs when the pump power is further increased. The F-CNT PVA sample also suffers potential thermal damage at pump power levels beyond this point due to its polymer nature. Once the stable HML condition is found, it was observed a hysteresis phenomena due to soliton stability while decreasing the pump power, which means the harmonic order is maintained to a certain level during the pump power alleviation process [165] it has been previously observed.

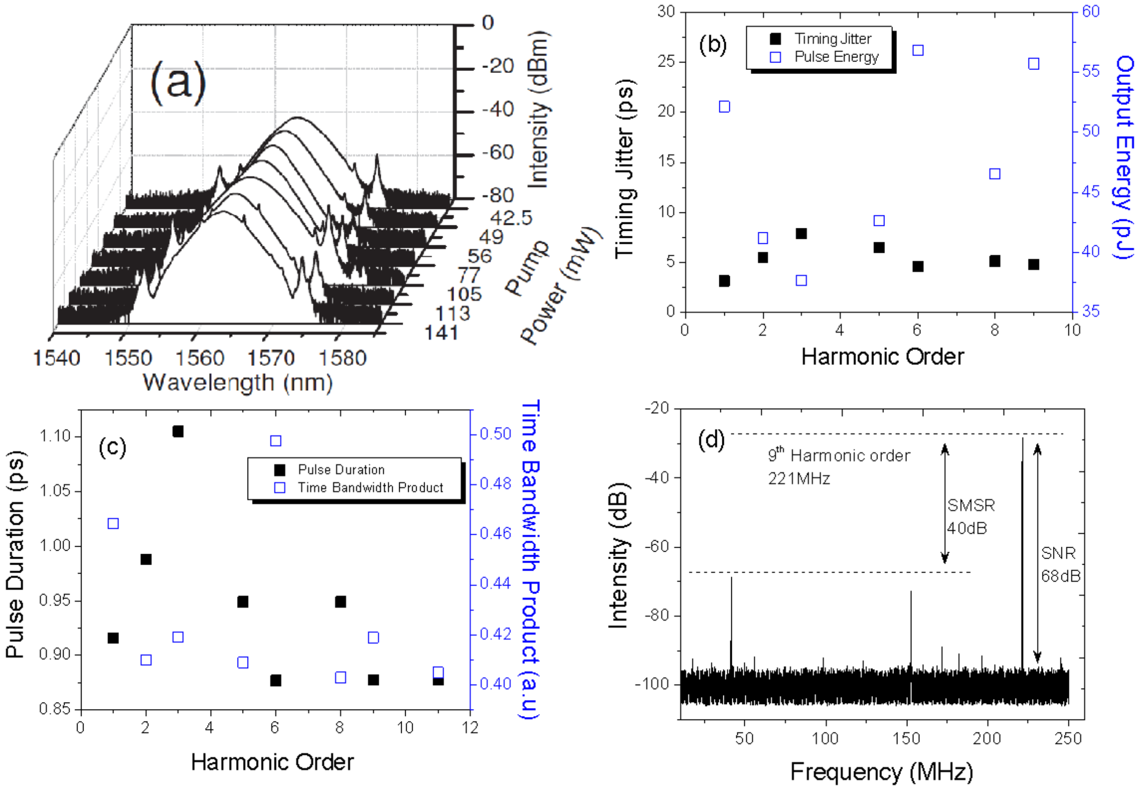

Figure 4-14 F-CNT-PVA mode locked EDFL (a) Evolution of optical spectrum under different pump power; (b) measured timing jitter (black solid square) and output energy (blue empty square) against the harmonic order; (c) measured pulse duration (black solid square) and time bandwidth product (blue empty square) over the harmonic order; (d) measured RF spectrum of the 9th HML at 221 MHz [143].

Next the C-CNT-PVA sample was examined for HML in the same EDFL by replacing the F-CNT-PVA sample with C-CNT-PVA at the end of the fibre ferrule. The laser showed the same threshold level and fundamental repetition rate. The laser with C-CNT-PVA could support a maximum of 10 harmonic orders at a pump power of 141 mW showing a repetition rate of 245 MHz. Figure 4-15 (a) shows the evolution of the optical spectrum of the laser from the fundamental frequency to its 10th harmonic order.

A similar central wavelength of 1563 nm is described compared to the laser with F-CNT-PVA sample. The SMSR for all harmonic orders with C-CNT-PVA is between 39 dB and 49 dB. The timing jitter and output pulse energy against the harmonic order are depicted in Figure 4-15 (b). Figure 4-15 (b) indicates that with the C-CNT-PVA sample, the EDFL shows a similar timing jitter performance and slightly lower output pulse energy compared to the F-CNT-PVA sample based laser. It can be seen that for the 7th order HML, the timing jitter is approximately 16 ps, which is much higher than the other harmonic orders. The reason for this is still unknown. In Figure 4-15 (c), the pulse duration and TBP against the harmonic order are illustrated which shows the C-CNT-PVA sample based EDFL outputs at similar pulse duration with slightly lower chirp. Figure 4-15 (d) shows the RF spectrum of the EDFL at its 9th harmonic order with 221 MHz repetition rate. At the 221 MHz repetition rate, the EDFL presents a SMSR of 40 dB with a SNR of 48 dB. Multiple pulsing was also observed when the pump power was in excess of 141 mW for the C-CNT-PVA sample. Further driving of the pump power may induce thermal damage to the CNT sample.

As described previously, the harmonic order is defined by the pump power and is limited to around 10. Confirming the discussion of pervious researchers [163], the evanescent field based CNT saturable absorber is able to support much higher harmonic orders. However, the CNT polymer films have the advantage of ease of manipulation and low cost. It is expected that a higher repetition rate could be mode locked by the CNT polymer films when cavity dispersion is properly managed. Moreover, the concentration of CNT may also affect the HML. For both samples, at its maximum harmonic order, the laser is stable for a few minutes, and this could have been because the high pump power damaged the PVA film which caused degradation of the CNT sample. For lower harmonic orders, with both samples, the laser gave stable performance over a duration of hours under laboratory conditions.

The principle of harmonic mode locking is still under debate. Grudinin *et al* [159] proposed that an acoustic effect plays an effective role in laser harmonic mode locking. Kutz *et al* [166] justified that the gain recovery could dominate the behavior of harmonic mode locking.

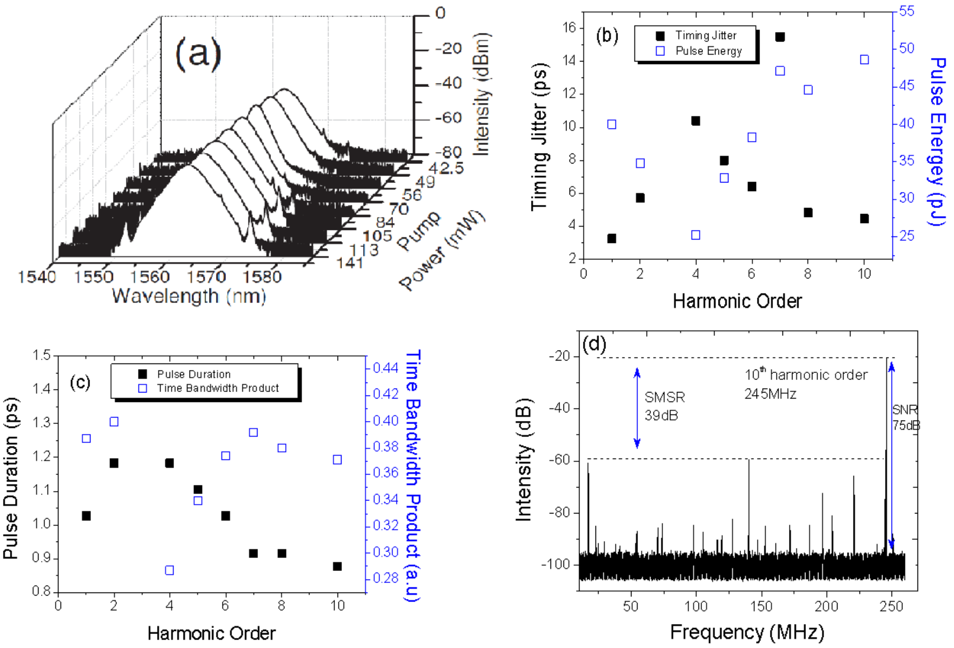

Figure 4-15 C-CNT-PVA mode locked EDFL (a) evolution of optical spectrum under different pump power; (b) measured timing jitter (black solid square) and output energy (blue empty square) against the harmonic order; (c) measured pulse duration (black solid square) and time bandwidth product (blue empty square) over the harmonic order; (d) measured RF spectrum of the 9th HML at 245 MHz [143].

4.4.4 Spectrum-, pulse width-, and wavelength switchable all-fibre mode-locked Yb laser with fibre based birefringent filter

Control of spectral width and pulse duration of the SWCNT mode locked Yb fibre laser were investigated using fibre Lyot filter (FLF) [167]. It is important that there are fewer possibilities for controlling pulse duration in all-fibre mode locked Ytterbium lasers in comparison with all-fibre mode-locked Erbium lasers, since there are no standard and commercially available non-expensive fibres with anomalous dispersion for the 1–1.1 μm spectral range. Compensation of positive dispersion in all-fibre Yb laser cavities is done either by using specialty fibres such as micro-structured fibre [168], long period gratings in higher order mode fibre [169], tapered fibre [170], or hollow-core photonic band-gap fibre [171] or by means of chirped fibre Bragg gratings also acting as spectral filters [172,173]. Although these methods provide the possibility of control over pulse duration, they suffer from different drawbacks: *e.g.* effective splicing micro-structured fibre to standard fibre is still an issue; and the tapered fibre core immediately exposed to the air may cause extra loss.

Figure 4-16 shows the schematic diagram for the all-fibre Yb ring laser. The laser cavity was constructed using standard single-mode fibres based components. Approximately 30 cm of single-mode Yb fibre with 1200 dB/km absorption at 975 nm was employed as the gain medium. Pump injection and single direction oscillation of the laser was performed by an integrated a wavelength division multiplexer with built-in optical isolator (IWDM). A 70/30 fused coupler was used to tap out the radiation from the ring resonator. The SA was represented by a polymer film containing SWNT. One piece of PM fibre was added between the IWDM and SA to serve as a fibre based Lyot filter if the cavity also consisted of elements with PDL. In the cavity PDL was inserted by fused IWDM and fused coupler. An in-line PC was used to fine-tune the birefringence of the laser cavity, which can otherwise lead to changes in a mode-locked regime. The total length of the laser cavity is 2.7 m corresponding to a fundamental repetition rate of 77 MHz.

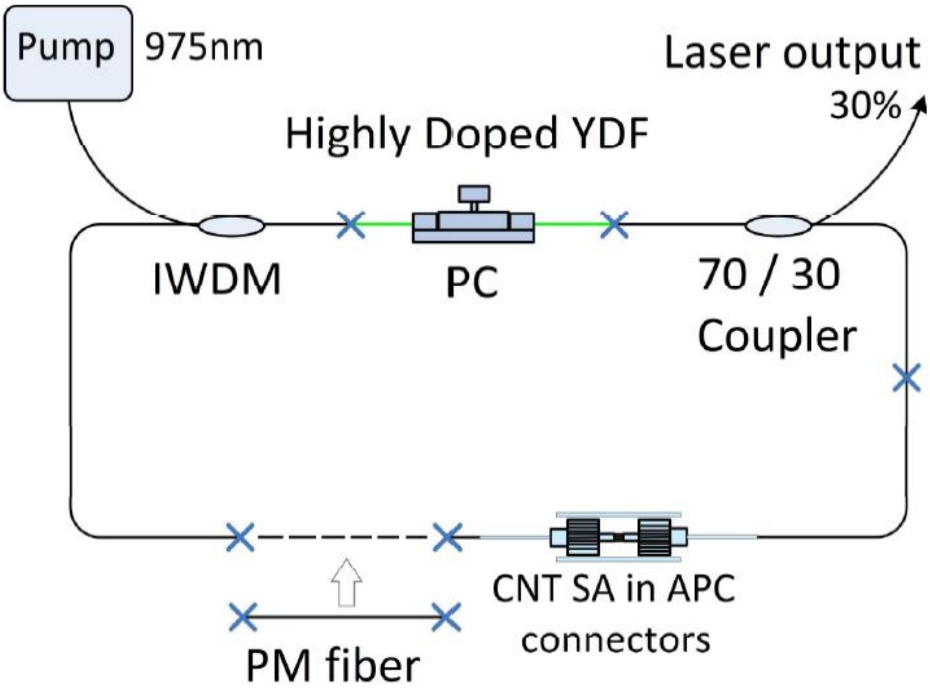

Figure 4-16 Diagram of the all-fibre mode-locked Yb laser. Cross marks indicate fibre splices [174].

The absorption spectrum of the SWNT sample subtracted on absorption of PVA is shown in Figure 4-17. Two near-IR bands centred at 1030 and 1160 nm, which typically indicate presence of semiconducting SWNTs with diameters ranging between 0.9 and 1.1 nm. The band at 1030 nm has a FWHM of approximately 100 nm and linear absorption around the working wavelength of the laser at 30% level. The fabricated film was clamped between two angled fibre connectors with index matching gel to minimize Fresnel loss.

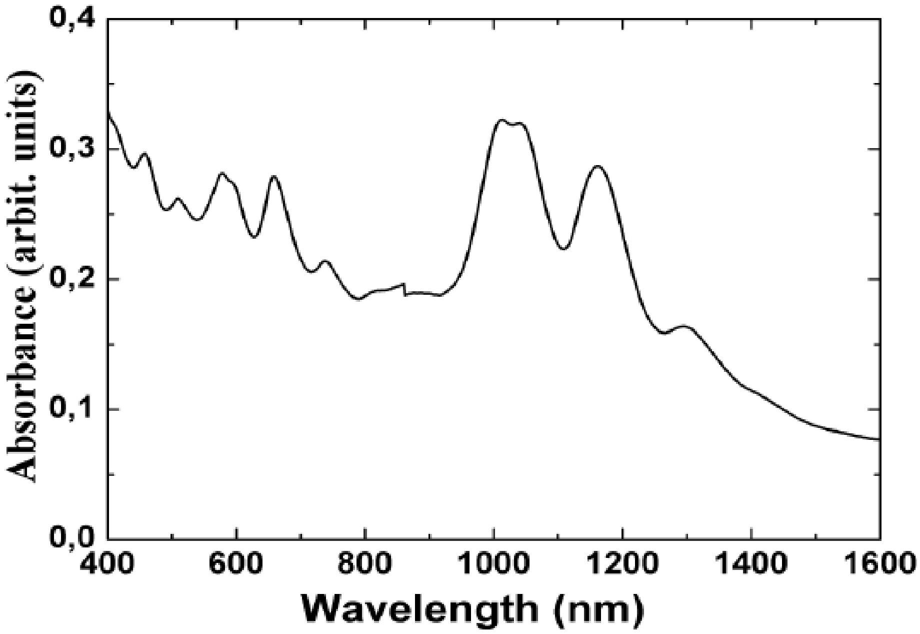

Figure 4-17 Absorption spectrum of SWNT sample [174].

Stable single-pulse mode-locked generation was achieved at 75 mW of pumping power. As the pumping level further increased, multi-pulsing was observed followed by Q-Switching. The average output power of the laser was 1–2 mW depending on the settings of the PC which defines the properties of the fibre filter. Without the PM fibre in the cavity, the measured full width half maximum (FWHM) of the spectrum was approximately 1.2 nm. Figures 4-18 (a) and 4-18 (b) demonstrate a laser output spectrum and pulse trains in a configuration without the PM fibre. Generation around the wavelength 1064 nm is explained by the transmittance of IWDM that we used.

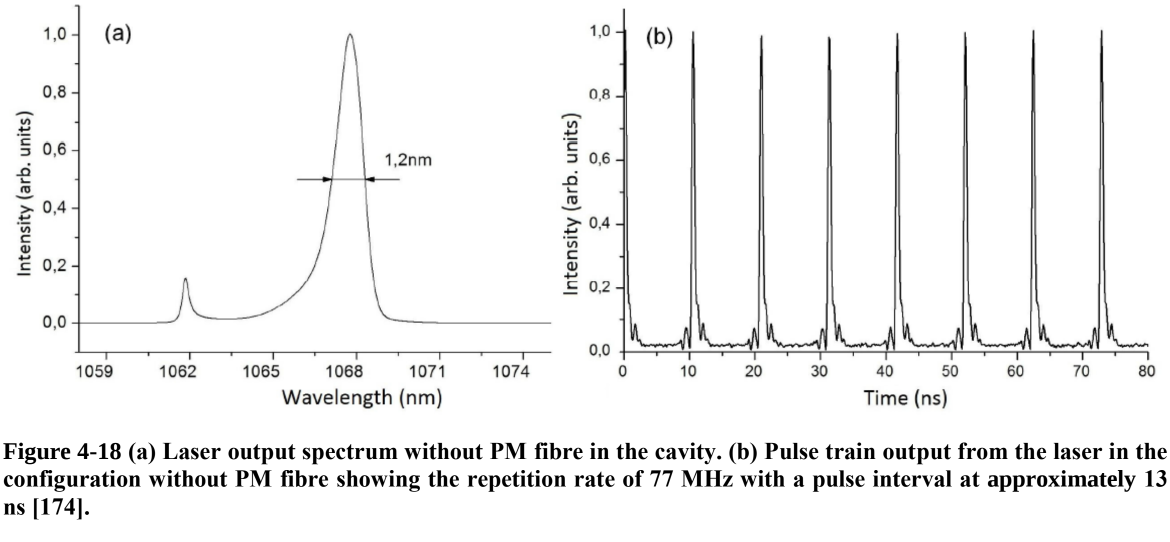

Figure 4-18 (a) Laser output spectrum without PM fibre in the cavity. (b) Pulse train output from the laser in the configuration without PM fibre showing the repetition rate of 77 MHz with a pulse interval at approximately 13 ns [174].

To study the impact of the fibre Lyot filter on the output spectrum and the pulse duration of the Yb fibre laser, the effects of various lengths of PM fibre were studied. The total cavity length was increased to 4.2 m and the replacement of FLF was performed as follows. After a section of PM fibre was spliced into the laser cavity, a piece of standard fibre of the same length was removed to maintain a constant cavity length and dispersion. By tuning the PC, modes of the laser could be easily locked. The output spectra of the laser with PM fibre sections 1, 1.5, and 2 m are presented in Figure 4-19, Figure 4-20 and Figure 4-21. It can be observed that at a fixed length of the PM fibre, tuning the PC allows tuning of the laser output wavelength. This tuning is particularly significant for the shortest length of PM fibre (1 m). At the shortest length of PM fibre, as predicted by our numerical calculations, we obtained the broadest output radiation spectra from the laser: 0.9–1.26 nm. As the PM fibre length increased to 2 m, the radiation spectrum contracted to 0.15–0.31 nm. Each curve in Figures 4-19 corresponds to an output radiation spectrum measured in mode locked operation, Figure 4-20 clearly demonstrates the dependence of output spectral width upon the setting of the PC at a fixed length of the PM fiber within the laser cavity.

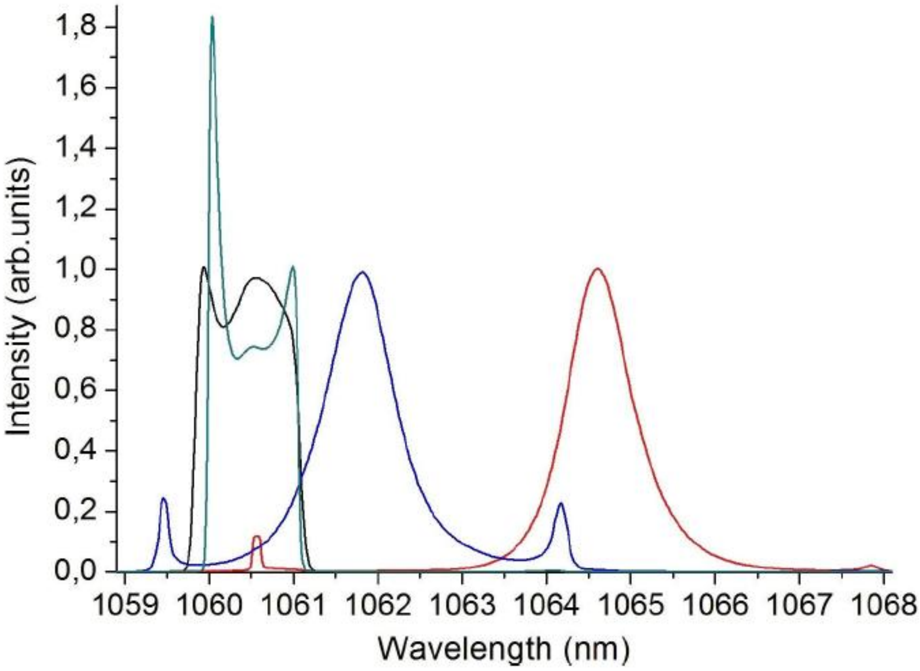

Figure 4-19 Output spectra of the Yb laser mode locked at different settings of the PC showing different FWHM with 1 m PM fibre in the laser cavity [174].

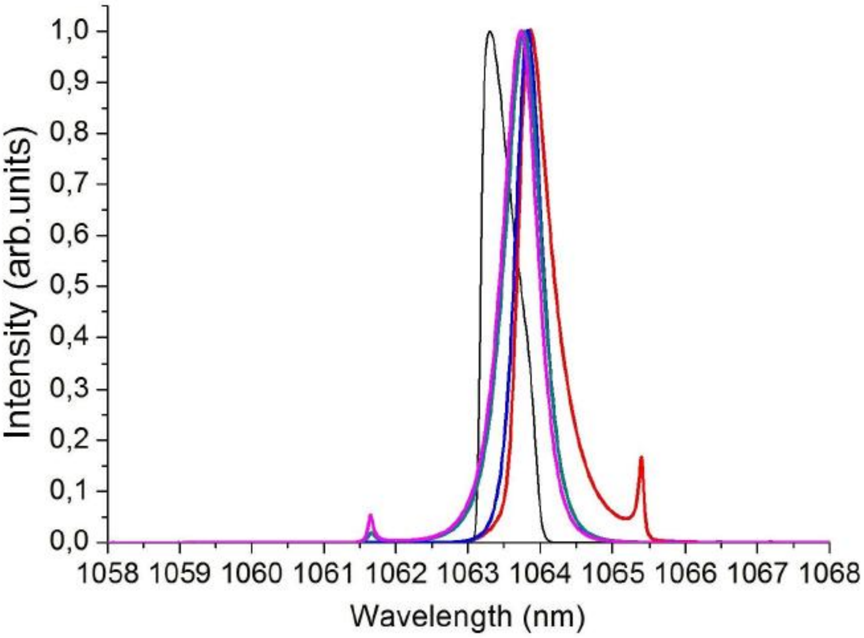

Figure 4-20 Output spectra of the Yb laser mode locked at different settings of the PC showing different FWHM with 1.5 m PM fibre in the laser cavity [174].

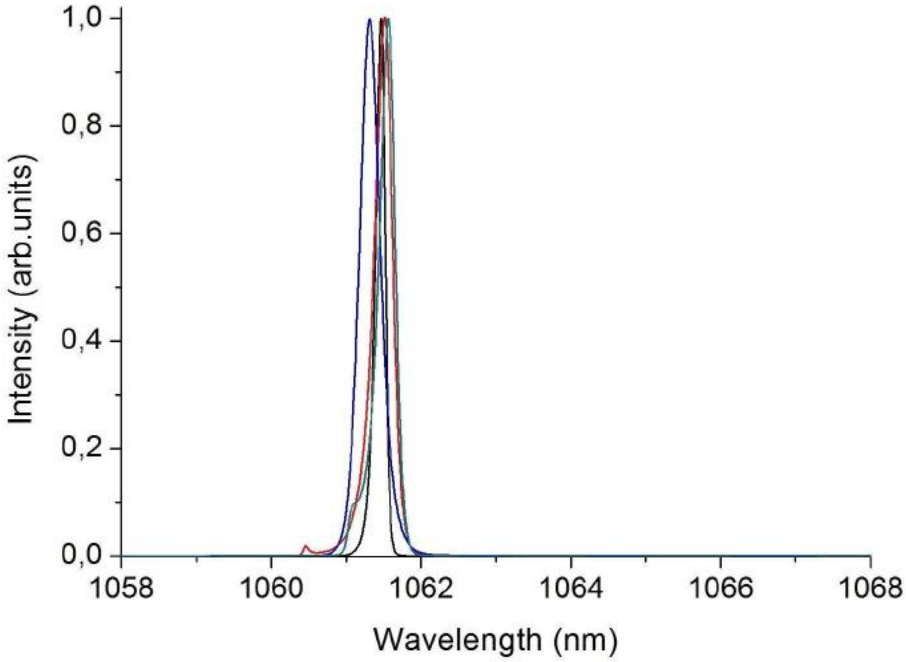

Figure 4-21 Output spectra of the Yb laser mode locked at different settings of PC showing different FWHM with 2 m PM fibre in the laser cavity [174].

Experimental data in Figure 4-21 clearly demonstrate the dependence of output spectral width upon the setting of the PC at a fixed length of the PM fibre within the laser cavity.

Thus, changing the PM fibre length within the cavity allows control of the spectral width of the laser output between broad limits, whereas the adjustment of PC parameters at a fixed PM fibre length made it possible to detune the laser's output wavelength (at relatively short PM fibre length) and to fine-tune the width of the laser output spectrum with longer PM fibre in the resonator. The output power of the laser radiation reached 1.5 mW and the pulse repetition rate was 50 MHz. To measure the pulse width, a scanning autocorrelator was used. For reliable signal the laser output was amplified by a fibre amplifier [175] up to an average power of 20 mW. Figures 4-22, 4-23 and 4-24 illustrate the recorded pulse auto-correlation functions and their corresponding spectra for PM fibres of different length. The auto-correlation function contrast indicates that the generated pulses have a certain amount of chirp. To estimate pulses duration, a theoretical analysis of the auto-correlation function was carried out with the chirp calculation. The corresponding results are presented in Figures 4-22, 4-23 and 4-24.

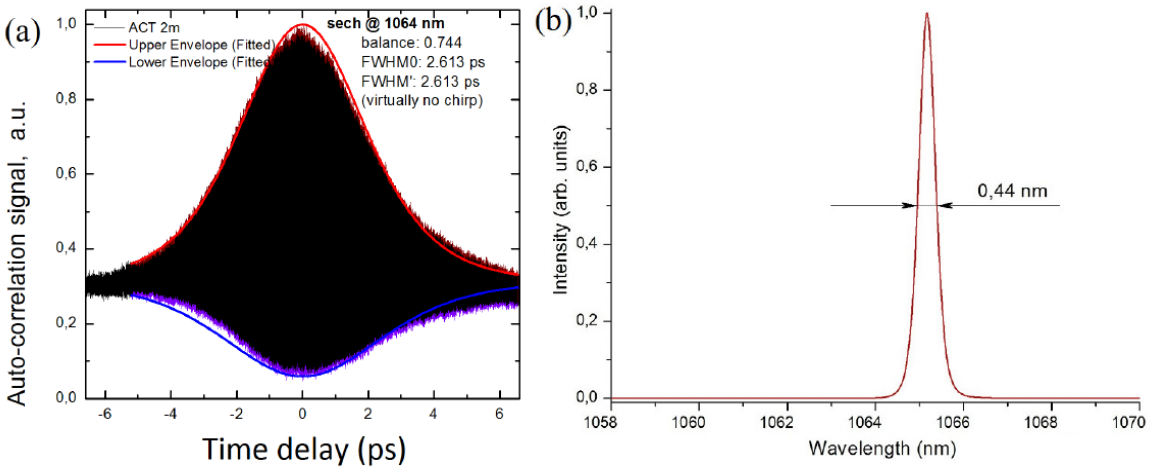

Figure 4-22 Resonator with a 2 m PM fibre: experimental and theoretical (red and blue envelopes) pulse auto-correlation functions (a) and laser output spectrum (b) [174].

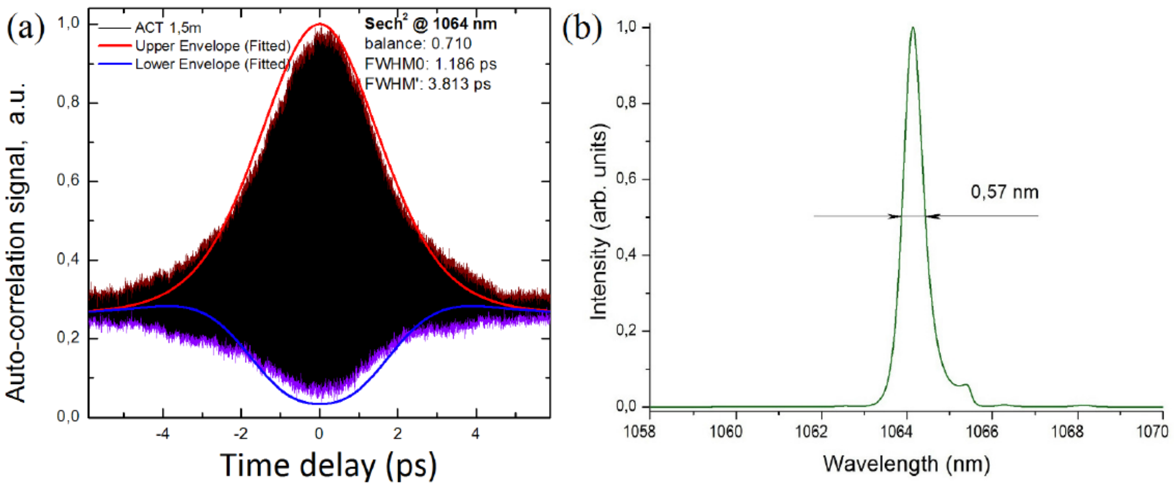

Figure 4-23 Resonator with a 1.5 m PM fibre: experimental and theoretical (red and blue envelopes) pulse auto-correlation functions (a) and laser output spectrum (b) [174].

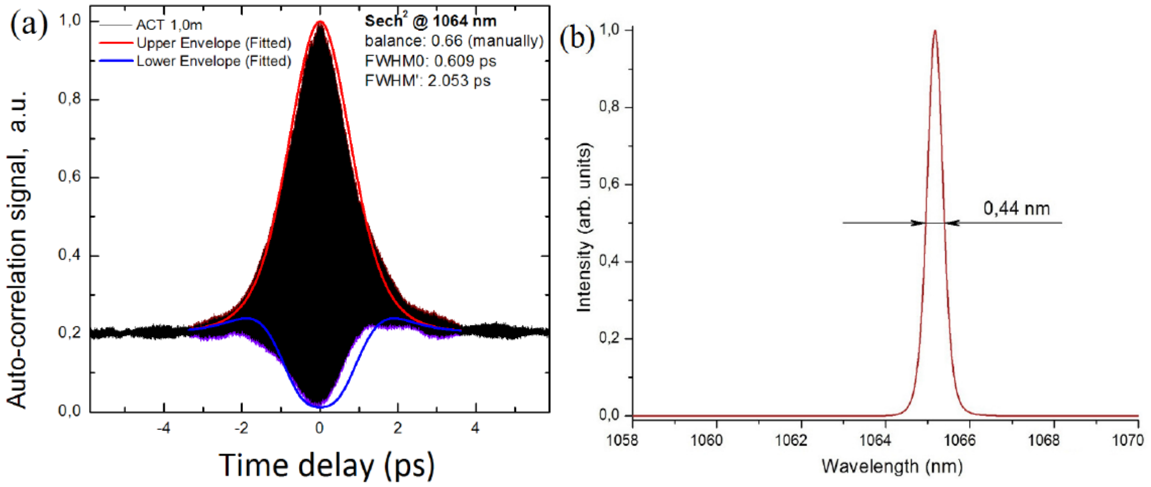

Figure 4-24 Resonator with a 1 m PM fibre: experimental and theoretical (red and blue envelopes) pulse auto-correlation functions (a) and laser output spectrum (b) [174].

It can be seen from these calculations that the birefringent filter allows controlling the chirp of the generated pulses. When a 2 m PM fibre is used in the laser cavity, the pulse duration is 2.61 ps, which is very close to the transform limited value of 2.21 ps. For a 1.5 m PM fibre, the output pulses exhibited more chirp: their duration was 3.8 ps, whereas the spectrally limited duration was 1.71 ps.

For a 1 m PM fibre, the pulse duration and the spectrally limited value were 2 and 1.2 ps respectively. So, a PM fibre in a laser cavity can function as a spectral selective filter in a SWNT mode locked Yb fibre laser. In the presence of a PC in such a cavity, the contrast of the filter's transmission function and the spectral position of its transmission peaks depend on the parameters of the PC.

4.4.5 Higher-order soliton generation in hybrid mode-locked thulium-doped fibre ring laser

Recently fibre lasers generating near 2 μm have attracted a great deal of attention due to a range of possible applications. The broad gain spectral band, extending from 1850 to 2100 nm provides more than 200 nm of available bandwidth, which is typical for thulium-doped fibres. Furthermore, thulium-doped fibre lasers exhibit excellent power scalability and high efficiency. Thulium’s gain spectrum covers several atmospheric transmission windows, offering numerous applications in remote sensing, laser radar [176] and free space or hollow core fibre telecommunications [176]. Obviously for these open-space applications eye-safe radiation is desirable. This can be achieved with thulium-doped fibre lasers due to the fact that the laser radiation at the wavelength band near 2 μm is entirely absorbed before it can reach and damage the eye’s retina. This wavelength region also includes the water absorption peaks, making such lasers a unique instrument for non-invasive surgery [177] or ophthalmology. On the other hand, there are lots of absorption lines of green-house gasses (CO_2 and N_2O) around 2 μm wavelength, that allow the use of thulium-doped lasers for gas detection and analysis [178].

High power 2 μm laser sources are well suited for nonlinear frequency conversion to obtain mid-IR and THz generation. Red-shifting of the generation band provides an increase of the fibre mode field size without sacrificing beam quality [179]. This helps to relax limitations for high-power applications imposed by optical nonlinearities. A higher threshold of nonlinear effects in thulium-doped fibre lasers is an advantage for high-power operation and telecommunication applications, however, this also complicates self-starting mode-locking through fast nonlinear polarization evolution (NPE) mechanism based on the nonlinear optical Kerr-effect in fibres. For example, to obtain an appropriate nonlinear phase shift for mode-locking initiation, all previous research has fouced on thulium-doped fibre lasers with a cavity length of more than 30 m [180,181]. However, a longer laser cavity may be responsible for pulse instabilities as discussed in such cases [182,183].

Most of current work on thulium-doped ultrafast fibre lasers has concentrated on a mode-locking regime initiated by semiconductor saturable absorber mirrors (SESAMs) [184], single-walled carbon nanotubes (SWNT) [131] and graphene based [185] saturable absorbers. Application of two simultaneous saturable absorbers, slow and fast, in a laser cavity helps to generate ultra-short pulses with high average power, temporal purity, and high frequency stability [186]. The comparatively slow saturable absorber is used for mode-locking initiation as it has a lower saturation threshold. The light modulator with a fast response time ensures efficient pulse formation and stabilization at substantially higher powers [186,187]. It is well known that saturable absorbers based on nonlinear optical Kerr-effect have the shortest response time, approximately 5 fs, based on the electric field interaction with the electrons of an active medium. Combination of NPE or nonlinear fibre loop mirrors with another saturable absorber has already been demonstrated [188,189] giving a shortest pulse duration of 230 fs [189].

The damage threshold of optical components has been a limitation for the output power of previous mode locked thulium doped ultrafast fibre lasers. Using a ferrule-type SWNT saturable absorber, the demonstrated average output power was below 20 mW due to destruction of the polymer composites [131]. So far, the highest pulse energy has been produced in a Figure-eight laser based of the double-clad thulium-doped fibre generating 685 fs pulses with the energy as much as 8.75 nJ [190]. A high-power and high-energy thulium doped all-fibre ring laser is demonstrated here, hybrid mode-locked by the coactions of SWNT and NPE.

Experiments setup; Figure 4-25 presents the schematic of the experimental setup of the thulium-doped fibre ring laser. Pump radiation from a CW single-mode laser diode at 1.55 μm has amplified with a commercial EDFA up to 1.2 W maximum output power is launched through a 1.56/1.9 μm wavelength division multiplexer (WDM) to a 1-m long thulium-doped active fibre (TDF). A commercial in-fibre polarization dependent isolator (PD-ISO) and a pair of polarization controllers (PC) are positioned after the active fibre to form the NPE based fast light amplitude modulator. A polymer film with dispersed SWNTs is used as a relatively slow saturable absorber, typical SWNT response time of 300-500 fs [12] to ensure self-starting mode locking. This is fixed between two angle-polished ferrules of optical FC/APC-connectors. An output coupler is positioned before the SWNT saturable absorber to decrease incident radiation power and therefore to prevent damage or degradation of the SWNT polymer film.

Coupling ratio was optimized during the experiment to obtain the highest lasing efficiency. The step-index ($\Delta n = 0.012$) of the active thulium doped aluminium-silica glass fibre has a 10 μm core containing 0.8 percent by weight thulium and 3.6 percent by weight with aluminium and a cutoff wavelength λ_c of 2.2 μm. The active fibre absorption at the pump wavelength of 1.55 μm was measured as 60 dB/m providing almost entire pump absorption in one meter of the active fibre. The second order dispersion was estimated to be ß = 76 ps^2/km at the wavelength of laser operation approximately 1.9 μm. The length of the laser cavity was varied from 2.7 to 22.5 m by inserting a section of passive SMF 2000 fibre.

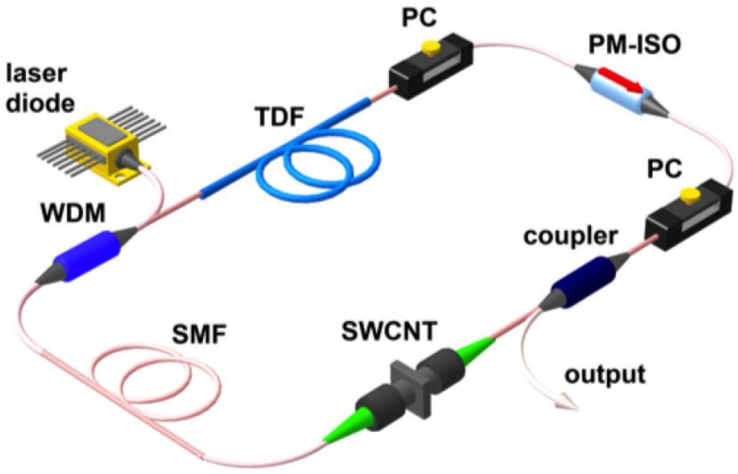

Figure 4-25 Schematic setup of the hybrid mode-locked thulium doped fibre laser [191].

A - Short cavity laser

The output-coupling ratio was firstly chosen to be 50/50 so that radiation power inside the cavity was equal to the output. The cavity length was shortened to 2.7 m corresponding to the pulse repetition rate of 72.5 MHz [192]. To explore the roles of the two types of saturable absorber in the hybrid mode-locking mechanism realization, the described laser was compared with another thulium-doped fibre ring laser mode-locked with the same SWNT-based saturable absorber. Both laser setups were built with identical components, except that a polarization sensitive isolator was replaced by a polarization independent one. In addition only one PC was retained in the cavity.

Figure 4-26 shows (a) experimental autocorrelation traces and (b) spectra of pulses generated in both hybrid and SWCNT-only mode-locked lasers at pump power of 320 mW. Both lasers can achieve mode-locking easily, with a generated pulse width of 590 fs and comparable spectral bandwidths of 6.58 and 6.78 nm respectively. The average output power of these lasers is 27 mW. It is evident that output characteristics of both lasers were similar; the spectrum of solo-SWNT mode locked laser is slightly red-shifted due to the difference in PC setups. This fact indicates that the SWNTs play a dominant role in mode-locking initiation and pulse formation at low pump powers below 400 mW, whereas the NPE threshold has not yet been achieved.

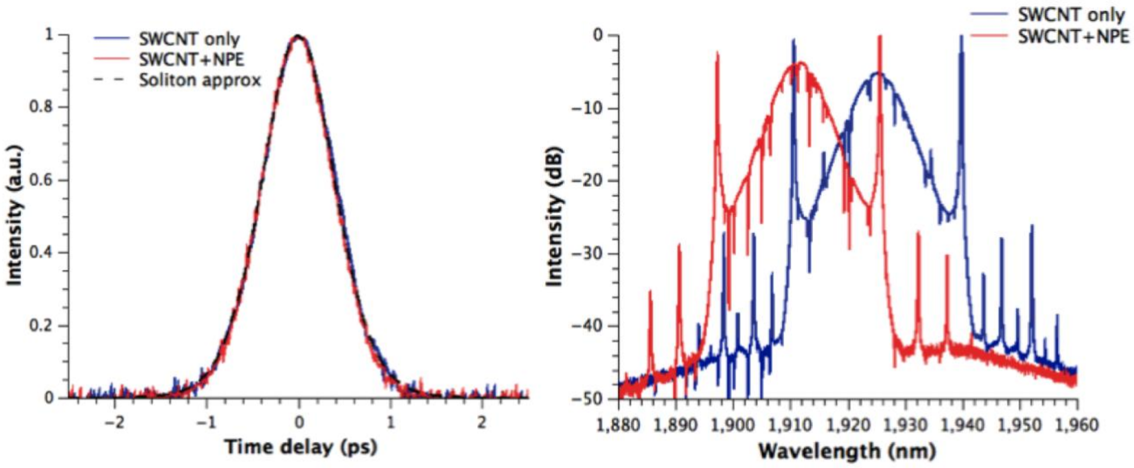

(a) (b)

Figure 4-26 Output autocorrelation traces (a) and spectra (b) at P_{pump} = 320 mW [191].

Throughout the increase in pump power, nonlinearity in the laser cavity affects generation to a greater degree and the NPE mechanism contribution to the pulse formation becomes more pronounced. During the pump power increase, NPE smoothly maintains mode-locking operation. However, it tends to break into non-regular multi-pulse generation and, finally, into Q-switching operation. This results in degradation of the PVA-based polymer film. The PVA polymer was preserved undamaged in the hybrid mode-locked laser.

Maximum average output power of 170 mW in the SWNT only mode-locked laser was achieved at the maximum pump power of 1.2 W (Figure 4-27). However, the laser pulses were generated at such a high-power mode for several seconds. After that the PVA-film degraded and the laser turned to CW operation.

In the case of hybrid mode-locking, the laser can steadily generate in two different regimes according to the polarization state adjustments giving approximately 300 mW output average power at the same slope efficiency of approximately 32.6 % (Figure 4-28). Output pulses had duration of 600 fs (state 1) and 1.28 ps (state 2) with spectral bandwidths of 8.7 and 3.1 nm respectively (Figure 4-27). Time bandwidth products for both states were calculated as approximately 0.411 and 0.316 respectively.

In both cases output spectra possess typical forms for soliton pulses with Kelly side-bands originating from periodic spectral interference between the soliton wave and a co-propagating dispersive wave. Due to high-intensive Kelly sidebands in the output spectrum in state 1, a pulse contains 68 % of all generated energy giving 2.93 nJ and the peak power of 4.88 kW, respectively. In state 2, however, side-bands contain a negligible part of the energy. The peak power in the pulse reached 3.19 kW corresponding to the pulse energy of 4.08 nJ.

The pulse characteristics of the SWNT-only mode-locked laser were close to above-mentioned state 1. The laser generated 600 fs pulses with a spectrum bandwidth of 10.86 nm and time bandwidth product of 0.54. It should be noted that a sharp spike at 1905 nm was observed in the spectrum (Figure 4-27 (b), green plot) showing that the mode locking operation was not complete and a high-power CW component is transmitted through the laser cavity. Pulse peak contains 65 % of all generated energy according to spectrum integration, corresponding to a value of 1.34 nJ and a peak power of 2.24 kW.

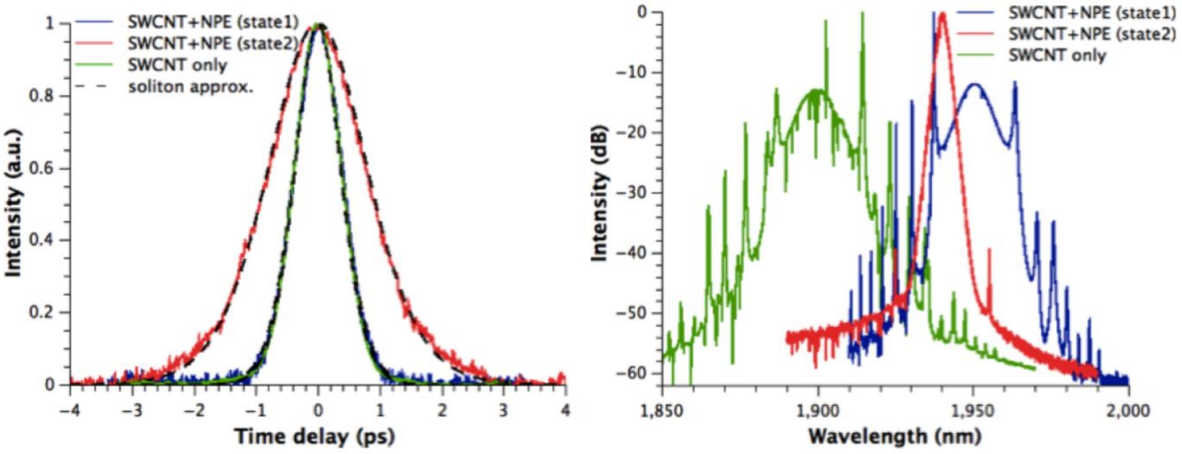

(a) (b)

Figure 4-27 Output autocorrelation traces (a) and spectra (b) at P_{pump} = 1.2 W [191].

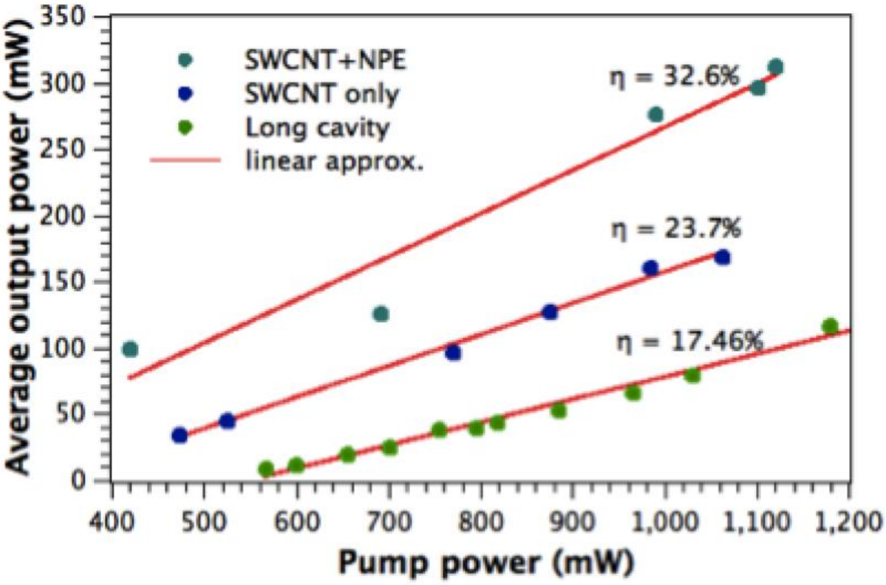

Figure 4-28 Laser slope efficiency [191].

The slope efficiency of SWNT only mode-locked laser was measured to be 23.7 % (Figure 4-28). It is worth noting that the pump radiation was entirely absorbed by the active fibre. This was proved by monitoring the average power at the wavelength of 1.55 μm, which did not exceed several milli-watts at the laser output when the pump power was higher than 1 W.

The long-term stability of the proposed laser was also studied. The laser generating 1.28 ps pulses at a 300 mW output power exhibited stable output under the laboratory conditions for 10 hours (Figure 4-29). The optical spectra of the laser were recorded at a 10-min interval. No obvious change was observed for the soliton parameters, such as the central wavelength, 3 dB spectral bandwidth, Kelly sideband positions and the spectral peak powers. Also, no obvious damage or degradation of SWNT polymer films was observed even when the same sample was used for self-starting mode locking the next day after several power cycles. The laser could effectively resist mechanical effects and perturbation. Considering the output coupling ratio of 50%, the radiation energy transmitted along the laser cavity to the SWNT module is equal to the output one, and rises to 4.08 nJ in the case shown in Figure 4-29.

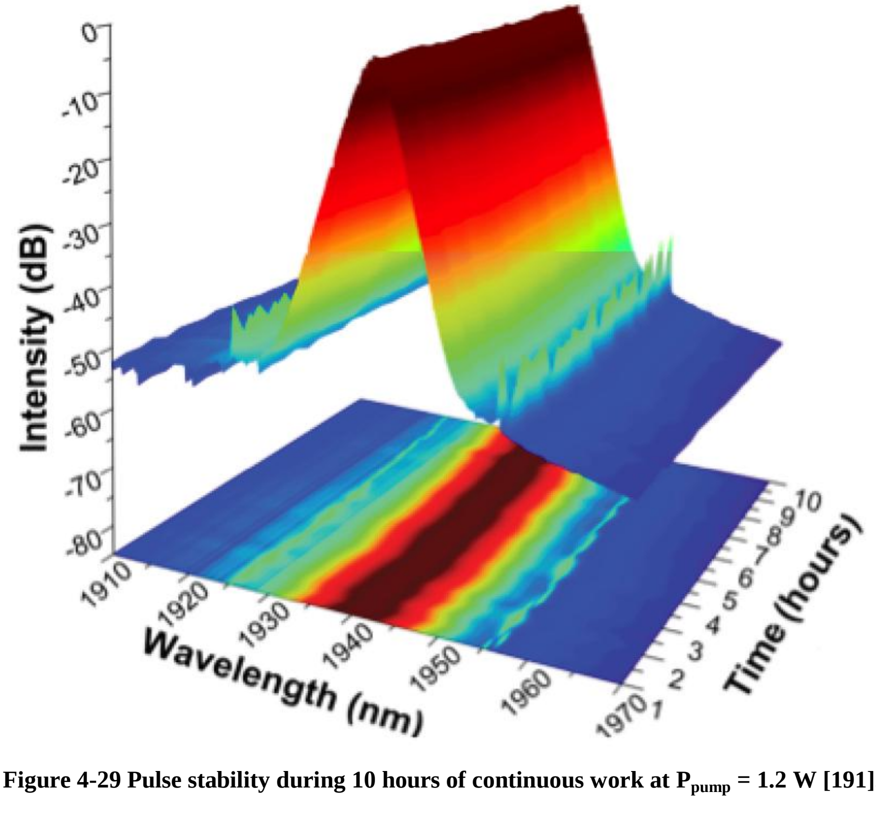

Figure 4-29 Pulse stability during 10 hours of continuous work at P_{pump} = 1.2 W [191].

Thus the PVA based SWNT polymer composite film could endure an optical fluence of at least 3.46 mJ/cm^2 without any significant damage, verifying its strong thermal stability.

With the pump power increase, no gain saturation was observed for pump powers higher than 1.2 W. Thus it is expected that through further laser cavity optimization on the saturable absorption parameters and with careful polarization adjustment, mode locked pulses of significantly higher pulse average powers and shorter duration could be generated, giving rise to higher pulse energy.

B- Long cavity laser

To achieve higher output energy and reduce the energy fluence transmitting through the PVA-based polymer film with incorporated SWNTs, 50/50 output coupler was replaced by a 30/70 coupler providing 70% output for generated energy. By careful initial PC adjustment, self-starting mode-locking was achieved at a pulse repetition rate between 6.37 and 9.6 MHz, which corresponds to a laser cavity length ranging between 31.4 and 20.8 m. Once the mode-locking was realized, polarization tuning was no longer needed during the pump power increase. The laser ran steadily for hours without any perturbation under laboratory conditions. In the whole available pump power range, the laser operated in the single pulse regime with no pulse breaking, Q-switching or multiple pulse operation observed. By changing the length of SMF-2000 inside the laser cavity lasing efficiency varied in a range from 11.2 to 17.46 % whereas output pulse duration at a maximum pump power of 1.2 W altered over a range between 640 and 875 fs respectively as is shown in Figure 4-30. A maximum efficiency of 17.46 % was obtained with a cavity length of 21.6 m. In this case the laser generated 840-fs pulses with a maximum average output power of 126.4 mW. The lasing slope efficiency in this case is depicted in Figure 4-28 (green plot). It is worth noting that power saturation was not observed even at the highest pump powers, meaning that it could be further increased.

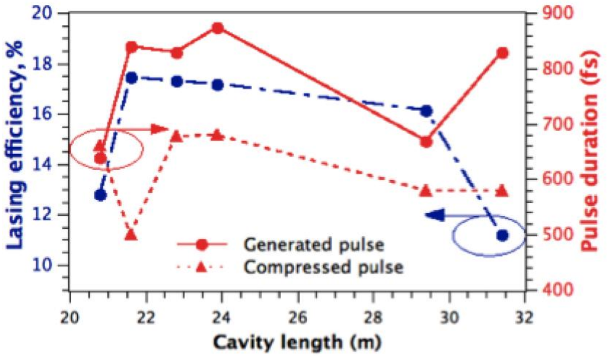

Figure 4-30 Output pulse parameters evolution by varying the cavity length [191].

The measured autocorrelation trace and spectrum of generated pulses in this case are presented in Figure 4-31 (blue solid line). The laser output spectrum possesses well-resolved Kelly sidebands, showing soliton pulse generation. It can be seen in Figure 4-31 (a) that the autocorrelation trace contains a noncompressed pedestal part. Nonlinear pulse chirp causes deviations from the ideal soliton pulse (see sech^2 approximation in Figure 4-31). By examining the output characteristics it was found that the pulse peak contains just 80% of the generated energy. Assuming a pulse repetition rate of 9.26 MHz, the pulse energy is estimated to be 10.92 nJ corresponding to a peak power of 13 kW.

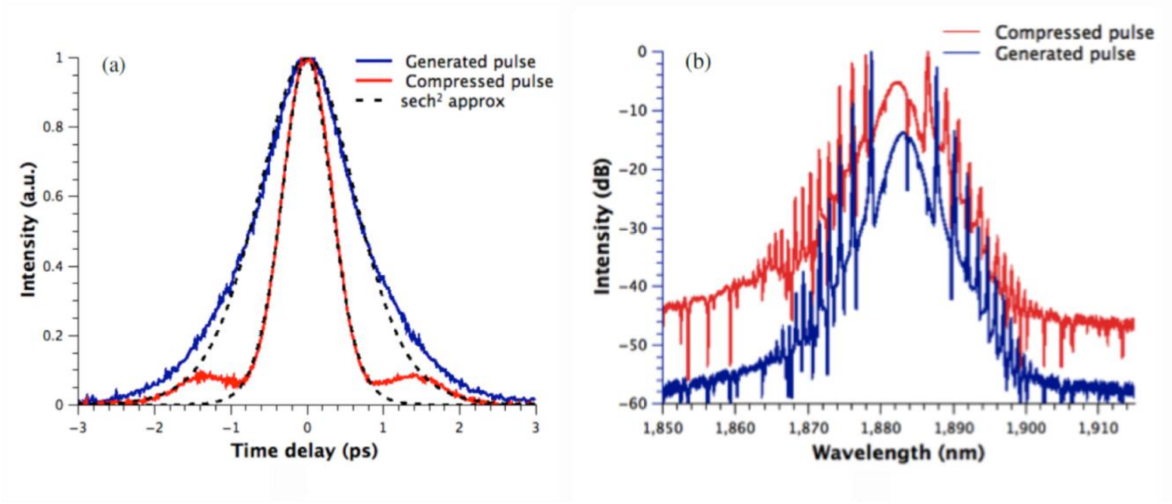

Figure 4-31 Output autocorrelation trace (a) and spectra (b) of the laser pulse at pump power P_{pump} = 1.2 W and cavity length L = 21.6 m [191].

To compress the pulse, the SMF-28 fibre section of variable length in the range from 2.5 to 5 m was inserted at the laser output as in previous work by other researchers [193]. The laser output parameters were strictly fixed during these experiments. The evolution of the shortest output pulse duration by varying cavity length is presented in Figure 4-30 (dashed plot). As is shown, the shortest pulse duration of 500 fs was achieved in the 21.6 m cavity length using 4.9 m long external fibre line giving a compression factor of 1.5X. This cavity length corresponds to the highest lasing efficiency as is shown in Figure 4-30. However, due to losses caused by external section of SMF-28 fibre, average output power decreased down to 117 mW.

The autocorrelation trace and spectrum of the compressed pulse are presented in Figure 4-31 (red traces). Though the pulse peak can be accurately approximated with a sech2 function, the pulse contains low intensive pulse pedestal (Figure 4-31 (a)). By autocorrelation traces and pulse spectra integration along with corresponding soliton function integration it was calculated that the pulse peak contains 86 % of the entire generated energy, reaching 10.87 nJ at a 9.26 MHz repetition rate, which corresponds to the pulse peak power as high as 21.7 kW.

Assuming that 70 % of the entire generated energy was coupled from the laser cavity, the pulse energy of 3.28 nJ was launched to the PVA-based polymer film with incorporated SWNT. According to previous experiments on the long-term stability, the polymer film possesses enough thermal reliability to ensure stable mode-locking at such high energies.

In conclusion, SWNTs have been used as saturable absorbers in the near IR spectral range in form of dispersion and composites for generation of ultra-short pulses with fibre lasers. We designed and developed new mode-locked devices based on SWNT-NMP with addition polymer solution filled in-fibre micro-chamber. A high stable pulse generation was showed. We developed and used SWNT-PVA films for mode-locking of Ytterbium, Erbium and Thulium-doped fibre laser in a spectral range 1000- 1800 nm. A harmonic mode locking (HML) of an Erbium-doped fibre laser was demonstrated. Generation of ultra-short pulses was achieved from Ytterbium-doped fibre laser. A hybrid passive mode-locked Thulium-doped all-fiber soliton laser was demonstrated. Application of SWCNTs-based saturable absorber (as comparatively slow one) facilitates mode-locking startup whereas the fast NPE mechanism based on the nonlinear optical Kerr effect allowed achieving high average output power and pulsing energy with the high long- and short-term stability.

Chapter 5

5. Conclusion

In conclusion, the CNT is a new material with unique optical properties, which has potential for use in various photonic applications. The initial motivation of this work was broadly to examine the optical properties of SWNTs and their photonic applications. The work demonstrated in this thesis has shown a number of key achievements in a range of areas including bundle engineering of SWNTs, photoluminescence intensity enhancement and the novel photonic applications of SWNT solution and composites.

The main scientific result of chapter 2, the work has progressed from initial trials for non covalent functionalization of carbon nanotubes and development of new dispersing agents (dispersants) for carbon nonmaterial (CNMs). I have shown that ions have a significant impact on CNT bundle formation in NMP. The addition of salt to the nanotube dispersion leads to self-assembly of nanotubes and formation of large CNT bundles that can be extracted from the solution by centrifugation. The all effect of salt addition increases with an increase of the salt concentration. I showed that salts can be used to regulate CNT concentration in samples as illustrated by observed changes in the intensities of PL and absorbance spectra of the samples at different salt concentrations. Self-assembly of nanotubes can be initiated by even small amounts of salts and the effect is reproducible. This provides an easy, robust and safe route to bundle engineering of pristine carbon nanotubes. Due to the general nature of the phenomena, it is likely to be observed in other CNM dispersions as well. The aim of this work is to attract the attention of the scientific community to the importance of salt effects on CNM dispersions. These findings provide new avenues for solvent engineering in nanoscience and nanotechnology as well as the development of new dispersing agents (dispersants) for CNMs.

In Chapter 3 we show on a novel nanophotonic system of PDs non-covalently attached to CNT micelle in water, which produce a significant PL amplification of CNT emission by through the energy transfer from PDs to SWNTs. Only positively charged astraphloxin or Cy3 molecules can interact with negatively charged micelles of CNT, because the tubes are covered by anionic surfactant. The coulomb attraction between the dye and surfactant molecules is a key issue in the emerging novel complexes. Result of experiments with water solutions of the dyes, CNT with surfactants, dyes with surfactants, and composition of dye-CNT-surfactant can be summarized as follows:

1.) Interaction of the dyes with CNT resulted in red shift of the dye’s intrinsic absorbance and PL maxima. Importantly, astraphloxin molecules interact with each other on CNT forming J-aggregates, whereas Cy3 molecules attach to CNT without interaction between the dye molecules.

2.) A strong amplification of PL from the excitonic levels of CNT in NIR range occurred under the red shifted excitation of positively charged astraphloxin or Cy3, which interact with CNT. The light absorbed by dye monomers does not contribute to amplification. We explain the effect of PL amplification as a non-radiative energy transfer process from the dyes aggregated to CNT.

3.) Upon rising dye concentration, amplification saturates and the number of monomers increases substantially. This shows that dye molecules interacting with CNT form only mono-molecular layer around the tubes.

Clarification of the energy transfer mechanism should be possible by studying different distances between CNT and dyes by extensive variation of surfactants and solvents, which could be pursued in the future. The Prominent features of PDs are a vast variety of substitutions, polymethine chain elongation, and the application of various anions and cations for neutralization of the charged dyes. This easy tailoring of PD molecular structure provides prospects for optimization of photonic and electronic properties of hybrid complexes of CNT-organic dye with tunable optical properties and potential for application as a photonic sensor.

Chapter 4 reports results on the application of both SWNT solutions and composites for ultrafast pulse generation in fibre lasers.

1). A homogeneous and stable dispersion of SWNTs in NMP was demonstrated with addition SBM polymer filled in-fibre microchamber for mode locking of EDFL. The polarization insensitive saturable absorber SWNT-PVP-NMP without any optimization and control offers durable and highly stable pulse generation. The application of CNT in NMP in the fibre microchamber also maintains the all-fibre format of the laser configuration. Laser with generates soliton pulses with temporal width of ~3.37 ps and an output power of ~29 mW (pulse energy of ~11 nJ) with a repetition rate of ~ 2.3 MHz at 1564 nm. SBM appears to stabilize SWNT dispersion and here results in the strong and steady optical absorption, PL, and saturable absorption. This dispersion was employed to achieve a stable mode-locked fibre laser with a 2.55 ps output pulse. This indicates significant potential for a liquid type saturable absorber for laser mode locking.

2). We used SWNT-Poly vinyl alcohol (PVA) films for mode-locking of Ytterbium, Erbium and Thulium-doped fibre laser in a spectral range 1000- 1800 nm.

- We demonstrated harmonic mode locking (HML) of an Erbium-doped fibre laser with chirped soliton pulses of ~1 ps pulse duration. EDFL shows a maximum of 10th harmonic order operation at 245 MHz with an output power of ~12 mW with the SWNTs-PVA saturable absorber. This is higher than previous results using a CNT- polymer film mode locker. EDFL also shows a higher SMSR ratio than some previous results. Although the absorption for both CNT-PVA samples is different, it did not make a significant difference to their performance in HML of EDFL.
- Generation of ultra-short pulses was demonstrated from Ytterbium-doped fibre laser with controlled duration, spectral width, and operational wavelength with a SA based on SWNT-PVA films within the wavelength range 1060–1066 nm. The average output power of the laser was 1.5 mW at a pulse repetition rate of 50 MHz. Utilization of a fibre Lyot filter made from several lengths of PM fibre in combination with a PC enabled control of the laser output spectrum width within the 0.15–1.25 nm range, with a pulse duration between 2–3.8 ps, and detuning the laser output wavelength by up to 5 nm.
- A hybrid passive mode-locked Thulium-doped all-fibre soliton laser was demonstrated. Application of a SWNT-based saturable absorber, although comparatively slow, facilitates mode-locking and setup. In contrast the fast NPE mechanism based on the nonlinear optical Kerr effect allowed achievement of a high average output power and pulse energy with high long- and short-term stability. The laser benefits from a simple ring cavity design with single-mode pumping by a high-power laser diode at 1.55 μm. Two different cavity schemes were studied, possessing different cavity lengths. The laser with a short cavity generates 600-fs or 1.28-ps pulses at a 72.5 MHz repetition rate with an average output power of 300 mW, more than one order of magnitude higher than earlier reported results for SWNT mode-locked fibre lasers. Such a high pulse energy and peak power with excellent long and short-term stability could find numerous applications, including supercontinuum generation in the mid-IR range. Typical sources existing are pumped by a master oscillator power amplifier (MOPA) consisting of a seed mode-locked fibre laser and one or several amplification stages. Such a complicated scheme presents a technical challeng for applications whereas obtaining high power directly from a seed laser without the chirped pulse amplification technique has advantages.

Future challenges will include: development of Carbon nonmaterial (CNM) polymer composites with enhanced and controllable optical and nonlinear optical properties, and development of new photonic sensors based on both functionalised CNMs and SWNT based fibre lasers for environmental monitoring.

References

1. Iijima S. Helical microtubules of graphitic carbon. nature. 1991;354:56–8.

2. Jorio, Ado, Dresselhaus, Mildred S., Dresselhaus G. Carbon Nanotubes. Springer-Verlag Berlin and Heidelberg GmbH & Co. K; 2008.

3. Weisman RB, Bachilo SM. Dependence of optical transition energies on structure for single-walled carbon nanotubes in aqueous suspension: an empirical Kataura plot. Nano Letters. 2003;3(9):1235–8.

4. Kataura H, Kumazawa Y, Maniwa Y, Umezu I. Optical properties of single-wall carbon nanotubes. Synthetic Metals. 1999;103:1–4.

5. Dresselhaus M, Dresselhaus G, Avouris P. Carbon nanotubes synthesis,structure,properties and applications. Springer Germany; 2001.

6. Kataura H, Kumazawa Y, Maniwa Y, Ohtsuka Y, Sen R, Suzuki S, et al. Diameter control of single-walled carbon nanotubes. Carbon. 2000 Jan;38:1691–7.

7. Rozhin AG, Sakakibara Y, Kataura H, Matsuzaki S, Ishida K, Achiba Y, et al. Anisotropic saturable absorption of single-wall carbon nanotubes aligned in polyvinyl alcohol. Chemical Physics Letters. 2005;405:288–93.

8. Kitiyanan B, Alvarez WE. Controlled production of single-wall carbon nanotubes by catalytic decomposition of CO on bimetallic Co–Mo catalysts. Chemical Physics Letters. 2000;317:497–503.

9. Bachilo SM, Balzano L, Herrera JE, Pompeo F, Resasco DE, Weisman RB. Narrow (n,m)-distribution of single-walled carbon nanotubes grown using a solid supported catalyst. Journal of the American Chemical Society. 2003;125(37):11186–7.

10. swentnano [Internet]. Available from: http://www.swentnano.com/tech/singlewallproducts_new.php

11. Bachilo SM, Strano MS, Kittrell C, Hauge RH, Smalley RE, Weisman RB. Structure-assigned optical spectra of single-walled carbon nanotubes. Science (New York, NY). 2002;298(5602):2361–6.

12. Hasan T, Sun Z, Wang F, Bonaccorso F, Tan PH, Rozhin AG, et al. Nanotube-Polymer Composites for Ultrafast Photonics. Advanced Materials. 2009;21:3874–99.

13. Matarredona O, Rhoads H, Li Z, Harwell JH, Balzano L, Resasco DE. Dispersion of Single-Walled Carbon Nanotubes in Aqueous Solutions of the Anionic Surfactant NaDDBS. The Journal of Physical Chemistry B. 2003;107(48):13357–67.

14. Moore VC, Strano MS, Haroz EH, Hauge RH, Smalley RE, Schmidt J, et al. Individually Suspended Single-Walled Carbon Nanotubes in Various Surfactants. Nano Letters. 2003;3(10):1379–82.

15. Islam MF, Rojas EA, Bergey DM, Johnson A. T, Yodh A. G. High Weight Fraction Surfactant Solubilization of Single-Wall Carbon Nanotubes in Water. Nano Letters. 2003;3(2):269–73.

16. Yang Y, Grulke E A., Zhang ZG, Wu G. Thermal and rheological properties of carbon nanotube-in-oil dispersions. Journal of Applied Physics. 2006;99(11):114307.

17. Hilding J, Grulke E A., George Zhang Z, Lockwood F. Dispersion of Carbon Nanotubes in Liquids. Journal of Dispersion Science and Technology. 2003;24(1):1–41.

18. Arnold MS, Green AA, Hulvat JF, Stupp SI, Hersam MC. Sorting carbon nanotubes by electronic structure using density differentiation. Nature nanotechnology. 2006;1(1):60–5.

19. Green A, Duch M, Hersam M. Isolation of single-walled carbon nanotube enantiomers by density differentiation. Nano Research. 2009;2:69–77.

20. Liu L, Barber A. H, Nuriel S, Wagner HD. Mechanical Properties of Functionalized Single-Walled Carbon-Nanotube/Poly(vinyl alcohol) Nanocomposites. Advanced Functional Materials. 2005;15(6):975–80.

21. Chen J, Hamon MA, Hu H, Chen Y, Rao apparao M, Eklund PC, et al. Solution properties of single walled carbon nanotubes. Science. 1998;282:95–8.

22. Giordani S, Bergin SD, Nicolosi V, Lebedkin S, Kappes MM, Blau WJ, et al. Debundling of single-walled nanotubes by dilution: observation of large populations of individual nanotubes in amide solvent dispersions. The journal of physical chemistry B. 2006;110(32):15708–18.

23. Mattia D, Gogotsi Y. Review: static and dynamic behavior of liquids inside carbon nanotubes. Microfluidics and Nanofluidics. 2008;5(3):289–305.

24. Hernandez Y, Nicolosi V, Lotya M, Blighe FM, Sun Z, De S, et al. High-yield production of graphene by liquid-phase exfoliation of graphite. Nature nanotechnology. 2008;3(9):563–8.

25. Baughman R.H., A. A. Zakhidov, Walt A. de Heer. Carbon nanotubes the route toward applications. Science. 2002;297:787–92.

26. Hirsch A. Functionalization of Single-Walled Carbon Nanotubes. Angewandte Chemie International Edition. 2002;41(11):1853–9.

27. Balasubramanian K, Burghard M. Chemically functionalized carbon nanotubes. Small (Weinheim an der Bergstrasse, Germany). 2005;1(2):180–92.

28. Wenseleers W, Vlasov II, Goovaerts E, Obraztsova ED, Lobach A. S, Bouwen A. Efficient Isolation and Solubilization of Pristine Single-Walled Nanotubes in Bile Salt Micelles. Advanced Functional Materials. 2004;14(11):1105–12.

29. Kume G, Gallotti M, Nunes G. Review on Anionic/Cationic Surfactant Mixtures. Journal of Surfactants and Detergents. 2007;11(1):1–11.

30. McDonald TJ, Engtrakul C, Jones M, Rumbles G, Heben MJ. Kinetics of PL Quenching during Single-Walled Carbon Nanotube Rebundling and Diameter-Dependent Surfactant Interactions. J. Phys. Chem. 2006;110:25339–46.

31. Manivannan S, Jeong IO, Ryu JH, Lee CS, Kim KS, Jang J, et al. Dispersion of single-walled carbon nanotubes in aqueous and organic solvents through a polymer wrapping functionalization. Journal of Materials Science: Materials in Electronics. 2008;20(3):223–9.

32. Zheng M, Jagota A, Strano MS, Santos AP, Barone P, Chou SG, et al. Structure based carbon nanotube sorting by sequence dependet DNA assembly. Science. 2003;302:1545–8.

33. Bahr JL, Yang J, Kosynkin DV, Bronikowski MJ, Smalley RE, Tour JM. Functionalization of carbon nanotubes by electrochemical reduction of aryl diazonium salts: a bucky paper electrode. Journal of the American Chemical Society. 2001;123(27):6536–42.

34. Hasan T, Scardaci V, Tan P, Rozhin AG, Milne WI, Ferrari AC. Stabilization and " Debundling " of Single-Wall Carbon Nanotube Dispersions in N -Methyl-2-pyrrolidone (NMP) by Polyvinylpyrrolidone (PVP). J Phys. Chem. 2007;111:12594–602.

35. Miyata Y, Yanagi K, Maniwa Y, Kataura H. Optical Evaluation of the Metal-to-Semiconductor Ratio of Single-Wall Carbon Nanotubes. J. Phys. Chem. 2008;112:13187–91.

36. Rozhin AG, Sakakibara Y, Namiki S, Tokumoto M, Kataura H, Achiba Y. Sub-200-fs pulsed erbium-doped fiber laser using a carbon nanotube-polyvinylalcohol mode locker. Applied Physics Letters. 2006;88(5):051118.

37. Wang F, Rozhin AG, Sun Z, Scardaci V, White IH, Ferrari AC. Soliton fiber laser mode-locked by a single-wall carbon nanotube-polymer composite. Physica Status Solidi (B). 2008 28;245(10):2319–22.

38. Saito R, Hofmann M, Dresselhaus G, Jorio A. Raman spectroscopy of graphene and carbon nanotubes. Advances in Physics. 2011;60:413–550.

39. O'Connell MJ, Bachilo SM, Huffman CB, Moore VC, Strano MS, Haroz EH, et al. Band gap fluorescence from individual single-walled carbon nanotubes. Science (New York, NY). 2002;297:593–6.

40. Wang F, Dukovic G, Brus LE, Heinz TF. The optical resonances in carbon nanotubes arise from excitons. Science (New York, NY). 2005;308:838–41.

41. Tan P, Rozhin A, Hasan T, Hu P, Scardaci V, Milne W, et al. Photoluminescence Spectroscopy of Carbon Nanotube Bundles: Evidence for Exciton Energy Transfer. Physical Review Letters. 2007;99(13):137402–6.

42. Walsh AG, Vamivakas a N, Yin Y, Cronin SB, Unlü MS, Goldberg BB, et al. Screening of excitons in single, suspended carbon nanotubes. Nano letters. 2007;7(6):1485–8.

43. Chen Y-C, Raravikar NR, Schadler LS, Ajayan PM, Zhao Y-P, Lu T-M, et al. Ultrafast optical switching properties of single-wall carbon nanotube polymer composites at 1.55 μm. Applied Physics Letters. 2002;81(6):975.

44. Lauret J-S, Voisin C, Cassabois G, Delalande C, Roussignol P, Jost O, et al. Ultrafast Carrier Dynamics in Single-Wall Carbon Nanotubes. Physical Review Letters. 2003;90(5):57404.

45. Bonaccorso F, Sun Z, Hasan T, Ferrari A. C. Graphene photonics and optoelectronics. Nature Photonics. Nature Publishing Group; 2010;4(9):611–22.

46. Boyd RW. Nonlinear Optics. second edi. San Diego: academic press; 2003.

47. Martinez A, Zhou K, Bennion I, Yamashita S. In-fiber microchannel device filled with a carbon nanotube dispersion for passive mode-lock lasing. Optics express. 2008;16(20):15425–30.

48. Y.W. Song, S. Yamashita, E. Einarsson and SM. All-fiber pulsed lasers passively mode locked by transferable vertically aligned carbon nanotube film. Optics letters. 2007;32:1399–401.

49. Okhotnikov O, Grudinin A, Pessa M. Ultra-fast fibre laser systems based on SESAM technology: new horizons and applications. New Journal of Physics. 2004;6:177–177.

50. Avouris P, Freitag M, Perebeinos V. Carbon-nanotube photonics and optoelectronics. Nature photonics. 2008;2:341–50.

51. Hong G, Tabakman SM, Welsher K, Wang H, Wang X, Dai H. Metal-Enhanced Fluorescence of Carbon Nanotubes. J A C S. 2010;132:15920–3.

52. Gong H, Peng R, Liu Z. Carbon nanotubes for biomedical imaging: the recent advances. Advanced drug delivery reviews. Elsevier B.V.; 2013;65(15):1951–63.

53. Liu Z, Tabakman S, Welsher K, Dai H. Carbon Nanotubes in Biology and Medicine: In vitro and in vivo Detection , Imaging and Drug Delivery. Nano Res. 2009;2:50–120.

54. Barone PW, Baik S, Heller DA, Strano MS. Near-infrared optical sensors based on single-walled carbon nanotubes. Nature Materials. 2005;4(1):86–92

55. Fadel TR, Steenblock ER, Stern E, Li N, Wang X, Haller GL, et al. Enhanced Cellular Activation with Single Walled Carbon Nanotube Bundles Presenting Antibody Stimuli 2008. Nano Letters. 2008;8(7):2070–6.

56. Fadel TR, Look M, Staffier PA, Haller GL, Pfefferle LD, Fahmy TM. Clustering of stimuli on single-walled carbon nanotube bundles enhances cellular activation. Langmuir: the ACS journal of surfaces and colloids. 2010 20;26(8):5645–54.

57. Forney MW, Poler JC. Significantly Enhanced Single-Walled Carbon Nanotube Dispersion Stability in Mixed Solvent Systems. Journal of Physical Chemistry C. 2011;115:10531–6.

58. Pham VH, Cuong TV, Hyr SH, Oh E, Kim EJ, Shin EW, et al. Chemical functionalization of graphene sheets by solvothermal reduction of a graphene oxide suspension in N-methyl-2-pyrrolidone. J. Mater.Chem. 2011;21:3371–7.

59. Bergin SD, Sun Z, Streich P, Hamilton J, Coleman JN. New Solvents for Nanotubes: Approaching the Dispersibility of Surfactants. J. Phys. Chem. 2010;114:231–7.

60. Connell MJO, Boul P, Ericson LM, Hu C, Wang Y, Haroz E, et al. Reversible water-solubilization of single-walled carbon nanotubes by polymer wrapping. Chemical Physics Letters. 2001;342:265–71.

61. Hwang J-Y, Nish A, Doig J, Douven S, Chen C-W, Chen L-C, et al. Polymer structure and solvent effects on the selective dispersion of single-walled carbon nanotubes. Journal of the American Chemical Society. 2008;130(11):3543–53.

62. Domard A, Rinaudo M, Terrassin C. New method for the quaternization of chitosan. Int J Biol Macromol. 1986;8:105–7.

63. Fedorov MV, Arif RN, Frolov AI, Kolar M, Romanova AO, Rozhin AG. Salting out in organic solvents: a new route to carbon nanotube bundle engineering. Physical chemistry chemical physics: Phys.Chem.Chem.Phys. 2011;13(27):12399–402.

64. Y.Marcus. Ion solvation. Chichester,UK: John wiley & Sons; 1985.

65. Frolov AI, Rozhin AG, Fedorov MV. Ion interactions with the carbon nanotube surface in aqueous solutions: understanding the molecular mechanisms. Chemphyschem: European journal of chemical physics and physical chemistry. 2010;11(12):2612–6.

66. L.Martinez, R.Andrade E.G.Birgin, J.M.Martinez. PACKMOL: A package for building initial configurations for molecular dynamics simulations. JComputational Chemistry. 2009;30(13):2157–64.

67. B.Hess, C.Kutzner, Spoel D.Van Der, E.Lindahl. GROMACS 4: Algorithms for highly efficient, load-balanced, and scalable molecular simulation. J. Chem.Theory comput.. 2008;3(4):435–47.

68. Jorgensen WL, Maxwell DS, Tirado-rives J. Development and Testing of the OPLS All-Atom Force Field on Conformational Energetics and Properties of Organic Liquids. J. Am. Chem. Soc..1996;118:11225–36.

69. Jensen KP, Jorgensen WL. Halide. Ammonium and Alkali Metal Ion Parameters for Modeling Aqueous Solutions. J. Chem. Theory comput.. 2006;2:1499–509.

70. Shih C, Lin S, Strano MS, Blankschtein D. Understanding the Stabilization of Liquid-Phase-Exfoliated Graphene in Polar Solvents: Molecular Dynamics Simulations and Kinetic Theory of Colloid Aggregation. J. Am. Chem. Soc. 2010;132:14638–48.

71. Aparicio S, Alcalde R, Da J, Leal M. Measurements and Predictive Models for the N-Methyl-2-pyrrolidone / Water / Methanol System a Garcı. J. Phys. Chem. B 2008;112:11361–73.

72. Aparicio S, Alcalde R. Characterization of two lactones in liquid phase: an experimental and computational approach. Phys. Chem. Chem. Phys. 2009;11:6455–67.

73. U.Essmann, Perera L., M.L.Berkowitz, T. Darden, H.Lee, L. G. Pedersen. A smooth particle mesh Ewald method. J Chem Phys. 1995;103:8577–93.

74. A.I.Frolov, Arif RN, K. Martin, Romanova, A. O., Fedorov, M. V., Rozhin AG. Molecular mechanisms of salt effects on carbon nanotube dispersions in an organic solvent (N-methyl-2-pyrrolidone). Chemical Science. 2012;3(2):541.

75. M.V. Fedorov, M. Goodman, S. Schumm. Solvent effects and hydration of a tripeptide in sodium halide aqueous solutions: an in silico studyw. Phys. Chem. Chem. Phys. 2007;9:5423–35.

76. Fedorov MV, Kornyshev AA. Molecular Physics: An International Journal at the Interface Between Chemistry and Physics Unravelling the solvent response to neutral and charged solutes. Mol Phys. 2007;105:1–16.

77. Collins KD. Charge Density-Dependent Strength. Biophys. J..1997;72:65–76.

78. R.D.Shannon. Revised effective ionic radii and systematic studies of interatomic distances in halides and chalcogenides. Acta crystallogr., Sect. A: Cryst. Phys. Diffr., Theor. Gen. Crystallogr. 1976;32:751–67.

79. Niyogi S, Densmore CG, Doorn SK. Electrolyte tuning of surfactant interfacial behavior for enhanced density-based separations of single-walled carbon nanotubes. Journal of the American Chemical Society. 2009;131:1144–53.

80. Niyogi S, Boukhalfa S, Chikkannanavar SB, McDonald TJ, Heben MJ, Doorn SK. Selective aggregation of single-walled carbon nanotubes via salt addition. Journal of the American Chemical Society. 2007;129(7):1898–9.

81. Dobrynin a, Rubinstein M. Theory of polyelectrolytes in solutions and at surfaces. Progress in Polymer Science. 2005;30:1049–118.

82. Ravi M, Bhavani S, Pavani Y, Rao VVRN. Investigation on electrical and dielectric properties of PVP: KCLO 4 polymer electrolyte films. Indian Journal of Pure and applied Physics. 2013;51:362–6.

83. Liu S, Ghosh K, Muthukumar M. Polyelectrolyte solutions with added salt: A simulation study. The Journal of Chemical Physics. 2003;119(3):1813.

84. Wong HS p., D.Akinwande. Carbon Nanotube and Graphene device physics. Cambridge , UK: Cambridge Unversity press; 2011.

85. Hirsch A. The era of carbon allotropes. Nature Materials. 2010;9(11):868–71.

86. Meng L, Fu C, Lu Q. Advanced technology for functionalization of carbon nanotubes. Progress in Natural Science. 2009;19(7):801–10.

87. Balasubramanian K, Burghard M. Chemically functionalized carbon nanotubes. Small. 2005;1(2):180–92.

88. Peng BX, Wong SS. Functional Covalent Chemistry of Carbon Nanotube Surfaces. Advanced Materials. 2009;21:625–42.

89. Y.lee, K.E. Geckele. Carbon Nanotubes in the Biological Interphase□: The Relevance of Noncovalence. Advanced Materials. 2010;22:4076–83.

90. Vardharajula S, Ali SZ, Tiwari P m., Eroglu E, Vig K, Dennis VA, et al. Functionalized carbon nanotubes: biomedical applications. Int. J. Nanomedicine. 2012;7:5361–74.

91. De Volder MFL, Tawfick SH, Baughman RH, Hart a J. Carbon nanotubes: present and future commercial applications. Science (New York, NY). 2013;339:535–9.

92. A.P.Demchenko. Introduction to Fluorescence Sensing. Springer; 2009.

93. S.Wolfbeis O. Fluorescence Methods and Applications: Spectroscopy, Imaging and Probes. Wiley-Blackwell; 2008.

94. Bergin SD, Nicolosi V, Cathcart H, Lotya M, Rickard D, Sun Z, et al. Large Populations of Individual Nanotubes in Surfactant-Based Dispersions without the Need for Ultracentrifugation. J. Phys. Chem. 2008;112:972–7.

95. Kim J-H, Heller D A, Jin H, Barone PW, Song C, Zhang J, et al. The rational design of nitric oxide selectivity in single-walled carbon nanotube near-infrared fluorescence sensors for biological detection. Nature chemistry. Nature Publishing Group; 2009;1:473–81.

96. Nismy NA, Jayawardena K, T. AD, Silva SRP. Photoluminescence Quenching in Carbon Nanotube-Polymer/Fullerene Films: Carbon Nanotubes as Exciton Dissociation Centres in Organic Photovoltaics. Advanced Materials. 2011;23(33):796–3800.

97. Yanagi K, Iakoubovskii K, Kazaoui S, Minami N, Maniwa Y, Miyata Y, et al. Light-harvesting function of β-carotene inside carbon nanotubes. Physical Review B. 2006;74(15):155420.

98. Yanagi K, Iakoubovskii K, Matsui H, Matsuzaki H, Okamoto H, Miyata Y, et al. Photosensitive function of encapsulated dye in carbon nanotubes. Journal of the American Chemical Society. 2007;129(16):4992–7.

99. Piao Y, Meany B, Powell LR, Valley N, Kwon H, Schatz GC, et al. Brightening of carbon nanotube photoluminescence through the incorporation of sp^3 defects. Nature chemistry. Nature Publishing Group; 2013;5(10):840–5.

100. Miyauchi Y, Iwamura M, Mouri S, Kawazoe T, Ohtsu M, Matsuda K. Brightening of excitons in carbon nanotubes on dimensionality modification. Nature Photonics. Nature Publishing Group; 2013;7(9):715–9.

101. Duque JG, Oudjedi L, Crochet JJ, Tretiak S, Lounis B, Doorn SK, et al. Mechanism of electrolyte-induced brightening in single-wall carbon nanotubes. Journal of the American Chemical Society. 2013;135(9):3379–82.

102. Casey JP, Bachilo SM, Weisman RB. Efficient photosensitized energy transfer and near-IR fluorescence from porphyrin–SWNT complexes. Journal of Materials Chemistry. 2008;18(13):1510.

103. Roquelet C, Langlois B, Vialla F, Garrot D, Lauret JS, Voisin C. Light harvesting with non covalent carbon nanotube/porphyrin compounds. Chemical Physics. 2013;413:45–54.

104. Ernst F, Heek T, Setaro A, Haag R, Reich S. Energy Transfer in Nanotube-Perylene Complexes. Advanced Functional Materials. 2012;22(18):3921–6.

105. Kachkovski AD. Polymethine Dyes. Kirk-Othmer Encyclopedia of Chemical Technology; 2000.

106. Eisele DM, Cone CW, Bloemsma EA, Vlaming SM, Kwaak CGF van der, Silbey RJ, et al. Utilizing redox-chemistry to elucidate the nature of exciton transitions in supramolecular dye nanotubes. Nature chemistry. 2012;4(655-662).

107. Hermann JP, Ducuing J. Third order polarizabilities of long chain molecules. J. Appl. Phys. 1974;45:5100–2.

108. Hales JM, Matichak J, Barlow S, Ohira S, Yesudas K, Brédas J-L, et al. Design of Polymethine Dyes with Large Third-Order Optical Nonlinearities and Loss Figures of Merit. Science. 2010;327:1485–8.

109. Mukhopadhyay S, Risko a C, Mardera a SR, Brédas J-L. Polymethine dyes for all-optical switching applications: a quantum-chemical characterization of counter-ion and aggregation effects on the third-order nonlinear optical response. Chemical Science. 2012;3:3103–12.

110. Kurdyukova IV, Ishchenko A a. Organic dyes based on fluorene and its derivatives. Russian Chemical Reviews. 2012;81(3):258–90.

111. Shandura MP, Kovtun YP, Yakubovskyi VP, Piryatinski YP, Lutsyk PM, Perminov RJ, et al. Dioxaborine Dyes as Fluorescent Probes for Amines and Carbon Nanotubes. Sensor letters. 2014;12:1–7, accepted.

112. Yao Q-H, Meng F-S, Li F-Y, Tian H, Huang C-H. Photoelectric conversion properties of four novel carboxylated hemicyanine dyes on TiO2 electrode. Journal of Materials Chemistry. 2003;13(5):1048–53.

113. Mojzych M, Henary M. Synthesis of Cyanine Dyes. Top heterocycl chem. 2008;14:1–9.

114. Lakowicz JR. Principles of Fluorescence Spectroscopy. Third. USA: Springer; 1999.

115. Zhang Y, Yuan S, Zhou W, Xu J, Li Y. Spectroscopic Evidence and Molecular Simulation Investigation of the π – π Interaction Between Pyrene Molecules and Carbon Nanotubes. Journal of Nanoscience and Nanotechnology. 2007 ;7(5):2366–75.

116. Pan B, Xing B. Adsorption mechanisms of organic chemicals on carbon nanotubes. Environ Sci Technol. 2008;42(24):9005–13.

117. Garmire E, Kost A. Nonlinear optics in semiconductors II. Academic press, San Diego: Semiconductors and Semimetals; 1999.

118. Garmire E. Resonant Optical Nonlinearities in Semiconductors. IEEE Journal of Selected Topics in Quantum Electronics. 2000;6(6):1094–110.

119. Keller U. Ultrafast solid state lasers. Volume 46. Wolf E, editor. Progress in optics,Elsevier; 2004.

120. Keller U. Recent developments in compact ultrafast lasers. Nature. 2003;424:831–8.

121. Isomäki A, Vainionpää A, Lyytikäinen J, Okhotnikov OG. Semiconductor Mirror for Optical Noise Suppression and Dynamic Dispersion Compensation. IEEE J. Quantum Electron. 2003;39:1481–5.

122. Tang Y, Siahmakoun A, Sergio G, Guina M, Pessa M. Optical switching in a resonant Fabry–Perot saturable absorber. Journal of Optics A: Pure and Applied Optics. 2006;8:991–5.

123. Rafailov EU, Cataluna MA, Sibbett W. Mode-locked quantum-dot lasers. Nature Photonics. 2007;1:395–401.

124. Rafailov EU, White SJ, Lagatsky AA, A.Miller, W.ASibbett, Livshits DA, et al. Fast Quantum-Dot Saturable Absorber for Passive Mode-Locking of Solid-State Lasers. IEEE Photon Tech Lett. 2004;16(11):2439–41.

125. Bohren CF, Huffman DR. Absorption and scattering of light by particales. New York: wiley-VCH; 1998.

126. Keller U, Weingarten KJ, Kartner FX, Kopf D, Braun B, Jung ID, et al. Semiconductor saturable absorber mirrors (SESAM's) for femtosecond to nanosecond pulse generation in solid-state lasers. IEEE J. Sel. Top Quant Electron. 1996;2(3):435–53.

127. Set SY, Yaguchi H, Tanaka Y, Jablonski M. Laser Mode Locking Using a Saturable Absorber Incorporating Carbon Nanotubes. 2004;22(1):51–6.

128. Schibli T, Minoshima K, Kataura H, Itoga E, Minami N, Kazaoui S, et al. Ultrashort pulse-generation by saturable absorber mirrors based on polymer-embedded carbon nanotubes. Optics Express. 2005;13(20):8025–31.

129. Nicholson JW, Windeler RS, Digiovanni DJ. Optically driven deposition of single-walled carbon- nanotube saturable absorbers on optical fiber end-faces. Optics Express. 2007;15(15):9176–83.

130. Cho WB, Yim JH, Choi SY, Lee S, Griebner U, Petrov V, et al. Mode-locked self-starting Cr:forsterite laser using a single-walled carbon nanotube saturable absorber. Optics letters. 2008;33(21):2449–51.

131. Solodyankin MA, Obraztsova ED, Lobach AS, Chernov AI, Tausenev AV, Konov VI, et al. Mode-locked 1.93 microm thulium fiber laser with a carbon nanotube absorber. Optics letters. 2008;33(12):1336–8.

132. Gambetta A, Galzerano G, Rozhin AG, Ferrari AC, Ramponi R, Laporta P, et al. Sub-100 fs pump-probe spectroscopy of Single Wall Carbon Nanotubes with a 100 MHz Er-fiber laser system. Optics Express. 2008;16(16):11727–34.

133. Nishizawa N, Seno Y, Sumimura K, Sakakibara Y, Itoga E, Kataura H, et al. All-polarization- maintaining Er-doped ultrashort-pulse fiber laser using carbon nanotube saturable absorber. Optics Express. 2008;16(13):9429–35.

134. Kivisto S, Hakulinen T, Kaskela A, Aitchison B, Brown DP, Nasibulin AG, et al. Carbon nanotube films for ultrafast broadband technology. Optics Express. 2009;17(4):2358–63.

135. A.Schmidt, S.Rivier, W.B.Cho, J.H.Yim, S.Y.Choi, S.Lee, et al. Sub-100 fs single-walled carbon nanotube saturable absorber mode-locked Yb-laser operation near 1 μm. Optics Express. 2009;17(22):20109–16.

136. Kelleher EJR, Travers JC, Ippen EP, Sun Z, Ferrari AC, Popov SV, et al. Generation and direct measurement of giant chirp in a passively mode-locked laser. Optics letters. 2009;34(22):3526–8.

137. Khudyakov DV, Lobach AS, Nadtochenko VA. Passive mode locking in a Ti:sapphire laser using a single-walled carbon nanotube saturable absorber at a wavelength of 810 nm. Optics letters. 2010;35(16):2675–7.

138. Kobtsev SM, Kukarin SV, Y. S. Fedotov. Mode-locked Yb fiber laser with saturable absorber based on carbon nanotubes. Laser Phys. 2011;21(2):283–6.

139. Castellani CES, Kelleher EJR, Travers JC, Popa D, Hasan T, Sun Z, et al. Ultrafast Raman laser mode-locked by nanotubes. Optics letters. 2011;36(20):3996–8.

140. Choi SY, Rotermund F, Jung H, Oh K, Yeom D. Femtosecond mode-locked fiber laser employing a hollow optical fiber filled with carbon nanotube dispersion as saturable absorber. Optics Express. 2009;17(24):1336–8.

141. Il NN, Obraztsova ED, Garnov SV, Mosaleva SE. Nonlinear transmission of single-wall carbon nanotubes in heavy water at a wavelength of 1.54 μm and self-mode locking in a Er^{3+}: glass laser obtained using a passive nanotube switch. Quantum Electronics. 2004;34(6):572–4.

142. Sakakibara Y, Tatsuura S, Kataura H, Tokumoto M, Achiba Y. Near-Infrared Saturable Absorption of Single-Wall Carbon Nanotubes Prepared by Laser Ablation Method Near-Infrared Saturable Absorption of Single-Wall Carbon Nanotubes Prepared by Laser Ablation Method. J. Appl. Phys. 2003;42:494–6.

143. Mou C, Arif R, Rozhin A, Turitsyn S. Passively harmonic mode locked erbium doped fiber soliton laser with carbon nanotubes based saturable absorber. Optical Materials Express. 2012;2(6):884.

144. Mou C, Rozhin A, Zhou K, Turitsyn S. Fiber laser mode locked by carbon nanotubes-N-methyl-2-Pryrrolidone solution in fiber microchannel. optical fiber communication conference. 2011;

145. Mou C, Rozhin AG, Arif R, Zhou K, Turitsyn S. Polarization insensitive in-fiber mode-locker based on carbon nanotube with N-methyl-2-pryrrolidone solvent filled fiber microchamber. Applied Physics Letters. 2012;100(10):101110.

146. Set SY, Yaguchi H, Tanaka Y, Jablonski M. Ultrafast fiber pulsed lasers incorporating carbon nanotubes. IEEE J. Sel. Top Quant. Electron. 2004;10(1):137–46.

147. Shohda F, Shirato T, Nakazawa M, Komatsu K, Kaino T. A passively mode-locked femtosecond soliton fiber laser at 1.5 μm with a CNT-doped polycarbonate saturable absorber. Optics Express. 2008;16(26):21191–8.

148. Tausenev AV, Obraztsova ED, Lobach AS, Chernov AI, Konov VI, Kryukov PG, et al. 177 fs erbium-doped fiber laser mode locked with a cellulose polymer film containing single-wall carbon nanotubes. Applied Physics Letters. 2008;92(171113).

149. Senoo Y, Nishizawa N, Sakakibara Y, Sumimura K, Itoga E, Kataura H, et al. Polarization-maintaining, high-energy, wavelength-tunable, Er-doped ultrashort pulse fiber laser using carbon-nanotube polyimide film. Optics Express. 2009;17(22):20233–41.

150. Mou C, Sergeyev S, Rozhin A, Turistyn S. All-fiber polarization locked vector soliton laser using carbon nanotubes. Optics letters. 2011;36(19):3831–3.

151. A.Martinez, S.Uchida, Y.W.Song, T.Ishigure, S.Yamashita. FabricationofCarbonnanotubepoly- methyl-methacrylate composites for nonlinear photonic devices. Optics Express. 2008;16(15):11337–43.

152. Shohda F, Nakazawa M, Mata J, Tsukamoto J. A 113 fs fiber laser operating at 1.56 μm using a cascadable film-type saturable absorber with P3HT-incorporated single-wall carbon nanotubes coated on polyamide. Optics Express. 2010;18(9):9712–21.

153. Sun Z, Rozhin AG, Wang F, Hasan T, Popa D, O’Neill W, et al. A compact, high power, ultrafast laser mode-locked by carbon nanotubes. Applied Physics Letters. 2009;95(25):253102.

154. Wang F, Rozhin AG, Scardaci V, Sun Z, Hennrich F, White IH, et al. Wideband-tuneable, nanotube mode-locked, fibre laser. nature nanotechnology. 2008;3(12):738–42.

155. Kelleher EJR, Travers JC, Sun Z, Rozhin AG, Ferrari AC, Popov SV, et al. Nanosecond-pulse fiber lasers mode-locked with nanotubes. Applied Physics Letters. 2009;95(11):111108.

156. Richardson DJ, Laming RI, Payne DN, Phillips MW, V. J. Matsas. 320 fs soliton generation with passively mode-locked erbium fiber laser. Electron Lett. 1991;27(9):730–2.

157. Grudinin AB, Richardson DJ, Payne DN. Passive harmonic modelocking of a fiber soliton ring lasers. Electron Lett. 1993;29(21):1860–1.

158. Gray S, Grudinin AB, Loh WH, Payne DN. Femtosecond harmonically mode-locked fiber laser with time jitter below 1 ps. Optics letters. 1995;20(2):189–91.

159. Grudinin AB, Gray S. Passive harmonic mode locking in soliton fiber lasers. J. Opt. Soc. Am. 1997;14(1):144–54.

160. Collings BC, Bergman K, Knox WH. Stable multigigahertz pulse-train formation in a short-cavity passively harmonic mode-locked erbium/ytterbium fiber laser. Optics letters. 1998;23(2):123–5.

161. Amrani F, Haboucha A, Salhi M, Leblond H, Komarov A, Grelu P, et al. Passively mode-locked erbium-doped double-clad fiber laser operating at the 322nd harmonic. Optics letters. 2009;34(14):2120–2.

162. Jiang K, Fu SN, Shum P, Lin CL. A wavelength-switchable passively harmonically mode-locked fiber laser with low pumping threshold using single-walled carbon nanotubes. IEEE Photon Technol. Lett. 2010;22(11):754–6.

163. Jun CS, Im JH, Yoo SH, Choi SY, Rotermund F, Yeom DI, et al. Low noise GHz passive harmonic mode-locking of soliton fiber laser using evanescent wave interaction with carbon nanotubes. Optics Express. 2011;10(20):19775–80.

164. Zhou SA, Ouzounov D g., Wise FW. passive harmonic mode-locking of a soliton Yb fiber laser at repetition rates to 1.5 GHz. Opt. lett. 2006;31(8):1041–3.

165. A.Komarov, H.Leblond, F.Sanchez. Multi stability and hysteresis phenomena in passively mode-locked fiber lasers. Phys. Rev. 2005;71(5):053809.

166. Kutz JN, Collings BC, Bergman K, Knox WH. Stabilized pulse spacing in soliton lasers due to gain depletion and recovery. IEEE J. Quantum Electron. 1998;34(9):1749–57.

167. Ozgoren K, Ilday FO. All-fiber all-normal dispersion laser with a fiber-based Lyot filter. Opt. lett. 2010;35(8):1296–8.

168. Lim H, Ilday F, Wise F. Femtosecond ytterbium fiber laser with photonic crystal fiber for dispersion control. Optics Express. 2002;10(25):1497–502.

169. Schultz M, Prochnow O, Ruehl A, Wandt D, Kracht D, Ramachandran S, et al. Sub-60-fs ytterbium-doped fiber laser with a fiber-based dispersion compensation. Optical & laser technologyology. 2007;32(16):2372–4.

170. Rusu M, Herda R, Kivisto S, Okhotnikov OG. Fiber taper for dispersion management in a mode-locked ytterbium fiber laser. Opt. lett. 2006;31(15):2257–9.

171. A.Isomaki, O.G.Okhotnikov. All-fiber ytterbium soliton mode-locked laser with dispersion control by solid-core photonic bandgap fiber. Optics Express. 2006;14(10):4368–73.

172. S. Kivisto RH, Okhotnikov OG. All-fiber supercontinuum source based on a mode-locked ytterbium laser with dispersion compensation by linearly chirped Bragg grating. Optics Express. 2008;16(1):265–70.

173. Gumenyuk R, Vartiainen I, Tuovinen H, Kivisto S, Chamorovskiy Y, Okhotnikov OG. Dispersion compensation technologies for femtosecond fiber system. Appl. Opt. 2011;50(6):797–801.

174. Fedotov YS, Kobtsev SM, Arif RN, Rozhin AG, Mou C, Turitsyn SK. switchable all-fiber mode-locked Yb laser with fiber based birefringent filter. Optics Express. 2012;20(16):20109–16.

175. A.B.Grudinin, D.N.Payne, P.W.Turner, L.J.A.Nilsson, M.N.Zervas, M.Ibsen, et al. Multi-fiber arrangements for high power fiber lasers and amplifiers. U S Patent 6,826,335 B1, 2004.

176. Petrovich MN, Poletti F, Wooler JP, Heidt AM, Baddela NK, Li Z, et al. First demonstration of 2m data transmission in a low-loss hollow core photonic bandgap fiber. in Proc ECOC. 2012;Th.3.A.5.

177. Huttmann G, Yao C, Endl E. New concepts in laser medicine: towards a laser surgery with cellular precision. Med. Las. Appl. 2005;20(2):135139.

178. K.Bremer, A.Pal, S.Yao, E.Lewis, R.Sen, T.Sun, et al. Sensitive detection of CO_2 implementing tunable thulium-doped all-fiber laser. Appl. Opt. 2013;52(17):39573963.

179. Goodno GD, Book LD, Rothenberg JE. Low-phase-noise, single-frequency, single-mode 608 W thulium fiber amplifier. Opt. lett. 2009;34:1204-1206.

180. Engelbrecht M, Haxsen F, Ruehl A, Wandt D, Kracht D. Ultrafast thulium-doped fiber-oscillator with pulse energy of 4.3 nJ. Opt. lett. 2008;33:690.

181. Wang Q, Chen T, Chen KP. Mode-Locked Ultrafast Thulium Fiber Laser with All-Fiber Dispersion Management. in Proc Conference on Lasers and Electro-Optics. 2010;paper CFK7.

182. Kobtsev S, Kukarin S, Smirnov S, Turitsyn SK, A L. Generation of double-scale femto/pico-second optical lumps in mode- locked fiber lasers. Optics Express. 2009;17:20707–13.

183. S.V.Smirnov, Kobtsev SM, S.V.Kukarin, S.K.Turitsyn. Mode- Locked Fibre Lasers with High-Energy Pulses. Laser Systems for Ap- plications. book Laser Pulses. In.Tech.; 2011: 39–58.

184. Kivist S, Hakulinen T, Guina M, Okhotnikov OG. Tunale Raman Soliton Source Using Mode-Locked Tm-Ho Fiber Laser. IEEE Photon Tech. Lett. 2007;19:934–6.

185. Zhang M, Kelleher EJ., Torrisi F, Sun Z, Hasan T, Popa D, et al. Tm-doped fiber laser mode-locked by graphene-polymer composite. Optics Express. 2012;4(2):159168.

186. Krtner FX, Au JA der, Keller U. Mode-Locking with Slow and Fast Saturable AbsorbersWhats the Difference? IEEE J. of Sel. Top. Quant. Electron. 1998;4(2):159168.

187. Guina M, Xiang N, Vainionpaa A, Okhotnikov OG, Sajavaara T, Keinonon J. Self-starting stretched-pulse fiber laser mode locked and stabilized with slow and fast semiconductor saturable absorbers. Opt. lett. 2001;26:1809–11.

188. Haxsen F, Wandt D, Morgner U, Neumann J, Kracht D. Hybrid mode-locked thulium soliton fiber laser. in Proc IEEE PHO. 2011;paper ThAA.

189. Chernysheva MA, Krylov AA, Kryukov PG, Arutyunyan NR, Pozharov AS, Obraztsova ED, et al. Thulium-doped mode- locked all-fiber laser based on NALM and carbon nanotube saturable absorber. Optics Express. 2012;20(26):B124–B130.

190. Rudy CW, Digonnet MJF, Byer RL. Thulium-doped ger- manosilicate mode-locked fiber lasers. in Proc FILAS. 2012;paper FTh4.

191. Chernysheva MA., Krylov AA., Arif RN, Rozhin AG, Rummelli MH, Turitsyn SK, et al. Higher-Order Soliton Generation in Hybrid Mode-Locked Thulium-Doped Fiber Ring Laser. IEEE Journal of Selected Topics in Quantum Electronics. 2014;20(5):1–8.

192. Chernysheva M, Krylov A, Mou C, Arif R, Rozhin A, Rmmeli MH, et al. 300-mW average output power hybrid mode- locked thulium-doped fiber laser. in Proc ECOC. 2013;P.1.

193. L.F.Mollenauer, R.H.Stolen, J.P.Gordon. Experimentalobservation pulse narrowing and solitons in optical fibers. Phys. Rev. Lett. 1980;45:10951098.